

XLII CBrAVIC

UFRRJ, Seropédica, RJ, 01 a 03 de dezembro de 2021



Imagen disponível em <https://portal.ufrj.br>

Book of Extended Abstracts

Realização:



CBrAVIC 2021
Formato: Livro digital
Veiculação: Digital
ISBN: 978-65-00-79418-2

**Brazilian Congress on Vacuum Applications
in Industry and Science**

Book of Extended Abstracts

edited by

Antonio Renato Bigansolli
Mauricio Antonio Algatti

**UFRRJ - Seropédica, RJ, Brazil
December 01-03, 2021**

Dados Internacionais de Catalogação na Publicação (CIP)
(Câmara Brasileira do Livro, SP, Brasil)

Brazilian Congress on Vacuum Applications in
Industry and Science (42. : 2023 : Seropédica,
RJ)

XLII CBrAVIC [livro eletrônico] : book of
extended abstracts / [organização Sociedade
Brasileira de Vácuo] ; edited by Antonio Renato
Bigansolli, Mauricio Antonio Algatti. -- 1. ed. --
São José dos Campos, SP : Ed. dos Autores, 2023.

PDF

Vários autores.

Bibliografia.

ISBN 978-65-00-79418-2

1. Ciência - Congresso 2. Ciência - Estudo
e ensino 3. Indústria 4. Pesquisa científica
5. Vácuo I. Sociedade Brasileira de Vácuo.
II. Bigansolli, Antonio Renato. III. Algatti,
Mauricio Antonio. IV. Título.

23-170709

CDD-001.42

Índices para catálogo sistemático:

1. Pesquisa científica 001.42

Aline Graziele Benitez - Bibliotecária - CRB-1/3129



Organização:



Apoio:



www.sbvacuo.org.br

Patrocínio:



Preface

This year the “CBrAVIC – The Brazilian Congress on Vacuum Applications in Industry and Science”, celebrating its 42th edition took place at UFRRJ – Seropédica's Campus of Universidade Federal Rural do Rio de Janeiro in Seropédica city, in the Rio de Janeiro State, Brazil.

This initiative makes evident the maturity and dynamism of national scientific community working in different areas of knowledge like Physics, Chemistry, Engineering, Biology, Medicine and so on. Following the tradition of CBrAVIC's previous editions, the Organizing Committee made all the efforts to congregate national and foreign researchers working in different knowledge areas in order to improve the Congress's scientific level by means of several Plenary Invited Talks by outstanding scientists presenting the state of art in different fields of Science and Technology.

The Organizing Committee is sure that this effort will strongly contribute for the personal and professional improvement of all conference's attendees. The Organizing Committee decided to realize this edition of CBrAVIC in the online format due the SARS-CoV-2 pandemic worldwide.

Therefore all the attendee's contributions will be presented online following the Conference's schedule previously published at the XLII CBrAVIC website. In spite of the limitations inherent to the online format, the Organizing Committee is sure that the enthusiasm of the attendees will not be prejudiced by those circumstances and that the scientific experiences exchanges among the attendees will be sound appreciated by everybody.

The Brazilian Vacuum Society hope that in the near future the normal activities will be back with the end of the SARS-CoV-2 pandemic and that the next edition of CBrAVIC will be held with the presence of all attendees in a very nice place, like UFRRJ Seropédica's Campus.



Prof. Dr. **Antonio Renato Bigansolli**
Chair of the Organizing Committee



Prof. Dr. **Mauricio Antonio Algatti**
Co-Chair of the Organizing Committee



Prof. Dr. **Julio Cesar Sagás**
Co-Chair of the Organizing Committee



Prof. Dr. **Nazir Monteiro dos Santos**
President of SBV

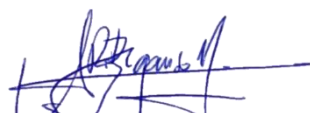
A título de prefácio

Este ano o “CBrAVIC – Congresso Brasileiro de Aplicações de Vácuo na Indústria e na Ciência”, comemora sua quadragésima segunda edição, nas dependências do Campus de Seropédica da Universidade Federal Rural do Rio de Janeiro entre os dias 01 a 03 de dezembro de 2021. Esta iniciativa evidencia a maturidade e o dinamismo da Comunidade Científica Nacional engajada nas diferentes áreas do conhecimento tais como Física, Química, Engenharia, Biologia, Medicina, etc.

Seguindo a tradição das edições anteriores, o Comitê Organizador procurou congregar pesquisadores Nacionais e Internacionais de diferentes áreas do conhecimento, objetivando o engrandecimento do evento através de Palestras Convidadas, da escolha de uma temática de ponta em Ciência e Tecnologia que viesse contribuir de forma significativa para o enriquecimento pessoal e profissional de todos os participantes.

O Comitê Organizador decidiu realizar esta edição do CBrAVIC no formato online devido à pandemia mundial de SARS-CoV-2. Desta feita todas os trabalhos serão apresentados na forma de apresentação de pôsteres, breves comunicações e palestras convidadas, seguindo a programação estabelecida no cronograma publicado previamente no website do XLII CBrAVIC.

Apesar das limitações inerentes ao formato de apresentação online, o Comitê Organizador tem certeza de que o entusiasmo dos participantes não será prejudicado por tais circunstâncias e que a troca de experiência científica entre os participantes será altamente apreciada por todos. A Sociedade Brasileira de Vácuo espera que num futuro próximo as atividades se normalizarão com o fim da pandemia de SARS-CoV-2 e que a próxima edição do CBrAVIC será realizada no formato presencial em um ambiente aprazível como o Campus de Seropédica da Universidade Federal do Rio de Janeiro.



Prof. Dr. **Antonio Renato Bigansolli**
Comite Organizador



Prof. Dr. **Mauricio Antonio Algatti**
Comite Organizador



Prof. Dr. **Julio Cesáro Sagás**
Comite Organizador



Prof. Dr. **Nazir Monteiro dos Santos**
Presidente da SBV

Principais temas a serem discutidos no XLII CBrAVIC:

1. Ciência e Tecnologia de Vácuo (CTV)
2. Ciência e Tecnologia de Plasmas (CTP)
3. Ciência e Tecnologia dos Materiais (CTM)
4. Superfícies, Interfaces e Filmes Finos (SIFF)
5. Energia: Fontes Renováveis e Tecnologia (EFRT)
6. Biomateriais, Biofilmes e Bioprocessos: Ciência e Tecnologia (BBBCT)
7. Vácuo na Indústria (VA)
8. Ciência e Tecnologia de Sensores e Dispositivos (CTSD)

PALESTRANTES CONVIDADOS (Invited Speakers)

Invited Plenary Speakers:

1. **Dra. Ana Gomes da Silva** – Universidade Nova de Lisboa - FCT-NOVA/UNL - Portugal
2. **Dr. André Avelino Pasa** - Universidade Federal de Santa Catarina – UFSC - Brasil
3. **Dr. Alfredo Cruz Orea** - Cinvestav – IPN – México
4. **Dr. José Luis Jiménez Pérez** - Cinvestav – IPN – México
5. **Dr. André Luis de Jesus Pereira** - Instituto Tecnológico de Aeronáutica – ITA - Brasil
6. **Dr. Marcelo Juni Ferreira** European Spallation Source - ESS
7. **Dr. Konstantin Georgiev Kostov** - Universidade Estadual Paulista - UNESP-Guaratinguetá – Brasil
8. **Dr. Clodomiro Alves Júnior** - Universidade Federal Rural do Semi-Árido – UFERSA - Brasil
9. **Dr. Gareth McGuinness and Dr. Harry Esmonde (Dublin University City)**
10. **Dra. Fernanda Roberta Marciano** - Universidade Federal do Piauí – UFPI - Brasil
11. **Dr. Carlos Roberto Grandini** - Universidade Estadual Paulista - Bauru UNESP-Bauru - Brasil

Technical Lecture:

John M. Screech – Senior Vacuum Applications Engineer – Agilent Technologies, Inc.

COMITÊ ORGANIZADOR (Organizing Committee):

Dr. Antonio Renato Bigansolli (Chair) – UFRRJ – Seropédica/RJ
Dr. Julio César Sagás (Co-Chair) – UDESC – Joinville/SC
Dr. Maurício Antonio Algatti (Co-Chair) – UNESP – Guaratinguetá/SP
Dr. Abel André Cândido Recco – UDESC – Joinville/SC
Dr. Álvaro José Damião – IEAV/CTA – São José dos Campos/SP
Ms. Ângelo Luiz Gobbi - LNNano – Campinas/SP
Dr. Carlos Fonzar Pintão – UNESP – Bauru/SP
Dr. Carlos Roberto Grandini – UNESP – Bauru/SP
Dr. Clodomiro Alves Júnior – UFERSA – Mossoró/RN
Dra. Daniela Becker – UDESC – Joinville/SC
Dra. Elidiane Cipriano Rangel – UNESP – Sorocaba/SP
Dra. Érica Freire Antunes – National Institute of Standard and Technology - USA
Dr. Evaldo José Corat – INPE – São José dos Campos/SP
Dr. João Moro – IFSP – Bragança Paulista/SP
Dr. Konstantin G. Kostov - UNESP - Guaratinguetá/SP
Dr. Leonardo Contijo – IFES – Vitória/ES
Dra. Luciana Sgarbi Rossino – FATEC – Sorocaba/SP
Dr. Luís César Fontana – UDESC – Joinville/SC
Dra Maria Lúcia Pereira da Silva - USP – São Paulo/SP
Dr. Mario Ueda – INPE – São José dos Campos/SP
Dra. Nazir Monteiro dos Santos – FATEC – ITAQUERA/SP
Dr. Pedro Augusto de Paula Nascente – UFSCar – São Carlos/SP
Dr. Péricles Lopes Sant'Ana – UNESP – Sorocaba/SP
Dr. Rogério Valentim Gelamo – UFTM – Uberaba/MG
Dr. Rogério Moraes de Oliveira – INPE – São José dos Campos/SP
Dr. Rogério Pinto Mota – UNESP - Guaratinguetá/SP

COMITÊ ORGANIZADOR LOCAL (Local Organizing Committee):

Dr. Antonio Renato Bigansolli (Chair) – UFRRJ – Seropédica/RJ
Dr. Danieli Martins do Carmo – UFRRJ – Seropédica/RJ
Dr. Belmira Benedita de Lima Kühn – UFRRJ – Seropédica/RJ
Dr. João Victor Nicolini – UFRRJ – Seropédica/RJ
Dr. Luiz Antonio Borges Júnior – UFRRJ – Seropédica/RJ
Dr. Marcelo Azevedo Neves – UFRRJ – Seropédica/RJ

Dr. Maria Ivone Martins Jacintho Barbosa – UFRRJ – Seropédica/RJ
Dr. Marisa Fernandes Mendes – UFRRJ – Seropédica/RJ
Dr. Renata Nunes Oliveira – UFRRJ – Seropédica/RJ
Dr. Roberto Carlos Costa Lelis – UFRRJ. – Seropédica/RJ
Dr. Rui de Góes Casqueira – UFRRJ – Seropédica/RJ
Dr. Simone Pereira Taguchi Borges – UFRRJ – Seropédica/RJ
D. Tessie Gouvêa da Cruz Lopes – UFRRJ – Seropédica/RJ

COMITÊ LOCAL ESTUDANTIL (Local Student Committee):

Ana Carolina Cavalcante – Discente/UFRRJ
Antonia Mônica Neres Santos – Mestranda/UFRRJ
Elise dos Santos Lauria – Discente/UFRRJ
Felipe Werlick Velloso dos Santos – Discente/UFRRJ
Fernanda Souza Oliveira – Discente/UFRRJ
Jessica Gonçalves Maia – Discente/UFRRJ
Jônatas de Oliveira Sousa – Discente/UFRRJ
Julia Gonçalves Maia – Discente/UFRRJ
Marcus Felipe de Oliveira Quetez - Discente/UFRRJ
Natália de Macedo do Lago – Discente/UFRRJ
Thaisa Correa Santiago – Discente/UFRRJ
Yanaira Dutra Lira – Discente/UFRRJ

COMITÊ CIENTÍFICO (Scientific Committee):

Dr. Antonio Renato Bigansolli – UFRRJ – Seropédica/RJ
Dr. Julio César Sagás – UDESC – Joinville/SC
Dr. Mauricio Antônio Algatti - UNESP - Guaratinguetá/SP
Dra. Adriana Silva - INPE - São José dos Campos/SP
Dr. Adriano Gonçalves dos Reis – UNESP - São José dos Campos/SP
Dra. Ana Neilde R Silva - USP - São Paulo/SP
Dr. André Ricardo Marcondes – INPE – São José dos Campos/SP
Ms. Ângelo Luiz Gobbi - LNNano – Campinas/SP
Dr. Carlos Roberto Grandini – UNESP – Bauru/SP
Dr. Cícero Rafael Cena da Silva - UFMS - Campo Grande/MS
Dr. Clodomiro Alves Júnior – UFERSA – Mossoró/RN
Dra. Cristiane Costa Wachesk - UNIFESP - São Paulo/SP

Dra. Danieli Aparecida Pereira Reis – UNIFESP – São José dos Campos/SP
Dra. Deborah Cristina Ribeiro dos Santos – SBV – Guaratinguetá/SP
Dr. Durval Rodrigues Júnior – EEL – Lorena/SP
Dra. Elidiane Cipriano Rangel – UNESP – Sorocaba/SP
Dra. Érica Freire Antunes – INPE – São José dos Campos/SP
Dr. Evaldo José Corat – INPE – São José dos Campos/SP
Dr. Fernando Luiz de Campos Carvalho – UNESP – São José dos Campos/SP
Dr. Francisco Tadeu Degasperi - CEETEPS – FATEC/SP
Dr. Gelson B. de Souza - UEPG - Ponta Grossa/PR
Dr. Gilberto Petraconi Filho – ITA/CTA – São José dos Campos/SP
Dra. Graziela da Silva Savonov – INPE - São José dos Campos/SP
Dr. João Moro - IFSP - Bragança Paulista/SP
Dr. Konstantin G. Kostov - UNESP - Guaratinguetá/SP
Dr. José Lucena Barbosa Júnior – UFRRJ – Seropédica/RJ
Dr. Luís César Fontana – UDESC – Joinville/SC
Dra. Maria Lúcia Pereira da Silva - USP – São Paulo/SP
Dra. Maria Margareth da Silva – ITA/CTA – São José dos Campos/SP
Dra. Marina Fuser Pillis - IPEN/CNEN - São Paulo/SP
Dr. Mario Ueda – INPE – São José dos Campos/SP
Dr. Michel Felipe Lima de Araújo – UDC – Foz do Iguaçu/PR
Dr. Milton Eiji Kayama - UNESP - Guaratinguetá/SP
Dr. Mostafa Dadashbaba - Yeditepe University - Istambul/Turquia
Dr. Nilson Cristino Cruz – UNESP - Sorocaba/SP
Dra. Neidenei Gomes Ferreira - INPE - São José dos Campos/SP
Dr. Pedro Augusto de Paula Nascente – UFSCar – São Carlos/SP
Dr. Péricles L. Sant'Ana - UNESP - Sorocaba/SP
Dra. Renata Antoun Simao - UFRJ - Rio de Janeiro/RJ
Dr. Roberto Yzumi Honda - UNESP - Guaratinguetá/SP
Dr. Rodrigo Sávio Pessoa – ITA/CTA - São José dos Campos/SP
Dr. Rogério de Almeida Vieira – UNIFESP – São Paulo/SP
Dr. Rogério Pinto Mota – UNESP - Guaratinguetá/SP
Dr. Rui de Góes Casqueira – UFRRJ – Seropédica/RJ
Dra. Samantha de Fátima Magalhães Mariano – INPE - São José dos Campos/SP
Dr. Steven Frederick Durrant - UNESP - Sorocaba/SP
Dra. Gabriela Araújo Ranieri – UNIFEI – Itajubá/MG
Dr. Rafael Toledo – UNILA – Foz do Iguaçu/PR

Sociedade Brasileira de Vácuo (Brazilian Vacuum Society)

Biênio 2021-2023 (Biennium 2021-2023)

DIRETORIA EXECUTIVA (Executive Board)

Presidente: Profa. Dra. Nazir Monteiro dos Santos (FATEC – São Paulo)

1º Vice Presidente: Prof. Dr. Luis Cesar Fontana (UDESC – Joinville -SC)

2º Vice Presidente: Prof. Dr. Antonio Renato Bigansolli (UFRRJ – Campus Seropédica – RJ)

Diretoria Científica: Júlio César Sagas (UDESC- Joinville - SC)

Diretoria Cultural: Prof. Dr. Álvaro José Damião (IEAv-CTA-São José dos Campos)

1º Secretário: Prof. Dr. Carlos Roberto Grandini (UNESP-Bauru)

2º Secretário: Prof. Dr^a Luciana Sgarbi Rossino (FATEC – Sorocaba – SP)

1º Tesoureiro: Prof. Dr. Rogério Pinto Motta (UNESP – Campus Guaratinguetá - SP)

2º Tesoureiro: Profa Dra Maria Lucia Pereira da Silva (USP/FATEC-São Paulo)

CONSELHO DELIBERATIVO (Deliberative Council)

A) Sócios Efetivos e/ou Honorários

Prof. Dr. Álvaro José Damião (IEAv-CTA-São José dos Campos)

Prof. Dr. Mário Ueda (INPE – São José dos Campos – SP)

Prof. Dr. Elidiane Cipriano Rangel (UNESP – Sorocaba – SP)

Prof. Dr. Érica Freire Antunes

SUPLENTES

Marcelo Azevedo (Agilent)

Marcelo Juni Ferreira (ESS ERIC)

B) Sócios Coletivos e/ou Mantenedores

Agilent

Avaco

Antoon Paar

IEAv

INPE

CONSELHO FISCAL (Fiscal Council)

Prof. Dr. Pedro Augusto de Paula Nascente (UFSCar)

MSc. Angelo Luiz. Gobbi (LNNano CNPEM)

Prof. Dr. Konstantin Georgiev Kostov (UNESP)

Prof. Dr. Mário Ueda (INPE)

Prof. Dr. Alfredo Gonçalves Cunha (UFES)

PROGRAMAÇÃO DAS PALESTRAS E APRESENTAÇÃO DE PÔSTERES

CONFERENCE'S TIMETABLE

Horários	29/11	30/11	01/12	02/12	03/12	04/12
08:00-hs						
09:00-hs				Abertura	Palestra-4 Produção de filmes finos de black-TiO ₂ por plasma de hidrogênio de cátodo oco para aplicações fotocatalíticas Dr. André Luis de Jesus Pereira (ITA)	Sessão de Pôster
10:00-hs	Minicurso: Tecnologia de Vácuo	Minicurso: Vácuo para professores do Ensino Médio		Palestra de abertura Ultrafast nonlinear nano-optics: from fundamentals to basic research and applications Dra. Ana Gomes da Silva (Univ. Nova de Lisboa)	Sessão de Pôster	Palestra-8 PANBioRA-project Dr. Gareth McGuinness Dr. Harry Esmonde (Dublin University City)
11:00-hs				Palestra-1 Room-temperature spin-field-effect transistor Dr. André Avelino Pasa (UFSC)	Palestra-5 Vacuum and accelerator science: ESS vacuum system Dr. Marcelo Júnio Ferreira (ESS)	Palestra-9 Filmes finos para aplicações biomédicas Dra. Fernanda Roberta Marciano (UFPI)
12:00-hs	Almoço					
14:00-hs			Palestra-2 Photothermal phenomena applied to optical and thermal characterization of materials Dr. Alfredo Cruz-Orea (Cinvestav-IPN)	Palestra-6 Development of cold-atmospheric-pressure plasma jets for biomedical applications Dr. Konstantin Georgiev-Kostov (UNESP-Guaratinguetá)	Palestra-10 Cellular metals as a solution for structural metallic biomaterials Dr. Carlos Roberto Grandini (UNESP-Bauru)	
15:00-hs	Minicurso: Tecnologia de Plasmas	Minicurso: Tecnologia de Plasmas	Sessão de Pôster	Sessão de Pôster	Encerramento	Minicurso: Técnicas de caracterização
16:00-hs			Palestra-3 Implementation of a 3D-printer by creating micro-scaffolds for tissue regeneration based on photocurable nanoresins Dr. José Luis Jiménez Pérez (Cinvestav-IPN)	Palestra-7 Interação do plasma com água hipersalina Dr. Clodomiro Alves Júnior (UFERSA)	Assembleia da SBV	
17:00-hs				Palestra técnica Agilent		

OPENING LECTURE

ULTRAFAST NONLINEAR NANO-OPTICS: FROM FUNDAMENTALS TO BASIC RESEARCH AND APPLICATIONS

Ana G Silva

NOVA School of Science and Technology, New University of Lisbon, Caparica, Portugal

Nonlinear optical spectroscopies have become important tools in surface and interface analysis where they can provide information on optical, electronic, magnetic, and vibronic properties, reaching a state of very high surface sensitivity. Nanostructures with their large fraction of surface to volume are interesting subjects for studies with interface sensitive optical techniques. The basic principles of Optical Second-harmonic generation (SHG) are reviewed. Applications of optical SHG and SHG spectroscopy to characterization of nanostructures, semiconductors surfaces and interfaces, nano crystals, metallic quantum wells, plasmonic structures, and 2D materials such as graphene will be discussed. Nonlinear optical spectroscopies and ultrafast phenomena have been in recent years developed also for environment and bio photonics applications. An overview of applications in different research fields will be presented.

References

- [1] R. W. Boyd, Nonlinear Optics, 4th Edition, Elsevier
- [2] Menzel, Nonlinear Optical Spectroscopy, In photonics. Advanced Texts in Physics, Springer, Berlin; Heidelberg
- [3] G. Cohen, Jahan Dawlaty, R. Fleming, Ultrafast Multidimensional Spectroscopy: Principles and Applications to Photosynthetic systems, IEEE, Journal of selected topics in quantum electronics, 1077-260X/\$26.00 © 2011 IEEE, 2011

Acknowledgments

The author would like to thank Portuguese science Foundation and Denmark Science Foundation for their financial support.

INVITED PLENARY LECTURE 1

ROOM TEMPERATURE SPIN FIELD-EFFECT TRANSISTOR

André Avelino Pasa *

Programa de Pós-graduação em Física, Universidade Federal de Santa Catarina, Florianópolis, Brazil

Spintronics or spin electronics is a new technology that is becoming the main technology for microelectronic devices. In this contribution, we will introduce the physical concepts behind spintronic devices that allow solid-state manipulation of electron spin to produce spin currents. Emphasis will be given to the fabrication of a spin field-effect transistor (SpinFET) with a graphene channel, permalloy ferromagnetic contacts, and an alumina tunnel barrier using standard large-scale microfabrication processes. Important results were obtained with local and non-local magnetoresistive measurements as a function of temperature and gate voltage. While the magnetoresistance is dependent on temperature and highly sensitive to gate voltage for spin-polarized currents, it is less dependent on temperature and less sensitive for spin currents.

References

[1] C. I. Araujo, H. A. Teixeira, O. O. Toro, C. Liao, J. Borme, L. C. Benetti, D. Schafer, I. S. Brandt, R. Ferreira, R., P. Alpuim, P. P. Freitas, A.A. Pasa, Room temperature two terminal tunnel magnetoresistance in a lateral graphene transistor, *Nanoscale*, 13 (47), 20028-20033 (2021).

Acknowledgments

The author would like to thank CNPQ for the financial support.

INVITED PLENARY LECTURE 2

PHOTOTHERMAL PHENOMENA APPLIED TO OPTICAL AND THERMAL CHARACTERIZATION OF MATERIALS

Alfredo Cruz Orea

CINVESTAV-IPN-Centro de Investigación y de Estudios Avanzados del Instituto Politécnico Nacional, 07360, Ciudad de México. México

It has been demonstrated, by several researchers, that Photothermal (PT) phenomena are useful for optical and thermal characterization of diverse materials. Based on these phenomena several PT techniques have been developed, which have been used to obtain optical absorption spectra of several types of samples, including media with high light scattering, such as the case of biological material. PT techniques have also been applied to obtain thermal properties of very diverse samples. In the present talk, the theory of some PT techniques will be briefly addressed, and some multidisciplinary applications of PT techniques will be presented, such as the thermal and optical characterization of foods, semiconductors and several biological materials of interest in different areas of knowledge as medicine, biotechnology (1-7), etc.

References

- [1] - Olvera LI, Villanueva GC, Cruz A, Sánchez N, Olvera SJ, Alvarado ML. Relationship between haemoglobin and glucose in type 1 experimental diabetes. IOP Conf. Series: Journal of Physics: Conf. Series 1221 (2019) 012070
- [2] - Hernández-Aguilar C, Domínguez-Pacheco A, Valderrama-Bravo C, Cruz-Orea A, Martínez Ortiz E, Ordoñez-Miranda J. Photoacoustic Spectroscopy in the Characterization of Bread with Turmeric Addition. Food and Bioprocess Technology (2020) 13:2104–2119
- [3] - Alvarado-Noguez ML, Hernández-Aguilar C, Domínguez-Pacheco FA, Cruz-Orea A, Sánchez-Sinéncio F. Photothermal Techniques Applied to the Thermal and Optical Characterization of Curcuma longa. International Journal of Thermophysics (2018) 39:99
- [4] - Macías M, Casallas-Moreno YL, Camacho-Reynoso M, Zambrano-Serrano MA, Pérez-Hernández BG, Yee-Rendón CM, Gurevich YG., López-López M, Cruz-Orea A. Thermal properties of cubic GaN/GaAs heterostructures grown by molecular beam epitaxy. Journal of Applied Physics 128, 135301 (2020)
- [5] - Luna-Sánchez JL, Jiménez-Pérez JL, Correa-Pacheco ZN, Macías-Mier M, Cruz-Orea A, Castañeda-Galván AA, Gutiérrez-Fuente R. Photoacoustic Spectroscopy for Curing Time Determination of an Acrylic Nanocomposite. International Journal of Thermophysics (2020) 41:99
- [6] - Carbajal-Valdés R, Rodríguez-Juárez A, Jiménez-Pérez JL, Sánchez-Ramírez JF, Cruz-Orea A, Correa-Pacheco Z.N, Macías M, Luna-Sánchez JL. Experimental investigation on thermal properties of Ag nanowire nanofluids at low concentrations. Thermochemical Acta, Volume 671, January 2019, Pages 83-88
- [7] - González-Domínguez JL, Cruz-Orea A, Rojas-Chávez H, Sánchez-Sinéncio F, Hernández Aguilar C, Domínguez-Pacheco FA. Thermal Efusivity of Human Fluids. International Journal of Thermophysics (2019) 40:25

Acknowledgments

The author would like to thank Consejo Nacional de Ciencia y Tecnología (CONACYT) for financial support.

INVITED PLENARY LECTURE 3

IMPLEMENTATION OF A 3D PRINTER BY MICRO-SCAFFOLDS ELABORATION FOR TISSUE REGENERATION BASED ON PHOTOCURABLE NANORESINS

J.L. Jimenez Perez^{1*}

¹*Unidad Profesional Interdisciplinaria en Ingeniería y Tecnologías Avanzadas, Instituto Politécnico Nacional, 1 Av. Instituto Politécnico Nacional 2580. La Laguna Ticomán, Ciudad de México. 07340. México.*

The aim of this work was the development of a prototype to obtain resin scaffolds through 3D printing for the elaboration of biocompatible materials of great interest in the medical area. This technique is promising in the generation of structures for applications in tissue engineering using biocompatible materials from biodegradable acrylic resins. On the other hand, a prototype was built and designed for 3D printing scaffolding using a UV laser controlled by a galvanometric mirror system and a mobile platform in the XYZ directions. In addition, the speed control of a stepper motor was used to print the layers of the photocurable resin. The LabVIEW program was used as the interface between the user and the control. In addition, a pair of microcontrollers were used, one for zero crossing detection and SCR firing and one for temperature sensor and stepper motor speed control. Finally, the system was integrated into an optical plate for testing and adjustment, obtaining micron-sized scaffolds. The purpose of this project was to use this technique of synthesis and 3D printing of polymeric scaffolds with carbon nanotubes as nanocomposites for the restoration of damaged tissues or organs, facilitating good tissue recovery. These biomaterials have different applications in nanomedicine and bone tissue engineering in the medical field.

INVITED PLENARY LECTURE 4

PRODUÇÃO DE FILMES FINOS DE BLACK-TiO₂ POR PLASMA DE HIDROGÊNIO DE CATÓDO OCO PARA APLICAÇÕES FOTOCATALÍTICAS

A. L. J. Pereira^{1*}, A. Godoy-Jr, B¹. Damasceno¹, H. C. S. Barros^{1,3}, B. Carvalho², M. C. Gomes³, D. M. G. Leite¹, M. Baldan², A. S. da Silva Sobrinho¹

¹*Instituto Tecnológico de Aeronáutica – ITA, Laboratório de Plasmas e Processos – LPP, São José dos Campos, 12228-900, SP, Brasil.*

²*Instituto Nacional de Pesquisas Espaciais – INPE, Av. dos Astronautas, 1758, Jardim da granja, São José dos Campos, SP, Brasil.*

³*Instituto Federal de São Paulo – IFSP, São José dos Campos, 12223-201, SP, Brasil.*

Neste trabalho será apresentado um novo método para se produzir filmes finos de black TiO₂ a partir de filmes puros de TiO₂ na fase anatase. O método consiste na imersão dos filmes de TiO₂ por apenas poucos minutos em um plasma de hidrogênio gerado por um sistema PECVD-RF com uma geometria de catodo oco, resultando em um eficiente escurecimento do TiO₂. O crescimento dos filmes puros de TiO₂ na fase anatase sobre substratos de vidro e c-Si se deu por meio do método de pulverização catódica (*magnetron sputtering*) e posterior tratamento térmico a 450 °C durante 2 h a fim de se conseguir uma preponderância da fase anatase. Antes e após o tratamento em plasma de H₂, as amostras foram caracterizadas quanto às suas características morfológicas, microestruturais, química, ótica, elétricas e de molhabilidade. Além disso, foi avaliado o potencial fotocatalítico dos filmes produzidos por meio da degradação do corante azul de metileno, além de uma investigação das características do plasma de hidrogênio gerado durante o processo de hidrogenação. Os resultados obtidos mostram que a utilização de um catodo oco para o processo de hidrogenação foi determinante para uma eficiente hidrogenação dos filmes de black TiO₂. Após o tratamento em plasma de hidrogênio os filmes apresentam um aumento significativo na absorção de luz em todo o espectro solar, uma diminuição significativa da resistência de folha, e um aumento significativo da área superficial. Estes resultados estão relacionados principalmente a um aumento das vacâncias de O e com o aumento da presença de grupos hidroxila OH na superfície dos filmes. Essas características levaram a uma melhoria significativa na sua atividade fotocatalítica sob irradiação UV-Vis.

INVITED PLENARY LECTURE 5

VACUUM AND ACCELERATOR SCIENCE: ESS VACUUM SYSTEM

Marcelo Juni Ferreira

European Spallation Source – ERIC, Technical Division, Vacuum Group, Lund, Sweden

Vacuum and particle accelerators development have been together since the technical and scientific evolution of the particle-gas interactions. It will be present the European Spallation Source (ESS), a multi-disciplinary research infrastructure for neutron, based on a 2GeV-5MW proton linear accelerator (LINAC), as a most updated version of vacuum science applied for accelerators [1]. The goal of ESS is to be the brightest neutron facility and to enable novel science in many fields such as biology research, environmental technologies and fundamental physics. The facility includes Super-Conductive Radio-frequency cavities (SRF) to accelerate a proton beam to produce neutron by spallation process on a helium-cooled tungsten wheel, possibility to host 42 neutron instruments. The ESS Vacuum Group has the overall responsibility for all technical vacuum systems used on the Accelerator, Target and Neutron Scattering Instruments (NSS). The team has the responsibility to provide internally or to the in-kind partners, guidance, on-going support and oversight during design, fabrication, installation, commissioning and operation. This allows an integrated approach to be adopted to ensure the implementation of a cost-effective vacuum program from the initial design through procurement and operation.

It will be given an overview from the vacuum requirements and engineering design of the ESS Vacuum System for the Accelerator, Target and Neutron Instruments. The ESS proton linear accelerator is under installation and initial conditioning (RFQ) at the Normal Conductive LINAC (NCL), the ion source and Low Energy Beam Transport (LEBT) description with some early result from the operation, status of vacuum control system. Also, the SRF installation with Linear Warm Units (LWU) [2], and preparations for the cryomodules installation. On the Target, the last updates on the monolith vessel welding, and early stage NSS instruments installations. An introduction about ESS Vacuum Laboratory and activities developed to support the design of ESS will be presented.

3. References

- [1] - McEntee J, “*A joined-up vision for vacuum*” CERN COURIER, Reporting on international high-energy physics, Applications/Opinion, (January, 2021) <https://cerncourier.com/a/a-joined-up-vision-for-vacuum/>
- [2] - Jarrigue C, Ravelli F, Ferreira MJ, “*Developing the Particle Free Vacuum System at ESS*”, vol 37 n. 3 (2018). <http://www.sbvacuo.org.br/rbav/index.php/rbav/article/view/1114>

Acknowledgments

Special thanks for all ESS project team along 11 years of design and test, and the Vacuum Group team interfacing all in-kinds and partners.

INVITED PLENARY LECTURE 6

DEVELOPMENT OF COLD ATMOSPHERIC PRESSURE PLASMA JETS FOR BIOMEDICAL APPLICATIONS

K. G. Kostov^{1*}, F. Nascimento¹, F. V. P. Kodaira¹, K. A. Petroski¹, A. A. Barbosa¹, A. C. P. L. Almeida¹, B. H. S. Leal¹, T. M. C. Nishime², G. M. G. Lima³,
M. H. Tanaka³, C. Y. Koga-Ito³

¹Faculty of Engineering – FEG, São Paulo State University – UNESP, Guaratinguetá, SP 12516-410, Brazil

²Leibniz Institute for Plasma Science and Technology – INP-Greifswald, Germany

³Institute of Science and Technology – ICT, São Paulo State University – UNESP, São José dos Campos
SP 12245-000, Brazil

Plasmas at atmospheric pressure generate highly reactive species, whose synergetic action can inactivate different microorganisms as well as stimulate eukaryotic cells growth and consequently tissue healing. Also, diverse studies have revealed that cold plasmas can induce apoptosis in different kinds of cancer cells without affecting the surrounding healthy tissues. Therefore, in the last decades a new multidisciplinary field called Plasma Medicine has emerged. Nowadays, cold atmospheric pressure plasmas have been routinely used in dermatology and for healing/disinfection of chronic wounds. Worldwide several cold atmospheric plasma systems have been certificated for medical applications and are currently commercially available. However, for some specific medical applications, like treatments of internal organs or inside body cavities, a new generation of cold atmospheric pressure plasma sources should be developed. In this work, we report the development, characterization and application of a cold atmospheric pressure plasma jet, which is produced at the tip of long flexible plastic tube [1]. This kind of remote plasma jet is produced far from the high voltage generator and can be easily manipulated by hands and directed to a target with otherwise different accesses (like inside patient's oral cavity). The device was successfully tested in *in-vitro* [2] and *in-vivo* [3] trials showing promising antibiofilm effect without cell toxicity.

References

- [1] K. G. Kostov, M. Machida, V. Prysiazhnyi and R. Y. Honda, *Plasma Sources Sci. Technol.*, vol. 24, p.025038 (2015).
- [2] T. M. C. Nishime, A. C. Borges, C. Y. Koga-Ito, M. Machida, R. O. Hein and K. G. Kostov, *Surf. Coat. Technol.*, vol. 312, p. 19, (2017).
- [3] A. C. Borges, G. M. G. Lima, T. M. C. Nishime, A. V. L. Gontijo, K. G. Kostov and C. Y. Koga-Ito, *PlosOne*, vol. 13, p. e0199832 (2018).

Acknowledgments

This work was supported by The São Paulo Research Foundation – FAPESP under grant 2019/05856-7; The National Council for Scientific and Technological Development – CNPq under grants 308127/2018-8 and 302405/2018-6 and The Coordination for the Improvement of Higher Personnel Education – CAPES, under programs PrInt and DS

INVITED PLENARY LECTURE 7

INTERACTION OF COLD ATMOSPHERIC PLASMA- HYPERSALINE WATER

Clodomiro Alves Junior

UFERSA - Univ Federal Rural do Semi-árido, Labplasma, 59.625-900, Mossoró, RN, Brazil

Industrial applications such as reverse osmosis desalination plants and salt production in evaporation tanks generate effluents composed of high concentrations of Mg, Na, K, Cl, and SO₄, referred to as hypersaline water. Until now, methods for disposing of these residues have been unsustainable and limited by high capital costs and lack of universal application. In recent years, atmospheric pressure cold plasma has gained prominence due to various research findings, established industrial implementations, as well as promising applications including nanomaterial synthesis, liquid sterilization, dye degradation, and medical applications. In this study, the interaction between plasma and hypersaline water will be investigated for potential application in salt extraction and/or separation.

Pulsed corona discharge (PCD) and dielectric barrier discharge (DBD) were employed, with either cathodic or anodic polarization, using different voltages and pulse frequencies. It was observed that under cathodic polarization, a considerable number of metal cations could be extracted from the solution in the form of precipitated salts. On the other hand, in the anodic configuration, despite showing higher spectral intensity for Na (589.5 nm), it was less efficient in salt precipitation. The results of this study suggest that changing the polarization also alters the plasma interaction mechanism, indicating it as an interesting technique to explore selective chemical extraction of saline water.

References

- [1] Ekanayake UGM et al. Sustain Mater Technol. 25:e00181. 2020.
- [2] L.F.A. Almada et al J. Phys. D. Appl. Phys. 54 (2021) 055202.
- [3] C P. Vanraes, A. Bogaerts, Appl. Phys. Rev. 5 (2018).
- [4] J.B.F.O. Barauna et al Materials Research. 20 (2017)
- [5] W. Voig, Pure Appl. Chem. 2015; 87(11-12): 1099–1126

Acknowledgments

The author would like to thank Capes, and CNPq for their financial support.

INVITED PLENARY LECTURE 8

Garrett McGuinness^{1,*} and Harry Esmonde¹

¹ DCU – School of Mechanical & Manufacturing Engineering, Dublin City University, Dublin 9, Ireland

Biomaterial-based solutions have found various applications in the healthcare system, ranging from advanced therapy medicines to medical devices. However, the existing methodologies for assessing the risks associated with biomaterials must be revised to ensure adequate evaluation across all applications. It is imperative to develop a new generalized testing system that can standardize the assessment of biomaterials. The PANBioRA consortium provides an innovative approach for selecting the most suitable implant biomaterial. By doing so, the consortium aims to mitigate and reduce potential complications that may arise post-implantation. The primary objective of PANBioRA is to develop a practical method for evaluating the cost and time implications of new biomaterials in both healthy and diseased conditions (generalized test), as well as for specific patients (personalized test). The PANBioRA consortium plans to develop a modular system that employs interdisciplinary techniques to predict a patient's specific response to a given biomaterial. This test system will integrate refined and miniaturized versions of existing methods and new evaluation technologies into a single instrument capable of performing multiple analyses at the cellular and microtissue levels. Through its multidisciplinary protocols and procedures, the PANBioRA testing system will set a new standard for evaluating biomaterials. The classification system developed within the PANBioRA project allows for the risk assessment of biomaterials at nano, micro, and Milli scales. Additionally, integrating a microfluidic system, which combines real-time monitoring tools such as electrochemical sensors, antibody-based cytokine detection, and mini-microscopes, will provide more continuous information using smaller biological samples and less biomaterial¹. The PANBioRA project has partnered with DCU to develop further and validate these methods and tools, which can be utilized independently or as part of the integrated model². Following the development and technical validation of the system, pre-clinical tests relevant to the risks associated with biomaterials will be conducted to demonstrate the effectiveness of the PANBioRA systems. In conclusion, the PANBioRA consortium is dedicated to revolutionizing the evaluation of biomaterials by establishing a standardized testing system. This innovative approach will enhance the selection of implant biomaterials and minimize potential complications. By integrating interdisciplinary techniques and advanced technologies, PANBioRA aims to set a new standard in biomaterial evaluation.

References

- [1] PANBioRA. (2020). *Personalised and generalised integrated biomaterial risk assessment*. [Https://Www.Panbiora.Eu/](https://Www.Panbiora.Eu/).
- [2] PANBioRA. (2021). *Outreach presentation at DCU introducing PANBioRA*. [Https://Www.Panbiora.Eu/News-Events/News-Details/Outreach-Presentation-at-Dcu-Introducing-Panbiora/](https://Www.Panbiora.Eu/News-Events/News-Details/Outreach-Presentation-at-Dcu-Introducing-Panbiora/).

Acknowledgments

The author would like to thank the PANBioRA project and DCU.

INVITED PLENARY LECTURE 9

FILMES FINOS PARA APLICAÇÕES BIOMÉDICAS

Fernanda Roberta Marciano

Programa de Pós-Graduação em Ciência e Engenharia de Materiais, Universidade Federal do Piauí, Teresina, PI, 64049-550, Brazil

Os filmes finos podem fornecer diferentes propriedades para a superfície do substrato. As suas propriedades podem ser significativamente aumentadas pela presença de nanopartículas em sua estrutura, com substanciais mudanças em suas propriedades. O foco da investigação deste trabalho está centrado na obtenção de filmes de carbono tipo-diamante (DLC) com nanopartículas incorporadas em sua estrutura. As vantagens desse novo filme estão em combinar as propriedades de dureza, baixa rugosidade, coeficiente de atrito e biocompatibilidade do DLC, adicionando as possibilidades de obtenção desse novo material híbrido em grandes áreas e altamente aderente aos substratos metálicos. Os resultados mostram filmes de DLC contendo nanopartículas de prata e de dióxido de titânio como agentes bactericidas; filmes de DLC contendo nanopartículas de diamante cristalino como agentes protetores contra corrosão eletroquímica. Esses filmes também mostraram-se eficientes contra a tribocorrosão. A homogeneidade dos filmes de DLC contendo nanopartículas foi avaliada sob diferentes formas de operação (carga e velocidade). Dessa forma, espera-se ampliar o potencial de aplicação para a utilização em áreas sujeitas ao atrito em ambiente corrosivo para aplicações biomédicas.

INVITED PLENARY LECTURE 10

CELLULAR METALS AS A SOLUTION FOR STRUCTURAL METALLIC BIOMATERIALS

Carlos Roberto Grandini

UNESP - Univ Estadual Paulista, Laboratório de Anelasticidade e Biomateriais, 17.033-360, Bauru, SP, Brazil

IBTN-Br – Institute of Biomaterials, Tribocorrosion, and Nanomedicine – Brazilian Branch, 17.033-360, Bauru, SP, Brazil

Metallic foams ('metfoams' or cellular metals) are a class of material unfamiliar to engineers and materials scientists. They are made possible by a range of novel processing techniques, which are still under development (1). In the most general term, cellular metals refer to a metallic body with any gaseous voids dispersed in it. The metallic phase divides space into closed cells which contain the gaseous phase. Cellular metals and porous metals have become the most promising lightweight multifunctional materials due to their superior combination of advanced properties mainly derived from their base material and cellular structure (2). They are used in a wide range of commercial, biomedical, industrial, and military applications.

In contrast to other cellular materials, cellular metals are non-flammable, recyclable, extremely tough, and chemically stable, and are excellent energy absorbers. Cellular metals enable an immediate weight reduction and material saving of components. Simultaneously, they can perform multiple functions due to their three-dimensional cellular structures. Despite these advantages, the commercial use of cellular metals is still limited due to the high production costs required to create stable cellular structures (topology and morphology). Another inhibitor to their application is the random variation in their mechanical, acoustic, and thermal behavior. However, new technical solutions ensure that these materials can be produced commercially with the required quality and reproducibility. Their integration into engineering structures can fully utilize their unique properties. The study for the use of cellular metals as structural biomaterials has increased significantly in recent years. Interconnected pores favor cell growth and ensure more excellent resistance in the tissue-implant relationship. In order to improve the integration of bone and tissue, several surface modification techniques have been used to tailor the topography (3). When the implant surface properties can mimic the physical and chemical properties of the biological structure, tissue and implant surface integration is accomplished by adhesion, spreading, and proliferation of cells on the implant surface (4). Key technologies and steps to design hybrid smart and multifunctional coatings on cellular metals for bone regeneration implants are outlined, including additive titanium and magnesium alloys manufacturing for permanent and temporary implant applications.

References

- [1] Evans AG, Hutchinson JW, Ashby MF. Cellular metals. *Current Opinion in Solid State and Materials Science*. 1998;3(3):288-303.
- [2] Duarte I, Fiedler T, Krstulović-Opara L, Vesenjak M. Cellular Metals: Fabrication, Properties, and Applications. *Metals*. 2020;10(11):1545.
- [3] Čaha I, Alves AC, Rocha LA, Toptan F. A Review on Bio-functionalization of β -Ti Alloys. *Journal of Bio- and Tribocorrosion*. 2020;6(4):135.
- [4] Santos-Coquillat A, Martínez-Campos E, Mora Sánchez H, Moreno L, Arrabal R, Mohedano M, et al. Hybrid functionalized coatings on Metallic Biomaterials for Tissue Engineering. *Surface and Coatings Technology*. 2021;422:127508.

Acknowledgments

The author would like to thank Capes, CNPq, and FAPESP for their financial support.

UNVEILING THE STRESS-INDUCED ORDERING OF POINT DEFECTS IN Ti-15Zr-BASED ALLOYS

Perosa, B. S.¹, Correa, D. R. N.^{1*}, Torrento, J. E.²; Grandini, C. R.²¹IFSP – Câmpus Sorocaba, Advanced Metallic Materials Group, Sorocaba (SP), Brazil²UNESP – Univ. Estadual Paulista, Laboratory of Anelasticity and Biomaterials, Bauru (SP), Brasil**1. Introduction**

Ti and its alloys have diverse industrial applications due to their favorable mechanical, chemical, and biological properties. Ti-15Zr-Mo alloys have been recently designed for biomedical applications, grouping interesting elastic modulus, mechanical strength, tribocorrosion resistance, and biocompatibility for use as metallic biomaterials [1]. As the mechanical properties are crucial parameters to evaluate the material's performance, a deep knowledge is quite important. In this sense, dynamo-mechanical analysis is an interesting tool, once it can provide specific information about the interaction of interstitial gases in metals and alloys [2]. In this sense, this study aims to evaluate the effect of substitutional and interstitial point defects on the anelastic behavior of Ti-15Zr-Mo alloys by dynamo-mechanical analysis.

2. Experimental

The Ti-15Zr-(0 to 20 %wt)Mo samples were cast in Ar arc-melting furnace, followed by a number of thermo-mechanical treatments which focused in three goals (Fig. 1a): homogenization (1273 K / 86.4 ks / 10^{-5} Torr / furnace cooling); Hot-rolling (1273 K / air cooling); solution (1123 K / 7.2 ks / 10^{-6} Torr / water quenching); oxygen doping (1123 K / 7.2 ks / 10^{-1} – 10^1 Torr O₂ / water quenching); aging (698 K / 14.4 – 43.2 ks / 10^{-6} Torr / water quenching). Then, the samples were characterized in DMA50 equipment (Metavib Inc.), in tensile mode, frequency in the range 1 – 40 Hz, heating rate of 1 K per min, from room temperature until 750 K. The data analysis was done with the Peak fitting module of the OriginLab® 8.0.

3. Results and Discussions

The internal friction and elastic modulus values as a function of temperature were affected by the chemical composition and processing steps due to distinct anelastic relaxation mechanisms. The amount of Mo changed the phase stability of the Ti-15Zr alloy from an hcp (α phase) to bcc structure (β phase), as a result, it facilitated the stress-induced ordering of oxygen in the metallic matrix, as indicated in Fig. 1b. After oxygen doping, the anelastic relaxation processes turned more evident, in special those related to clusters (e.g. Ti-O-O). Regarding the aging treatment, it provided an interstitial diffusion of light elements located at the grain boundaries to intergranular regions, as a result, the anelastic relaxation processes were more intense than the solutionized samples. Overall, our study shows that it is possible to handle the stress-induced ordering of point defects (substitutional and interstitial elements) by proper chemical composition and processing design.

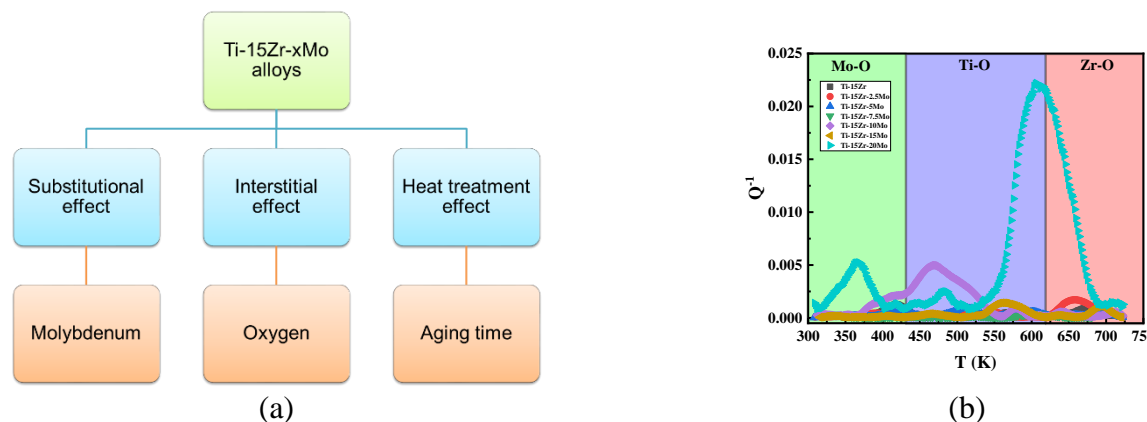


Fig. 1. (a) Research design diagram and (b) Internal friction as a function of Mo measured at 10 Hz.

4. References

[1] J. E. Torrento et al., Journal of Alloys and Compounds, **873**, 159641, (2021).
 [2] D. R. N. Correa et al., Materials Research, **20**(3), 688-693 (2017).

Acknowledgments

The authors thank the Brazilian funding agencies FAPESP and CNPq for the financial support.

TITANIUM DIOXIDE DECORATED REDUCED GRAPHENE OXIDE FILMS FOR PHOTOCATALYTIC APPLICATION

Rodrigo T. Bento¹, Olandir V. Correa¹, Marina F. Pillis^{1*}

¹*Instituto de Pesquisas Energéticas e Nucleares (IPEN-CNEN/SP), São Paulo, Brazil*

1. Introduction

Titanium dioxide (TiO_2) films obtained by sol-gel method have been widely investigated as a promising photocatalyst in water and air decontamination [1]. Nevertheless, it has not yet been found a satisfactory way for the TiO_2 films to present appropriate photocatalytic activity under visible light. Recent studies have demonstrated the possibility of applying TiO_2 /reduced graphene oxide (rGO) heterojunctions on the water treatment with high efficiency [2]. However, there are few studies focused on the photocatalysis mechanism of such heterojunctions under visible light, using simpler, low-cost, and eco-friendly synthesis routes. In this way, the present study aims the synthesis, characterization, and visible light photocatalytic behavior of TiO_2 /rGO composite films successfully deposited on borosilicate glass substrates by a facile airbrush spray-coating technique.

2. Experimental

Firstly, TiO_2 films were obtained by sol-gel method, from a solution of titanium (IV) isopropoxide diluted in isopropanol (v:v, 1:10), and deposited on borosilicate glass by airbrush spray-coating technique, at room temperature. The angle of the cold spray was fixed in 45° , and the feed rate was 17 mm.s^{-1} . The films were dried at 100°C for 60 min, and then heat treated at 550°C for 30 min. Then, the films were coated with rGO nanosheets UVC-reduced for 2, 8, and 24 h, from a suspension containing 0.6 g of rGO in 60 ml of isopropanol. After spraying rGO on the TiO_2 surface, the films were dried at 100°C for 60 min. The samples were characterized by Raman spectroscopy, Atomic force microscopy (AFM), and the photocatalytic activity observed by the methyl orange dye (MO) removal (5 mg.L^{-1}) under visible light.

3. Results and Discussions

The results showed that under visible light, the photocatalytic activity of the films improved considerably from the formation of TiO_2 /rGO heterojunction. After 300 min of visible light irradiation, approximately 49 % of the dye was removed from the water by using the TiO_2 /rGO-2h UVC nanocomposite film. The heterojunctions containing rGO UVC-obtained at 8 and 24 h, respectively, exhibited efficiencies of 34 % and 10 %, approximately. Such behavior suggests that the photocatalytic activity of heterojunctions is strongly dependent on the synthesis time of rGO production. The longer the UVC reduction time, the lower the concentration of oxygenated groups present in the rGO. MO photolysis curve shows that, without the presence of the catalyst, there was no dye removal under visible light. The pure TiO_2 film also did not show photoactivity. The results suggest that the TiO_2 /rGO heterojunction films have a promising application for the eco-friendly water treatment.

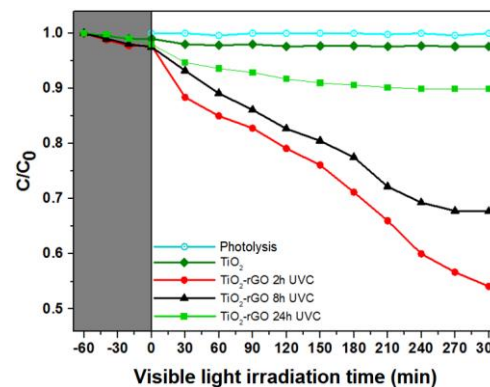


Fig. 1. Photocatalytic behavior of TiO_2 /rGO heterojunctions on the methyl orange dye removal under visible light.

4. References

- [1] J.G. Mahy et al., *Catalysts*, **11**, 768, (2021).
- [2] A. Diamantopoulou et al., *Applied Catalysis B: Environmental*, **240**, 277-290, (2019).

Acknowledgments

The authors are grateful to the Brazilian agency CNPq (Proc. 168935/2018-0) for the grant support.

APPLICATION OF COLD PLASMA JETS WITH FUNNEL-SHAPED OUTPUT FOR THE TREATMENT OF POLYMERIC SAMPLES

B.H.S. Leal^{1*}; F.V.P. Kodaira¹; K. G. Kostov¹

Universidade Estadual Paulista (UNESP), Faculdade de Engenharia de Guaratinguetá (FEG), Guaratinguetá, SP, Brazil

1. Introduction

The treatment of materials by plasma jets at atmospheric pressure (JPPA) has been gaining popularity as an alternative to conventional surface treatments, because besides promoting specific and unique changes, the process does not generate waste, thus being considered a "green" process. Plasma is composed of reactive and energetic species capable of modifying the surface structure of a material but keeping its volume intact. The plasma treatment is able to change the molecular structure and even incorporate new functional groups on the polymer surface, these changes promote changes in properties such as wettability, adhesion, biocompatibility, among others [1]. A common characteristic among JPPAs is the small treatment area, limited by the size of the generated plume. For some processes this characteristic of the jets is a quality, but for other applications it is a limitation. In this work we use a jet with conical exit in order to increase the area treated by the plasma [2].

2. Experimental

To perform the treatments, a glass funnel was used with a pointed metal electrode inserted inside and a grounded circular electrode covered with glass that is also used as sample holder and is positioned under the jet. This reactor generates a filamentary discharge in the working gas (Ar). The source used to power the system was a MINIPULS-6 AC voltage generator. An oscilloscope was used to perform the electrical characterization of the device. The treatments occurred on 1 mm thick, 50 mm long and 20 mm wide polymeric samples of high-density polyethylene (HDPE) and polypropylene (PP). Both are commercial polymers highly used in the packaging and storage industries. The samples were treated for the times of 40, 60, 120, 180 and 300 seconds. Once treated the samples were characterized as to their molecular structure by Fourier transform infrared spectroscopy (FTIR).

3. Results and Discussions

The measurements of the surface contact angle indicated a homogeneous treatment along the treated surface at all treatment times analyzed. It was also possible to obtain the treatment efficiency as a function of exposure time. The hydrophobic recoveries of the surfaces were recorded over a period of 168 h after the treatments. The infrared spectrum did not indicate in any of the treatments substantial alteration of the chemical bonds, so that no new absorption peaks or relevant changes in the ratio between the peaks in the same spectrum were detected.

4. References

- [1] R. Y. Santos, A. L. R.; Kostov, K. G.; Honda, "Estudo de polímeros comerciais tratados a plasma em pressão atmosférica," Aleph, p. 82 f.: il., 2010.
- [2] T. S. M. Mui, R. P. Mota, A. Quade, L. R. de O. Hein, and K. G. Kostov, "Uniform surface modification of polyethylene terephthalate (PET) by atmospheric pressure plasma jet with a horn-like nozzle," *Surf. Coatings Technol.*, vol. 352, no. May, pp. 338–347, 2018, doi: 10.1016/j.surfcoat.2018.08.014.

Acknowledgements

The authors would like to acknowledge CAPES for the financial support in Brazil.

DUPLEX TREATMENT OF AISI D2 TOOL STEEL: NITRETATION BY PLASMA AND REACTIVE DEPOSITION OF TIN AND TiAlN FILMS VIA MAGNETRON SPUTTERING

Marcio Luiz Moretti¹, and Abel André Cândido Recco^{2*}^{1,2} *Laboratory of Plasmas, Films and Surfaces - Santa Catarina State University, Joinville, SC, Brazil***1. Introduction**

In this work, thin films of TiN and TiAlN were obtained via reactive sputter cathodic deposition on AISI D2 plasma nitrided tool steel and non-nitrided steel. The Nitriding and depositions were realized in two different reactors, characterizing the duplex treatment. The present work proposes to investigate the influence of the plasma nitrided layer on the mechanical properties of coatings and on the quality of adhesion of films to the substrates. The hardness (H) and the modulus of elasticity (E) of the films were determined through instrumented indentation tests (EII), and the adhesion of the film to the substrate was qualitatively evaluated through the Rockwell C test - DIN-CEN/TS 1071-8Standard. There is no significant variation in H and E of films obtained by duplex treatment and reactive deposition. However, the coatings obtained by duplex treatment were classified with the best indexes in the quality of adhesion of the films to the substrates. The improvement in adhesion can be attributed to the preliminary treatment of nitriding and the compressive loads acting on the nitrided surface [1,2].

2. Experimental

The Treatment via plasma nitriding was realized in a working atmosphere containing 5.0% nitrogen, 73.5% hydrogen and 21.5% argon by volume for 120.0 \pm 0.5 minutes, with experimental conditions that inhibit the formation of the layer of compounds and promote an increase in the diffusion zone. The Reactive cathodic sputtering depositions were performed using a triode magnetron sputtering system and a direct current voltage source. In both depositions, was used the argon inert gas flow, deposition temperature, current density and polarization voltage of the substrate constant and equal to 2.8 ± 0.1 sccm, $300 \pm 5^\circ$ C, 2.00 A and -50 VDC. The nitrogen flux used in the deposition of TiN and TiAlN films was 4.6 ± 0.1 sccm and 6.8 ± 0.3 sccm, respectively.

3. Results and Discussions

Tables 1 and 2 present the values of hardness (H) and module of elasticity (E) of TiN and TiAlN thin films, and the quality indices of adhesion of the films to substrates. There were no significant variations in the values of hardness and module of elasticity between coatings obtained via reactive sputter cathodic deposition and by duplex treatment. However, both films obtained by the duplex treatment of plasma nitriding followed by reactive deposition showed the best quality indices of adhesion of the coatings to the substrates. The adhesion of the films to the substrates may have been influenced by the compressive loads acting on the nitrided layer. Compressive loads provide mechanical support to the substrate surface, promoting an increase in loading and unloading load capacity [3].

Tab.1.Hardness (H)and module of elasticity(E) of TiN and TiAlN thinfilms via EII

Coating	Treatment	H (GPa)	E (GPa)
TiN	Duplex	25 ± 1	331 ± 25
TiN	Deposition	24 ± 2	296 ± 21
TiAlN	Duplex	23 ± 2	320 ± 30
TiAlN	Deposition	21 ± 4	317 ± 28

Tab.2. Adhesion Index of the film to the substrate via Rockwell C – DIN-CEN/TS 1071-8 Standard

Coating	Treatment	Adhesion Index
TiN	Duplex	HF-1
TiN	Deposition	HF-2
TiAlN	Duplex	HF-4
TiAlN	Deposition	HF-6

4. References

- [1] ROUSSEAU, A.F., et al. Microstructural and tribological characterization of a nitriding/TiAlN PVD coating duplex treatment applied to M2 High Speed Steel tools. *Surface & Coatings Technology*, 272, 403-408, (2015).
- [2] ABREU, L. H. P., et al. Plasma nitriding of AISI M2 steel: performance evaluation in forming tools. *Surface Engineering*, 508-551, (2020).
- [3] TORRES, R. D., et al. Influence of the nitriding and TiAlN/TiN coating thickness on the sliding wear behavior of duplex treated AISI H13 steel. *Surface & Coatings Technology*, 205, 1381-1385, (2010).

EFFECT OF HEAT TREATMENTS ON THE MICROSTRUCTURE OF Ti-(10 - x)Al-xV (x = 0, 2, AND 4 wt%) ALLOYS

Pinto B. O.^{1*}, Torrento, J. E.¹, Grandini, C. R.¹, Correa, D. R. N².¹UNESP – Univ. Estadual Paulista, Laboratory of Anelasticity and Biomaterials, Bauru (SP), Brazil²IFSP – Campus Sorocaba, Advanced Metallic Materials Group, Sorocaba (SP), Brazil

1. Introduction

For the manufacture of biomaterials, metallic materials are the most popular, due to their beneficial mechanical and corrosion performance. The Ti-6Al-4V alloy (ASTM F136) is the most worldwide used form of titanium, being employed in the aerospace, automobile, and biomedical industries [1]. The microstructure and properties of titanium alloys are directly dependent of the processing and heat treatment history [2]. This study aimed to produce and characterize the phase composition of novel Ti-Al-V based alloys, in order to assess their potential use as healthcare appliances.

2. Experimental

Commercially pure metals were cut and separated in the correspondent mass ratio of Ti-(10-x)Al-xV (x = 0, 2, and 4 wt%). The materials were then previous etched in a solution of nitric acid (HNO₃) and hydrofluoric acid (HF) in a 4:1 ratio proportion, and ultrasonic cleaned for 15 minutes. The samples were produced in an arc-melting furnace with argon inert gas atmosphere. A homogenization heat treatment was conducted in a quartz tube, with vacuum in the order 10⁻⁷ Torr, heating rate of 10 °C per min, with temperature plateau of 1000 °C, over a period of 24 hours, and then furnace cooled. After that, the samples was subjected to hot-rolling, with heating at 1000 °C, reduced thickness to approximately 5 mm, and air cooled. Finally, the samples were submitted to a solution treatment at 900 °C for 2 hours, with water cooling. The microstructure and phase composition of the samples were evaluated by XRD measurements, and optical and SEM imaging. Chemical composition was evaluated by and EDS detector coupled in the SEM equipment.

3. Results and Discussions

The samples exhibited a dual $\alpha + \beta$ phase composition (Fig 1), being the microstructure composed by lamellar structures disposed along the granular matrix. Some minor fraction of metastable martensite α' precipitates were also formed. The dual phase composition formed due to the combination between the α - stabilizer action of aluminum (Al) and the β -stabilizer action of vanadium (V). The results were corroborated with the theoretical predictions, having great potential for use as biomaterials.

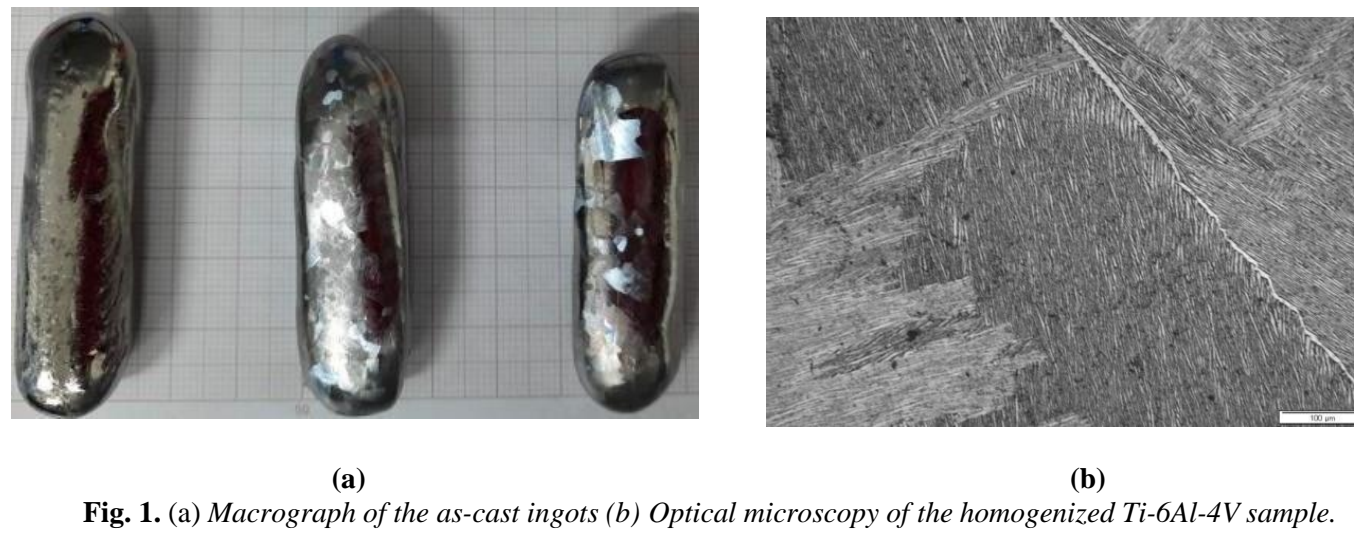


Fig. 1. (a) Macrograph of the as-cast ingots (b) Optical microscopy of the homogenized Ti-6Al-4V sample.

4. References

- [1] D. R. N. Correa et al., Journal of Materials and Technology, 4(2), 180-185 (2015).
- [2] J. E. Torrento et al., Materials Letters, 269, 1276621, (2020).

Acknowledgments

The authors thank the Brazilian funding agencies FAPESP and CNPq for the financial support.

STRUCTURAL PROPERTIES OF Zn-Nb CO-DOPED TiO₂ FILMS OBTAINED IN HiPIMS

Joel Stryhalski^{2*}, Alexandre Laur¹, Julio Cesar Sagás³, Luis Cesar Fontana³, Marcos Massi¹

¹*Mackenzie Presbyterian University, Engineering School, São Paulo, Brazil*

²*Federal Institute of Santa Catarina, Department of Physics, Jaraguá do Sul, Brazil*

³*Santa Catarina State University, Laboratory of Plasmas, Films and Surfaces, Joinville, Brazil*

1. Introduction

Titanium dioxide (TiO₂) has been extensively investigated in the last decades due to the interest of this material in different devices [1], [2] and many researches are focused on changing the TiO₂ properties using dopants. This strategy induces stress in lattice changing electronic distribution and mechanical properties. Due to electronic properties, and the industry interest Nb [3] and Zn [4] was investigated as TiO₂ dopant in High Power Impulse Magnetron Sputtering (HiPIMS) technique.

2. Experimental

In a magnetron sputtering system, using HiPIMS technique, three discharge pulse widths: 40 µs, 50 µs, and 70 µs (in 600 Hz and -660V) was performed to obtain Zn and Nb co-doped TiO₂ on borosilicate glass substrates (1×20×50 mm³). The required deposition conditions have been identified by systematically studying the phase formation and microstructure as a function of pulse width and target mode operation. A substrate bias pulse of -30 V was synchronized with magnetron but with a fixed width of 100 µs pulse and substrate temperature was fixed in 200 °C. Target-substrate distance was 6.0 cm and Ar and O₂ flow rates were 86.0 and 2.5 sccm, respectively, to work in 5.0 mTorr (0.66 Pa), the discharge power density was 6.41 W/cm² for 1 hour.

3. Results and Discussions

Increasing the pulse width, the deposition changes from compound mode to metallic mode. XRD results show only anatase phase of TiO₂, as can be seen in Figure 1, where one can observe that larger pulses results in lower crystallinity peak. No zinc nor niobium oxides peaks were observed, which indicates that both zinc and niobium oxides, if formed, are amorphous or substituted Ti atoms in TiO₂ structure. In XPS peak fit analysis, Figure 2, it was observed that "as-deposited" ZnNb:TiO₂ films have an increase in substoichiometric Ti³⁺ phase in larger pulse, confirming the oxygen deficiency during deposition.

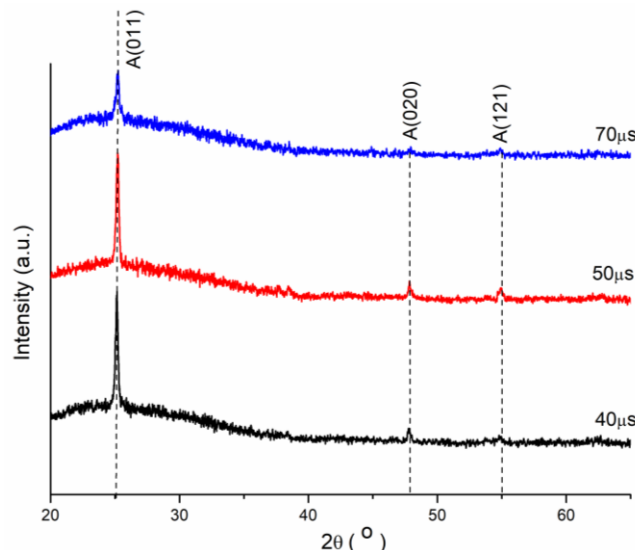


Fig. 1. DRX peaks, only anatase was observed, but larger pulses reduce peak intensity

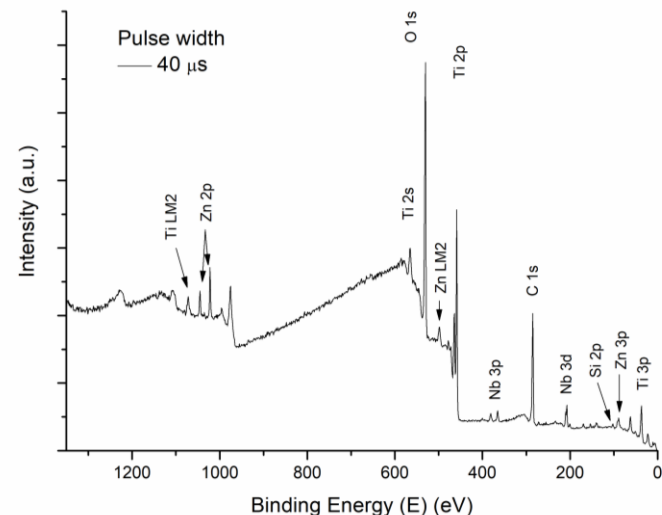


Fig. 2. XPS peak fit analysis of Ti 2p region in 70 µs

4. References

- [1] U. Diebold, Surface Science Reports, pp. 48-(2003) 53-229, 2003.
- [2] Y. Furubayashi, et al, Applied Physics Letters, pp. 252101-252101-3, 2005.
- [3] J. Wu, et al. Scientific Reports, p. 3(2012) 1283, 2012.
- [4] K. Ellmer, A. Klein and B. Rech, Springer, 2008.

Acknowledgments

Authors are grateful for CAPES-PrINT (grant # 88887.310339/2018-00, MackPesquisa, LabPlasma- UDESC, IFSC-Rau and Anton Paar Brasil.

Zn-Nb CO-DOPED TiO_2 FILMS GROWTH THROUGH HiPIMS: ELECTRICAL AND OPTICAL PROPERTIES

Joel Stryhalski^{2*}, Alexandre Laur¹, Julio Cesar Sagás³, Luis Cesar Fontana³, Marcos Massi¹

¹*Mackenzie Presbyterian University, Engineering School, São Paulo, Brazil*

²*Federal Institute of Santa Catarina, Department of Physics, Jaraguá do Sul, Brazil*

³*Santa Catarina State University, Laboratory of Plasmas, Films and Surfaces, Joinville, Brazil*

1. Introduction

Titanium dioxide (TiO_2) has been extensively investigated in the last decades due to the interest of this material in different devices [1], [2] and many researches are focused on changing the TiO_2 properties using dopants. This strategy induces stress in lattice changing electronic distribution. Due to electronic properties, and the industry interest Nb [3] and Zn [4] was investigated as TiO_2 dopant in High Power Impulse Magnetron Sputtering (HiPIMS) technique.

2. Experimental

A magnetron sputtering system using HiPIMS technique was used to obtain Zn and Nb co-doped TiO_2 on borosilicate glass substrates ($1 \times 20 \times 50 \text{ mm}^3$). The required deposition conditions have been identified by systematically studying the phase formation and microstructure as a function of pulse width and target mode operation. A substrate bias pulse of -30 V was synchronized with magnetron but with a fixed width of 100 μs pulse and substrate temperature was fixed in 200 °C. Target-substrate distance was 6.0 cm and Ar and O₂ flow rate was 86.0 and 2.5 sccm respectively to work in 5.0 mTorr (0.66 Pa), the discharge power density used was 6.41 W/cm² for 1 hour to obtain films.

3. Results and Discussions

Increasing the pulse width, the deposition changes from compound mode to metallic mode. The XRD results show only anatase TiO_2 but, despite this, electrical resistivity reaches $10^4 \Omega \cdot \text{cm}$ for larger pulses, keeping 90% of transmittance in visible region (Figure 1). An hypothesis for this phenomenon is that during the metallic deposition (in larger pulses) of Nb and Zn change electron distributions which change the Fermi level and electronic distributions. It can be seen in Tauc plots (Figure 2) a double gap: $\approx 3.5 \text{ eV}$ for all samples indicating an indirect anatase band gap E_{g1} , but a clear Burstein-Moss shift of 0.3 eV is observed. A second gap is caused by dopant effects and reach 2.80 eV.

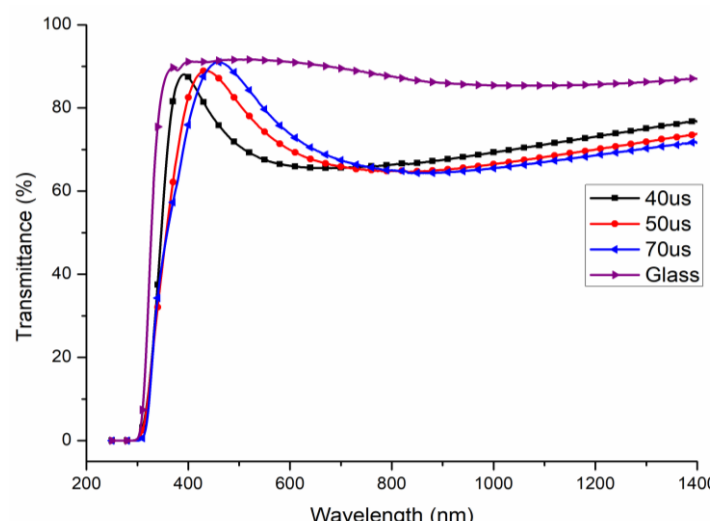


Fig. 1. Transmittance spectrum

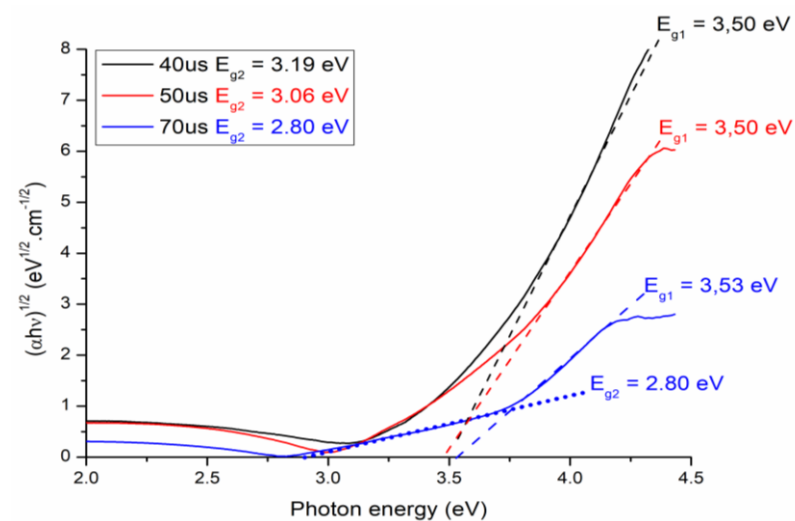


Fig. 2. Tauc plot for band gap energy

4. References

- [1] U. Diebold, Surface Science Reports, pp. 48-(2003) 53-229, 2003.
- [2] Y. Furubayashi, et al, Applied Physics Letters, pp. 252101-252101-3, 2005.
- [3] J. Wu, et al. Scientific Reports, p. 3(2012) 1283, 2012.
- [4] K. Ellmer, A. Klein and B. Rech, Springer, 2008.

Acknowledgments

Authors are grateful for CAPES-PrINT (grant # 88887.310339/2018-00, MackPesquisa, LabPlasma- UDESC, IFSC-Rau and Anton Paar Brasil.

EFFECTS OF AGING TREATMENTS IN A NOVEL Bio-HEA BASED ON TiZrNbTaMn FOR POTENTIAL USE AS ORTHOPEDICAL IMPLANTS

Jhuliene Elen Torrento^{1*}, Tiago Santos Pereira Sousa¹, Carlos Roberto Grandini¹, Diego Rafael Nespeque Correa^{1,2}

¹Univ. Estadual Paulista - Laboratório de Anelasticidade e Biomateriais, Bauru (SP), Brazil

²Instituto Federal de Educação, Ciência e Tecnologia de São Paulo, Sorocaba (SP), Brazil

1. Introduction

In the last years, high entropy alloys (HEAs) have been developed for many applications and recognized for their superior strength, ductility, and corrosion resistance, which has attracted attention by the biomedical industry. Thus, the current research effort is looking for the development of Bio-HEAs with properties compatible with the use as implantable materials [1]. This project aims to characterize a novel Bio-HEA based on TiZrNbTaMn subjected to aging treatments, for possible application as biomedical implants.

2. Experimental

In this study, TiNbZrTaMn and TiNbZrTaMo alloys were produced in non-equiautomic proportions, following some *ab initio* design predictions. The ingots were cast by argon arc-melting and subjected to a heat treatment for microstructural homogenization. Then, aging treatments were performed at 573 K, 673 K, and 773 K for 6 hours (Fig. 1). The samples were characterized by EDS, XRD, optical, scanning electron and transmission electron microscopy, elastic modulus, and Vickers microhardness measurements.

3. Results and Discussions

The chemical characterizations indicated a good quality of the samples produced (Fig. 2), and the structural characterization indicated the majority of BCC crystalline structure, as predicted by the *ab initio* design parameters, with the secondary phase precipitation with a hexagonal structure in the TiZrNbTaMo alloy. In the microstructural characterization, both alloys in the as-cast condition showed an irregular formation. After the heat treatments, it is possible to observe grain boundaries, characteristic of the BCC crystalline structure. For the TiZrNbTaMo alloy, in the boundary region, it is also noted some acicular structures indicated some microstructural modifications, which was confirmed by transmission electron microscopy. The studied samples showed a low elastic modulus (around 80 GPa). The TiZrNbTaMo alloy showed substantial variation in elastic modulus that may be related to the precipitation of secondary phases in the microstructure after heat treatments. Both bio-HEAs showed high Vickers microhardness to some commercial biomedical biomaterials (SS 316L, CP-Ti grade 2, and Ti-6Al-4V ELI). This study produced new Bio-HEAs, and the TiZrNbTaMn alloy showed the best potential for use in the orthopedical area, grouping low elastic modulus and high microhardness.

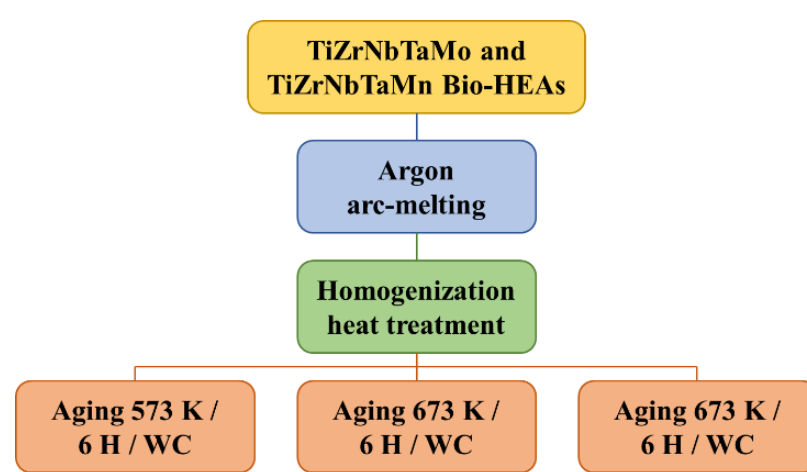


Fig. 1. Bio-HEAs processing diagram.



Fig. 2. Photograph of as-cast samples.

4. References

[1] T. NAGASE et al., Materials Science and Engineering: C **107**, 110322 (2020)

Acknowledgments

The authors thank CNPq and FAPESP (grant #2018/24931-7) for the financial support.

ISOTHERMAL DECOMPOSITION OF THE AISI 420 LOW-TEMPERATURE NITRIDED LAYER

Zanella, I. G^{1*}, F. I; Brunatto, S. F¹; Cardoso, R. P.²¹*Federal University of Paraná, Curitiba, Brazil*²*Federal University of Santa Catarina, Florianópolis, Brazil.***1. Introduction**

Plasma assisted thermochemical treatments are being increasingly applied in industry to treat different types of materials. These treatments provide changes in the material surface characteristics, generally improving corrosion resistance and wear resistance. For the AISI 420 martensitic stainless steel, studies carried out by [1] showed that the application of nitriding for as-quenched samples present the best results. For such case, the nitrided layer presents metastable phases. However, the thermal stability of the phases formed on the surface of the nitrided material was only carried out for austenitic stainless steels [2]. So, in this study the impact of isothermal treatments on the phases present on the low-temperature nitrided AISI 420 martensitic stainless steel was performed.

2. Experimental Apparatus

The apparatus used in this work is described in [3], however, an auxiliary heating system was added to allow heating independently from the plasma. The pulsed power supply applied to generate the plasma has a frequency of 4.2 kHz and the average power transferred to the plasma is controlled by adjusting the duty cycle (time on (t ON) of the pulse). Before nitriding, AISI 420 martensitic stainless steel samples were heated and kept at 1050°C for 1 hour and air cooled. Plasma nitriding was carried out at 350 °C and, 3 Torr for 12 h and the gas mixture was composed of 70% N₂ + 20% H₂ + 10% Ar. To evaluate the isothermal decomposition of the phases formed after nitriding, a 350 °C heat treatment was performed for nitrided samples for 1, 4 and 16 h, in an atmosphere composed of 80% of H₂ and 20% Ar, where only the auxiliary heating system is responsible for heating. The samples were characterized by X-ray diffraction (XRD), microhardness and scanning electron microscopy (SEM).

3. Results and Discussions

Figure 1 presents the XRD analysis, for annealed (α) and as-quenched (α') conditions. In addition, the 350°C nitrided and the isothermally treated samples are also shown. It can be observed that for times of 1, 4 and 16 h the peak at ~38°C shifts to the right. In contrast, the main peak at ~43°, after 1 hour at 350°C, begins to separate into two peaks (as shown in figure 1), as the treatment time increases, the intensity of the peaks increases. Indicating that there was a reorganization of nitrogen in the phases present on the surface of the material. In figure 2, the top hardness performed under the studied conditions are presented. It can be observed that the hardness for the nitrided sample and for the isothermally treated samples have very similar hardness.

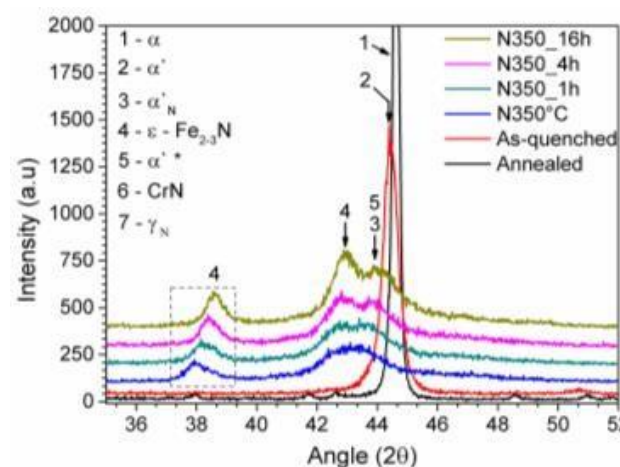


Fig. 1 - X-ray diffraction patterns for sample nitrided for 12 h and isothermically treated samples.

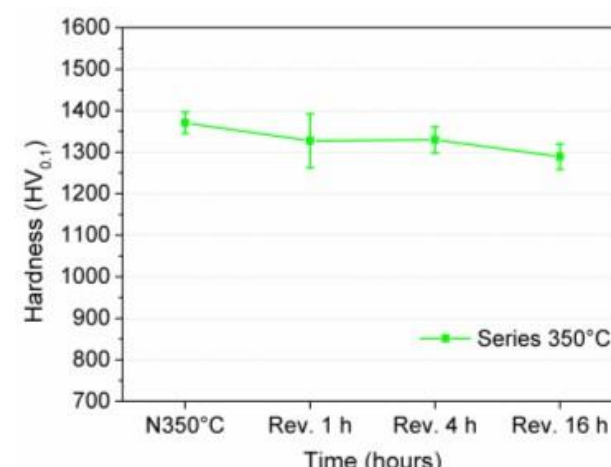


Fig. 2. Top hardness for samples nitrided for 12 h and for isothermically treated samples.

4. References

- [1] R.P. Cardoso, C.J. Scheuer, S.F. Brunatto, Stainless Steel: Low-Temperature Nitriding Kinetics, *Encycl. Iron, Steel, Their Alloy.* (2016) 3283–3293.
- [2] A.P. TSCHIPTSCHIN, A.S. NISHIKAWA, L.L. VARELA, C.E. PINEDO, Thermal stability of expanded austenite formed on a DC plasma nitrided 316L austenitic stainless steel, *Thin Solid Films.* 644 (2017) 156–165.
- [3] C.J. Scheuer, R.P. Cardoso, M. Mafra, S.F. Brunatto, AISI 420 martensitic stainless steel low-temperature plasma assisted carburizing kinetics, *Surf. Coatings Technol.* 214 (2013) 30–37.

Acknowledgments

Author would like to thank UFPR, PG-Mec, CAPES, CNPQ, CME/UFPR and LORXI.

ATOMIC FORCE MICROSCOPY ANALYSIS OF SODIUM ALENDRONATE PARTICLES COATED WITH PCL

Yasmin dos Anjos Garcia^{1*}, Talita Goulart da Silva¹, Cristiane Evelise Ribeiro da Silva², Roberta HelenaMendonça¹

¹PPGEO/IT - Chemical Engineering Department - Rural Federal University of Rio de Janeiro (UFRRJ)

² Materials and Products Test Division - National Institute of Technology (INT)

1. Introduction

The development of biomaterials applied for osteoporosis treatment can be a promising alternative. Bisphosphonate, such as sodium alendronate (ALD), has been used to treat osteoporosis. Although oral administration has been associated with side effects such as gastro-esophageal reflux. Moreover, there are some requirements to take the medicine, which also hinder the patient's compliance, for one breakfast and avoid the decubitus position after using the drug. Thus, the aim of this work was evaluate by atomic force microscopy a Polycaprolactone (PCL) and ALD-based powder as a potential input for manufacturing biomaterials by selective laser sintering (SLS), compression molding (CM), solvent casting (SC), among others [1].

2. Experimental

PCL was solubilized in acetone (20% w/v). Then, this solution was dripped on ALD trihydrate as described by Silva et al., 2021. The mixture of ALD and PCL was kept at room temperature for 24 hours to evaporate the solvent and obtain the coated powder. The samples were evaluated by AFM-JPK instruments, Nanowizard model in intermittent contact mode using silicon nitride needles (MikroMasch™ NSC16) and XRD using X-ray diffractometer (Rigaku, model Mini Flex II) operated with CuK α source ($\lambda = 1.5418 \text{ \AA}$) under the following conditions: scan speed of 2°/min and 2 θ scan range of 2-60° [1].

3. Results and Discussions

Figure 1 shows AFM images of particles coated with PCL. In topography images, Figure 1 (a) it is possible to note the presence of clusters, probably due the presence of PCL. It indicates that the dry process have to be improved, avoiding particle agglomeration. Phase images (Figure 1 (b)) suggests that the ALD particles were well coated by PCL. XRD of the coated particles showed that the ALD characteristics picks were preserved. In conclusion, the coating process was efficient, since, the properties of the ALD were preserved.

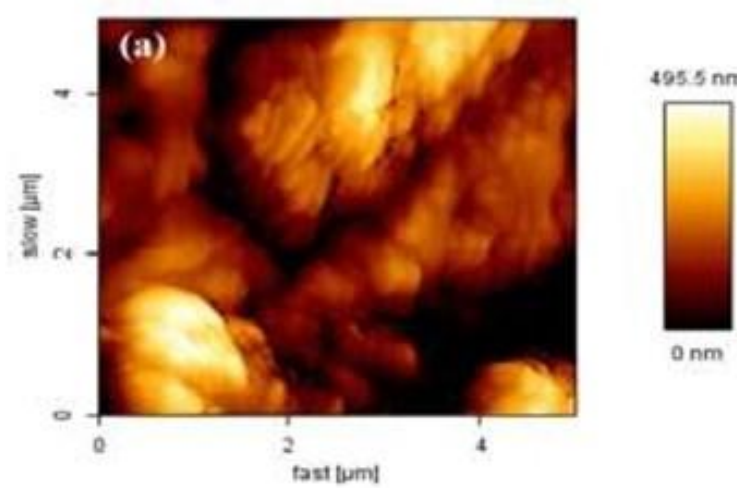


Fig.1. Atomic force microscopy images of ALD particles coated with PCL – (a).

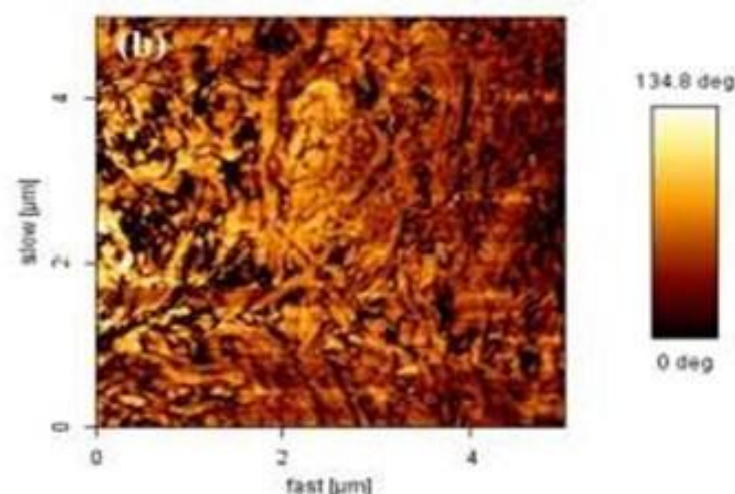


Fig.2. Atomic force microscopy images of ALD particles coated with PCL – (b).

4. References

[1] T. S. Goulart, D. P. Baptista, B. F. C. Patrício, M. A. Sarcinelli, H. V. R. Antunes, S. Letichevsky and R. H. Mendonça, "Polycaprolactone/alendronate systems intended for production of biomaterials". *Journal of Applied Polymer Science*, 138(28), 50678, (2021).

Acknowledgments

This study was financed in part by the Coordination of Improvement of Higher Education Personnel (CAPES).

The authors would like to acknowledge National Council for Scientific and Technological Development (CNPq), National System of Nanotechnology Laboratories (MCTI/SisNANO/INT-CENANO-CNPq Process number 442604/2019-0) and Rio's Innovation Hub for Health Nanosystems (NanoSaúde/FAPERJ) for the support. Finally, the authors would like to thank Perstorp Group and Farmácia Alternativa for donating the PCL and ALD supplies, respectively.

POLY(ACRYLIC ACID)/ CHITOSAN SPONGES LOADED WITH SUNFLOWER OIL – SWELLING PREDICTION APPLING THIN PLATE SPLINE INTERPOLATION

Yasmin dos Anjos Garcia^{1*}, Talita Goulart da Silva¹, Tiago dos Santos Mendonça², Cristiane Evelise Ribeiro da Silva³, Maurício de Jesus Monteiro³, Sonia Letichevsky⁴, Roberta Helena Mendonça¹

¹PPGEQ/IT - Chemical Engineering Department – Rural Federal University of Rio de Janeiro ²Theoretical Physics Department - Physics Institute A. D. Tavares, State University of Rio de Janeiro ³Materials and Products Test Division - National Institute of Technology - INT

⁴Chemical and Materials Engineering Department – PUC - Rio de Janeiro

1. Introduction

Sponges has been attracting interest for wound healing strategies due to their micro-porosity and capability to absorb a great amount of fluids. The use of chitosan (Chi) sponges has been considered in the treatment of wound dressing applications. Poly (acrylic acid) (PAA), obtained from acrylic acid, is a hydrophilic polymer and it has been used as a gelling agent in drugs and in the synthesis of hydrogels for controlled release of drugs. Mixtures of Chi and PAA have been used in the controlled release of drugs. Sunflower oil (SO) has been used in the treatment of wounds [1]. The aim of this work was to study the sunflower oil incorporation in Chi/PAA sponges (a material with potential use in wound healing not only to absorb the exudate, for example, but to provide the beneficial effects of sunflower oil in the treatment of wounds) applying thin plate interpolation method [2].

2. Experimental

Sponges of Chi/PAA (% Chi in the sample (S10 (10%) S25 (25 %), S50 (50 %) were produced by lyophilization process (LIOTOP, model L 101) and dipped on SO. The mass variation (MV) analysis was carried out to study the SO. Thus, the MV values were calculated by eq. (1), where M_t is sample's mass at time t and M_0 the mass of the dry samples. The resulting MV data were fitted in order to evaluate the effect of composition in SO absorption kinetics. The TPSIM application was performed using the software and a polynomial fit p55 was applied, simultaneously, to the experimental and the interpolated data, to obtain a 3D surface that correlates MV, composition and time as described in [2]

$$MV = \left(\frac{M_t - M_0}{M_0} \right) \times 100\% \quad (1)$$

3. Results and Discussions

The composition of the sample affects the mass variation. According to Fig. 1, absorption is faster in the early stages. After that, mass stabilization occurs for chitosan contents ranging from 100 to 60 % wt. For samples with a higher proportion of PAA, due to mechanical properties, excess swelling causes mass losses. In conclusion, Chi/PAA sponges are able to be loaded with SO.

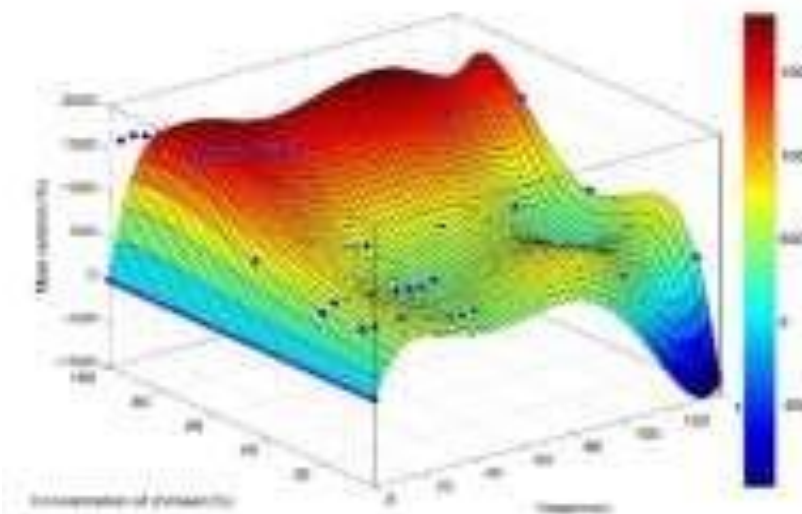


Fig. 1. Analysis of the mass variation (MV) – Chi/PAA sponges.

4. References

- [1] R. H. Mendonça, et.al., "Production Process of Fluid Absorption Drug Carrying. Brazil. (2019). Patent: Inovation Priviledge. Register No: BR1020190139021, Title: "Production Process of Fluid Absorption Drug Carrying", Registration institution: INPI – National Institute of Industrial Property. Deposit: 04/07/2019.
- [2] G. F. Silva, T. G. Silva, V. G. Gobbi, et.al., "Swelling degree prediction of polyhydroxybutyrate/chitosan matrices loaded with "Arnica-do-Brasil". Journal of Applied Polymer Science, 136(32), 47838, (2019).

Acknowledgments

Coordination of Improvement of Higher Education Personnel - Brazil (CAPES). The authors would also like to acknowledge National Council for Scientific and Technological Development (CNPQ) for their financial support as well as the Program PICV, PROIC and Nanosaúde Hub: E-26/010.000983/2019 – FAPERJ.

EVALUATION OF X-RAY DIFFRACTOMETRY IN ALUMINA GROWN ON AA2024-T3 ASSISTED BY PLASMA ELECTROLYTIC OXIDATIONLucas, R.R.^{1*}, Mota, R.P.¹, Abrahão, A.B.R.M.², Botelho, E.C.³¹Dep. of Physics, School of Engineering, São Paulo State University (UNESP), Brazil²Pindamonhangaba Faculty of Technology (FATEC-PINDA), Brazil³Dep. of Materials and Technology, School of Engineering, São Paulo State University (UNESP) Brazil**1. Introduction**

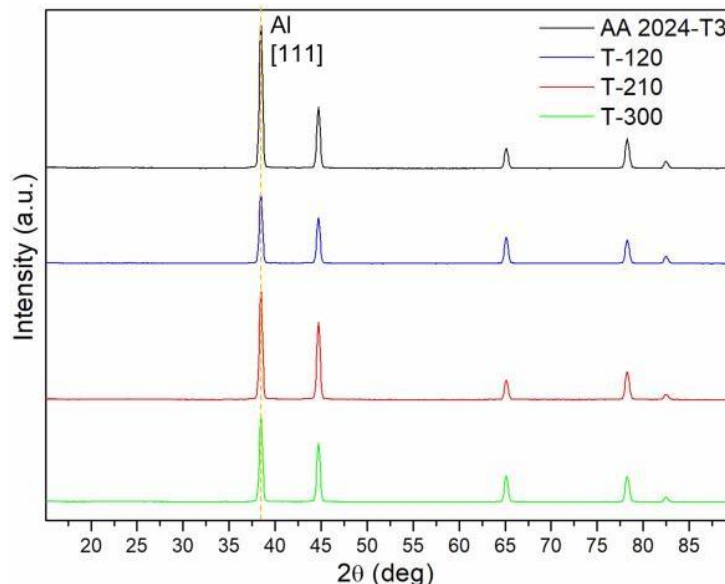
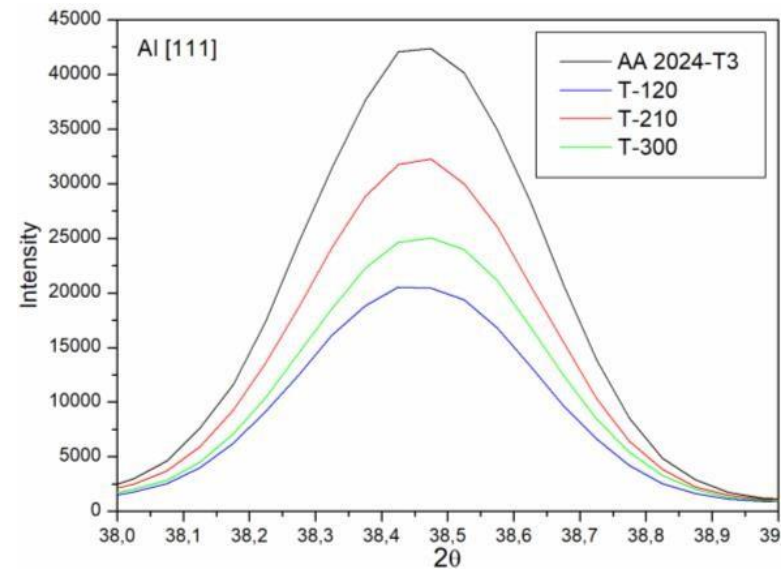
The Plasma electrolytic oxidation (PEO), unlike conventional anodizing, tends to generate oxide coatings on aluminum alloys with optimized physical and chemical properties. With the use of environmentally friendly electrolytes and significantly shorter process times [1, 2]. A typical characterization to be performed on these films is the x-ray diffractometry, to determine the crystalline phases present, films produced by PEO generally have different crystalline phases such as γ -Al₂O₃, α -Al₂O₃, etc., in contrast, films resulting from conventional anodizing have amorphous phases [1-3].

2. Experimental

Substrates with dimensions of 25 x 25 x 3 mm, properly cleaned with isopropyl alcohol in an ultrasonic vat, were subjected to electrolytic oxidation to plasma, with a potential of 380 volts with times of 120, 210 and 300 seconds. The experimental system to develop the treatment consists of a Variac 0 ~ 180 VAC, a bending circuit and voltage rectifier, a mechanical stirrer, a stainless steel becker (as a counter electrode) and multimeters (to follow the applied potential and current). The crystallinity of the coatings produced was characterized by X-ray diffraction, with equipment from Panalytical X'Pert PRO, with a $\text{K}\alpha\text{Cu}$ (40 kV, 40 mA) configuration, scanning at 2θ from 15° to 90° with a 0.05° step.

3. Results and Discussions

From the XRD analysis, it was possible to plot the spectra present in Figure 1. It is possible to observe spectra of the untreated alloy and the other treatments; peaks present at 38.5° / 44.7° / 65.1° / 78.2° / 82.5° are attributed to aluminum diffractions [2]. When performing an image magnification of 38.5° (Figure 2) in the grouped spectra, it is verified the difference in intensity of the aluminum diffraction of the untreated alloy with the other treated samples. The process performed with 120 seconds showed lower aluminum diffraction intensity than the other treated samples and the substrate, due to the formation of the alumina oxide coating [2].

**Figure 1.** XRD spectra of PEO.**Figure 2.** Peak of Aluminum [111].**4. References**

- [1] JADHAV, P.; BONGALE, A.; KUMAR, S. A review of process characteristics of plasma electrolytic oxidation of aluminium alloy. *Journal of Physics: Conference Series* 1854 (2021) 012030.
- [2] LUCAS, R.; GONÇALVES, L.; SANTOS, D. Morphological and chemical characterization of oxide films produced by plasma anodization of 5052 aluminum alloy in solution containing sodium silicate and sodium phosphate. *RBAV* 39 (2020) 33-41.
- [3] MELO, J. et al. Obtenção e sinterização de filmes de alumina porosa através da anodização de folhas de alumínio. *51º Congresso Brasileiro de Cerâmica* (2007), Bahia.

ON THE PHYSICAL AND ELECTROCHEMICAL PROPERTIES OF MLG-BASED ELECTRODE SURFACES MODIFIED BY MICROWAVE-ASSISTED REACTIVE PLASMA.

Gabriel de Moraes Moura¹, Camila Cristina da Silva¹, Emiliane Andrade Araújo Naves¹, Jeferson Aparecido Moreto¹, Deusmaque Carneiro Ferreira¹, Paulo Roberto de Oliveira¹, Cristiane Kalinke², Jair Scarmínio³, Abner de Siervo⁴, Thiago Henrique R. da Cunha⁵, Rogério Valentim Gelamo^{1*}

¹Institute of Technological and Exact Sciences, Federal University of Triângulo Mineiro (UFTM); ²Institute of Chemistry, University of Campinas (Unicamp);

³Physics Department, State University of Londrina (UEL); ⁴Gleb Wataghin Institute of Physics (IFGW), University of Campinas (Unicamp); ⁵Center of Technology in Nanomaterials and Graphene (CTNano), Federal University of Minas Gerais (UFMG).

1. Introduction

Recently, our research group demonstrated the advantages of using flexible multilayer graphene paper electrodes [1]. In addition, the reactive plasma technique is often employed to activate the surface of materials both chemically and physically. Plasma intensity, partial pressure of oxygen and reaction time can affect the electrode properties. The surface morphology, the generation of C-C bond defects, surface chemical composition, interfacial free energy, and electrochemical properties may be analyzed for the MLG electrodes as a function of the plasma treatment parameters. The results should indicate that plasma treatment variable adjustments can be used to modulate specific surface properties and with potential applicability in electrochemical sensors and supercapacitors.

2. Experimental

The MLG electrode surfaces modified by the reactive plasma treatments were characterized by five specific physical and electrochemical properties. Plasma treatments were carried out under three different plasma conditions: oxygen gas pressure into the reactor, plasma intensity, and reaction time. The goal was to develop a quick strategy to investigate the influence of plasma treatment parameters on the physical and electrochemical properties of the MLG electrodes.

3. Results and Discussions

The treatment promoting changes in the surface morphology of the MLG electrodes, generating surface C-bond defects and altering both the electrode surface free energy and the electrochemical properties of these electrodes. As cathode in an electrochemical cell, improved electron transfer capacity was observed for those MLG electrodes that underwent the longest plasma treatment time (180 s), reducing 85% of the charge transfer resistance when compared to the pristine MLG electrode. Moreover, these electrodes showed a large electroactive surface area promoted by a high concentration of oxidized sites. High capacitances were obtained for MLG electrodes treated in the intense plasma region for the longest time experimented (180 s). They were in fact 1450% higher than the non-treated MLG electrode, which suggests potential employment in electrochemical capacitor devices.

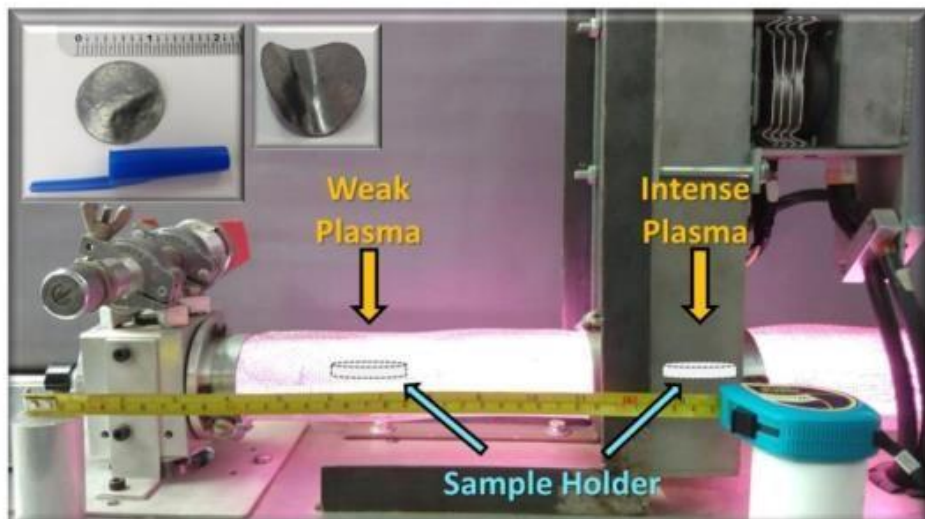


Fig. 1. Setup of reactive plasma used for MLG treatments.

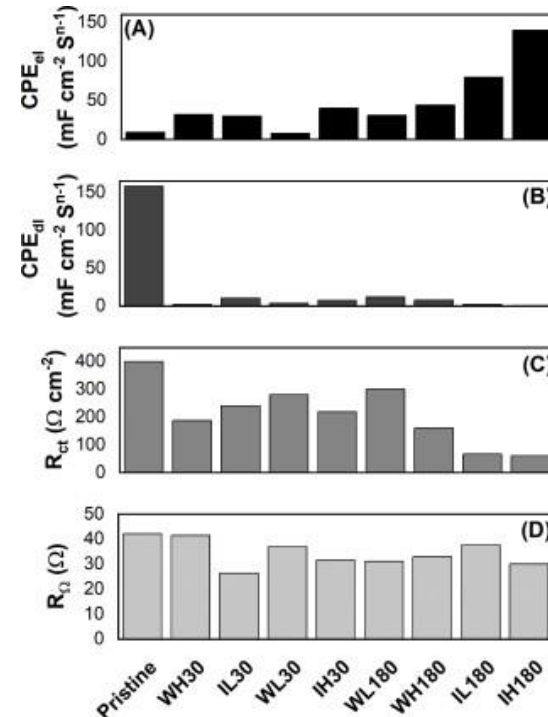


Fig. 2 (A, D). Average values of the electrochemical impedance spectroscopy (EIS) parameters of the MLG electrodes.

4. References

[1] G. de Souza Augusto, *et al.*, *Electrochim. Acta*. 285 (2018) 241–253.

Acknowledgments

CNPq, (FAPEMIG-Brazil) (Grant APQ-01359-21), Capes and UFTM.

NEW APPROACHES TO PREVENT THE CORROSION PROCESS OF THE 2198-T851 ALUMINIUM ALLOY CONTAINING NIOBIUM OXIDE-BASED COATING

Leonardo dos Reis Freitas¹, Rogério V. Gelamo², Cláudia Eliana Bruno Marino³, João Pedro Lopes do Nascimento¹, Jeferson Aparecido Moreto^{1*}

¹Institute of Exact Sciences, Naturals and Education, Federal University of Triângulo Mineiro (UFTM). Avenida Doutor Randolfo Borges Júnior, Univerdecidade, 38064200 - Uberaba, Minas Gerais, Brazil.

²Institute of Technological and Exact Sciences, Federal University of Triângulo Mineiro (UFTM). Avenida Doutor Randolfo Borges Júnior, Univerdecidade, 38064200 - Uberaba, Minas Gerais, Brazil.

³Mechanical Engineering Department, Federal University of Paraná, 81531-990, Curitiba, Paraná, Brazil.

1. Introduction

Recently, our research group demonstrated the advantages of use of niobium oxide thin films on the surface of different materials obtained through reactive sputtering technique [1, 2]. Considering the attractive properties of the niobium oxide coating, this work aims to propose an applied and innovative research for the functionalization of the 2198-T851 (Al-Cu-Li) aluminium alloy used as aircraft material. Here, new insights regarding the effect of long-term immersion corrosion on the 2198-T851 aluminium alloy containing niobium oxide thin film was verified by using global electrochemical techniques in 0.6 mol L⁻¹ NaCl solution.

2. Experimental or Theory

The structural and morphological properties of the niobium oxide thin films were characterized by using SEM/EDX, AFM, FTIR and Raman spectroscopy. Global electrochemical tests (OCP, PPc, CV, and EIS) were performed in 0.6 mol L⁻¹ NaCl solution.

3. Results and Discussions

The results demonstrated that the reactive sputtering technique was advantageous for producing thin films on the 2198-T851 aluminium surface. Raman spectroscopy results revealed a band near 650 cm⁻¹ related to Nb-O single bonds, whilst the band centred at 868 cm⁻¹ may be attributed to Nb=O double bonds. Potentiodynamic polarization curves indicated that the niobium oxide acts as a protective barrier, since a difference of about 210 mV was observed between E_{pitting} and E_{corr} . The 2198-T851 aluminium alloy functionalized with niobium oxide thin film presented a superior behaviour compared to the bare material up to 7 days of immersion in an aggressive environment (see Fig. 1 (a,b)).

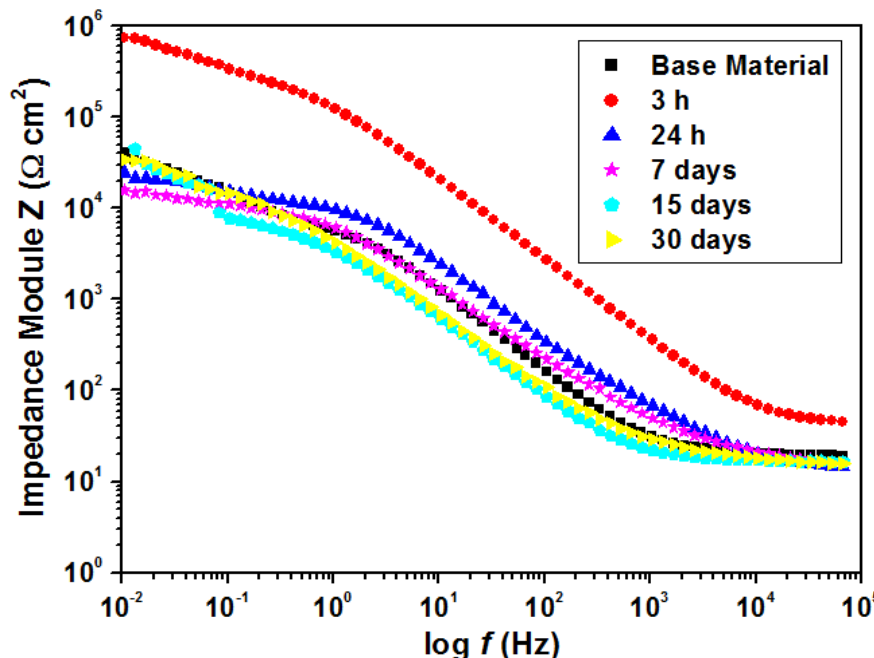


Fig. 1 (a). Bode plots of Electrochemical Impedance Spectroscopy spectra of uncoated and coated 2198T851 aluminium alloy exposed to 0.6 mol L⁻¹ NaCl solution. Impedance Module vs. Frequency.

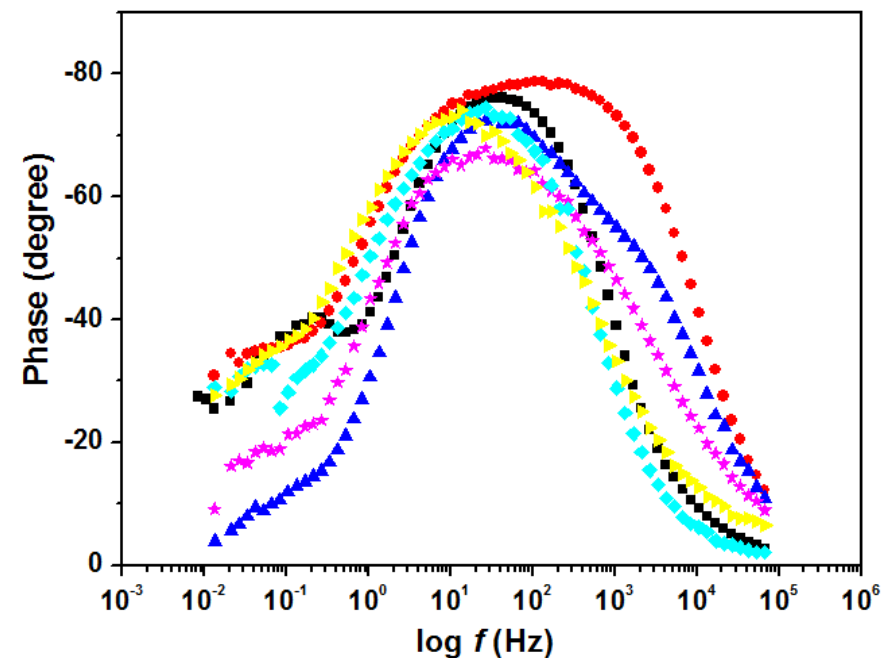


Fig. 1 (b). Bode plots of Electrochemical Impedance Spectroscopy spectra of uncoated and coated 2198T851 aluminium alloy exposed to 0.6 mol L⁻¹ NaCl solution. Phase vs. Frequency.

4. References

- [1] Bino et al, Applied Surface Science, **557**, 149739 (2021).
- [2] Moreto et al, J Mater Sci: Mater Med **32**, 25 (2021)

Acknowledgments

CNPq (Grant 303659/2019-0) as well as Research Supporting Foundation of Minas Gerais State (FAPEMIG-Brazil) (Grant APQ-02276-18).

OPTICAL CHARACTERIZATION OF DBD PLASMA JETS PRODUCED INSIDE A TUBE USING DIFFERENT SETTINGS

Ana Carla de Paula Leite Almeida ^{1*}, Ananias Alves Barbosa ¹, Fellype do Nascimento ¹, Konstantin Georgiev Kostov ¹¹Faculty of Engineering, UNESP, Guaratinguetá, SP, Brazil**1. Introduction**

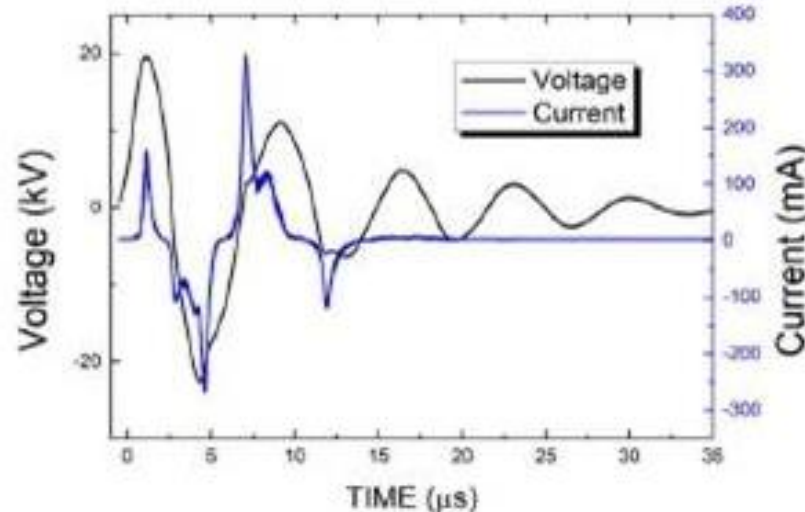
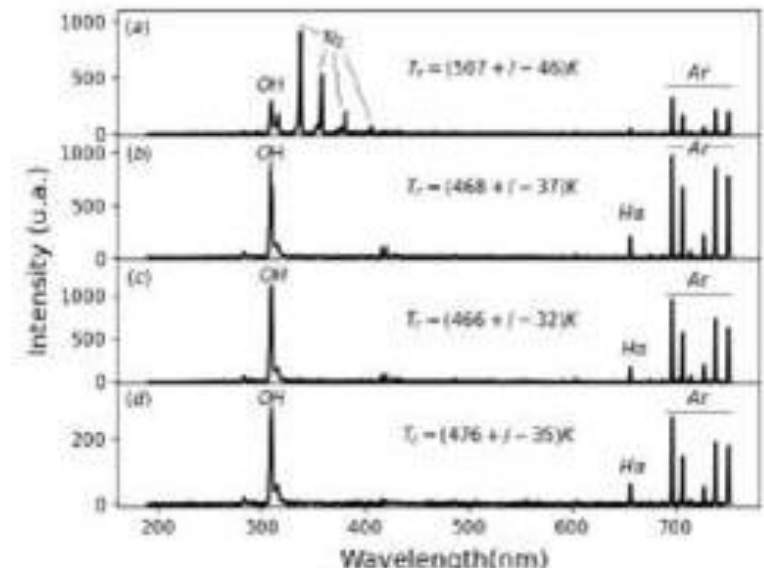
Recent studies have shown that the reactive oxygen and nitrogen species (RONS) produced within atmospheric pressure plasma jets (APPJs) play an important role for the successful application of this kind of plasmas in several areas. This motivates the development of new applications of APP in medical procedures such as wound healing and treatment of cancerous tissues as well as the investigation of RONS present in the plasma jet and some of their parameters like the rotational temperature (T_r), and other plasma parameters like its electrical characteristics and how they influence the plasma treatment. In this work, we present the T_r results obtained from OH molecules and the electrical characterization of plasma jets applied inside of a silicon tube with different settings.

2. Experimental

The plasma jets studied in this work were produced inside a silicon tube and at the end of a long and flexible plastic tube, with the last one connected to a dielectric barrier discharge (DBD) reactor. The DBD reactor is a cylindrical pin-electrode type, to which high voltage pulses, whose waveform is shown in Fig. 1, were applied. We employed different configurations for the long tube by changing the number of holes from which the plasma jets were extracted to be applied into the silicon tube. Argon was used as the working gas, and a flow rate of 2.0 l/min was employed in all the experiments. Spectroscopic measurements were performed using a spectrometer from Avantes (model AvaSpec-ULS-RS-TEC), with spectral resolution of (0.784) nm. Then, T_r values were obtained by comparing the measured and simulated spectra. For this purpose, it was used spectroscopic emissions from the OH molecular bands in the wavelength range from 305 to 313 nm.

3. Results and Discussions

Figure 2 shows the spectra obtained for the different configurations we have studied, together with the respective T_r value obtained in each case. We concluded that once a plasma jet interacts directly with the surface of the silicon tube, the intensity of the emissions from the OH molecules follows the same trend of the Argon ones. Although the production of OH and H α in the plasma jet changes depending on the number of holes from which the jets are extracted, the T_r values do not change significantly, keeping around 479 K for all configurations.

**Fig. 1.** Measured voltage and current waveforms for working gas Ar.**Fig. 2.** Spectrum obtained from the plasma jet at the end of: (a) the 2-hole tube, (b) the 3-hole tube, (c) the 4-hole tube and (d) the 6-hole one.**4. References**

[1] X. Lu, G. V. Naidis, M. Laroussi et al, Phys. Rep., 630, 630, 1–84, (2016)

Acknowledgments

This work was supported by CAPES and FAPESP.

INFLUENCE OF AGGREGATES OF DIMENSION STONE WASTE IN THE PROPERTIES OF CONCRETE FOR INTERLOCKING PAVERS

Fernanda Souza Oliveira¹, Simone Pereira Taguchi Borges¹

¹Universidade Federal Rural do Rio de Janeiro, Seropédica, Rio de Janeiro, Brazil

1. Introduction

Dimension stones are worldwide used as building and finishing material, and the waste produced in the process causes serious environmental problems [1]. The objective of this work is to use dimension stone waste to produce hexagonal interlocking pavements, with technological properties compatible with the standards [2], encouraging the development of ecologically sustainable products.

2. Experimental

This study aimed to evaluate the properties of hexagonal pavers using marble and granite waste as coarse aggregate. The concrete composition was calculated considering the mixture of Portland cement CII, fine aggregate (sand), coarse aggregate (dimension stone waste with size equivalent to Gravel 1), and water, in the respective proportion, 1:1.2:3. The amount of water used was calculated by the water/cement ratio obtained by Abrams curves resulting in 0.4. Cylindrical PVC molds with Ø50x100 mm [3] greased with Vedacit's Desmol CD. The concrete was agitated for 30 seconds to eliminate bubbles and distribute the mass into the mold until complete filled. Three specimens of each composition (crushed stone, granite, and marble) were prepared, and water absorption test (WA) was performed. The WA average value must be less than 6%, according to the standard [3]. The stresses were simulated using Autodesk Inventor software using the hexagonal pavers as model.

3. Results and Discussions

The crushed stone (B) models showed an average water absorption of 3.28%; those with marble (M) waste 3.06% and granite waste (G) presents 3.70%, presents values below the average of standard limit [2], as shown in Fig. 1. The stress analysis for hexagonal paver (Fig.2) shows the first principal stress value of 73.74 MPa, while the simulated displacement was 0.12 mm, and these values corresponding to the standard [3]. These results show it can be expected that the interlocked pavers with dimension stone waste has an attractiveness to be used commercially, due the price calculated around R\$ 20.00 per m², which represents approximately 28% less than the market value. Thus, the use of waste in the hexagonal pavers reduces the raw material used in the process, mitigating the environmental impacts generated by the mining companies, and this adds added value to the product. This eco-friendly product has potential to be a viable alternative for the application as paver for light traffic.

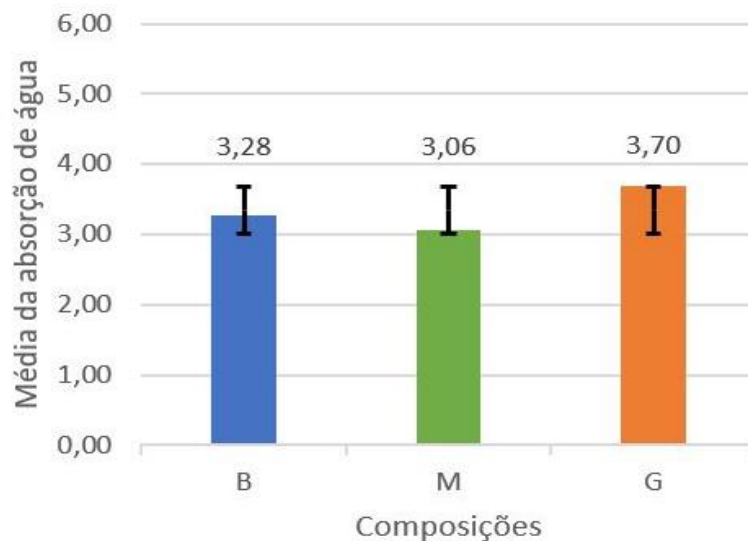


Fig. 1. Average water absorption of the concrete samples

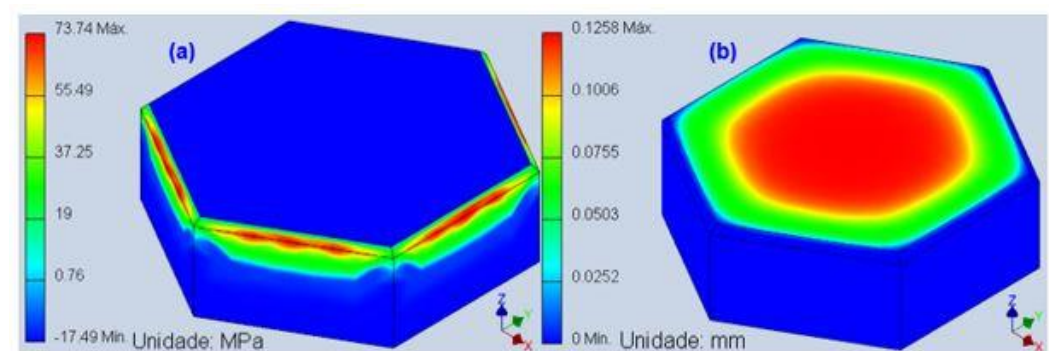


Fig. 2. Simulation of first principal stress (a) and strain (b) in hexagonal pavers

4. References

- [1] Neves, M.A., Taguchi, S.P., da Silva, D.R., Vieira, F.T. Geol. USP, Sér. cient., São Paulo, v. 19, n. 1, p. 33-42, 2019.
- [2] ABNT – Associação Brasileira de Normas Técnicas. NBR 9781 – Peças de concreto para pavimentação – Especificação e métodos de ensaio. RJ, Fev. 2013.
- [3] _____. NBR 5739 - Concreto - Ensaio de compressão de corpos de prova cilíndricos. Rio de Janeiro. 2018.

Acknowledgments

Our special thanks to UFRRJ and CNPq for the scholarships.

IMPROVING THE LOCALISED CORROSION RESISTANCE OF THE Ti-6Al-4V ALLOY THROUGH NIOBIUM OXIDE COATINGS

João Pedro Lopes do Nascimento^{1*}, Brunela Pereira da Silva², Idalina Vieira Aoki², Jair Scarminio³, Rogério Valentim Gelamo³, Jeferson Aparecido Moreto¹.¹*Institute of Exact Sciences, Naturals and Education, Federal University of Triângulo Mineiro (UFTM)*²*Polytechnic School, Department of Chemical Engineering, University of São Paulo (USP)*³*Center of Exact Sciences, Physics Department, State University of Londrina (UEL)*⁴*Institute of Technological and Exact Sciences, Federal University of Triângulo Mineiro (UFTM)***1. Introduction**

When Ti-6Al-4V alloy is subjected to presence of F^- aggressive ions, the TiO_2 thin film spontaneously produced on the alloy surface is broken, leading the material to a localised corrosion process. Recently, our research team verified a powerful effect of the niobium oxide coating as surface corrosion protection of the titanium and aluminium alloy [1, 2]. In the present study, we assessed the localised corrosion process of the coated and uncoated Ti-6Al-4V alloy by using Scanning Vibrating Electrode Technique (SVET) in 0.01 mol L⁻¹ NaF solution.

2. Experimental

The niobium oxide thin films were deposited on the Ti-6Al-4V alloy surface by using reactive sputtering technique. The thin films were morphologically and structurally characterized by using optical microscopy (OM), SEM/EDX, AFM, FTIR, XPS and XRD. The SVET measurements were performed up to 15 h of immersion in 0.01 mol L⁻¹ NaF solution, pH 2.0, at room temperature. The morphology of the coated and uncoated surfaces were assessed by OM before and after the SVET tests.

3. Results and Discussions

Our results indicated the reactive sputtering technique was suitable to produce polycrystalline niobium oxide coatings on the Ti-6Al-4V alloy, with a thickness about 300-450 nm. It was possible to verify the coated Ti-6Al-4V alloy displayed lower values of ionic current densities in SVET tests even in the presence of F^- aggressive ions when compared to the bare material, demonstrating the thin film acts as a protective barrier layer. The SVET maps obtained by the beginning of exposure and after 15 h of immersion in NaF aggressive medium, as well as the optical images of the respective surfaces by the end of exposure are depicted in **Fig. 1 (a,b)** and **Fig. 2 (a,b)**, respectively.

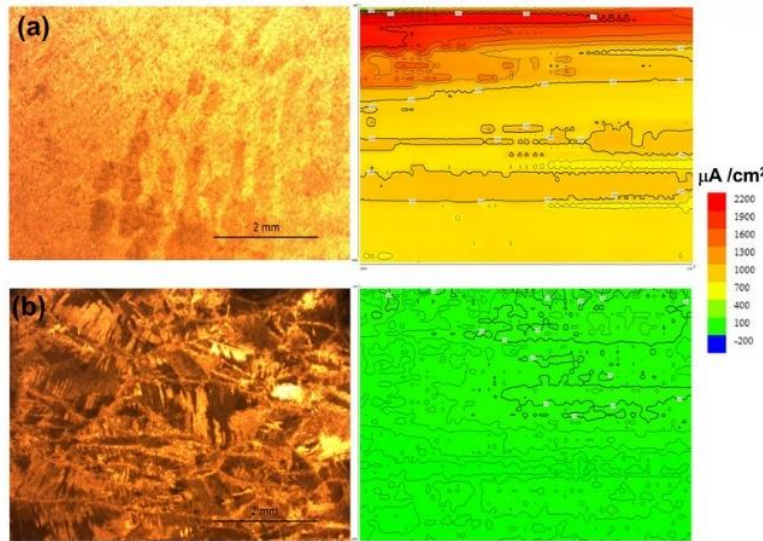


Fig. 1. Current density distributions of uncoated Ti-6Al-4V alloy after (a) 1 h, (b) 15 h and OM images at each immersion time in the presence of F^- aggressive ions.

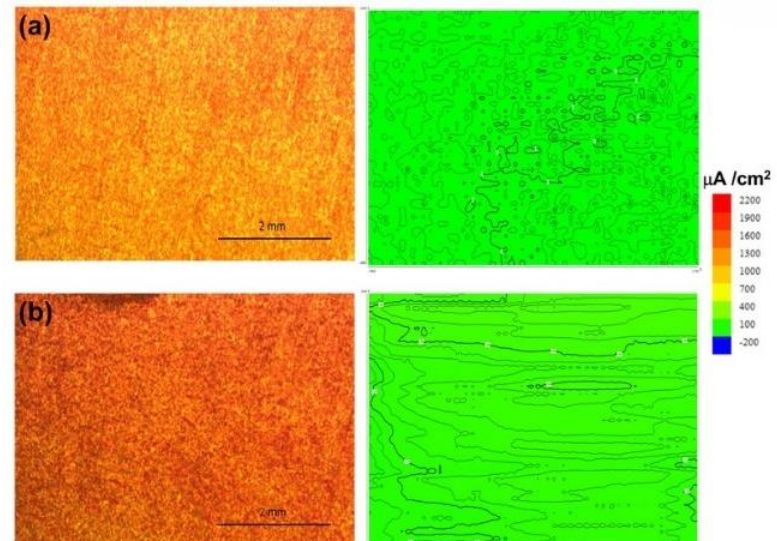


Fig. 2. Current density distributions of coated Ti-6Al-4V alloy after (a) 1 h, (b) 15 h and OM images at each immersion time in the presence of F^- aggressive ions.

4. References

[1] Bino et al, *Appl. Surf. Sci.* 557, 149739, (2021).
 [2] Moreto et al, *Appl. Surf. Sci.* 556, 149750, (2021).

Acknowledgments

CNPq (Grants 303659/2019-0, 140187/2017-0, 310504/2020-1) as well as Research Supporting Foundation of Minas Gerais State (FAPEMIG-Brazil) (Grant APQ-02276-18).

EFFECT OF DIAMOND-LIKE CARBON FILM ON TRIBOLOGICAL BEHAVIOR OF TOOL STEEL AISI M2

Miguel Rubira Danelon^{1*}, Rômulo Ribeiro Magalhães de Sousa², Larissa Solano de Almeida¹, Marcos Dorigão Manfrinato^{1,3}, Luciana Sgarbi Rossino^{1,3}

¹*Federal University of São Carlos – UFSCAR – Sorocaba Campus – Sorocaba/SP*

²*Federal University of Piauí – UFPI – Teresina/PI*

³*Sorocaba Technological College – FATEC-So – Sorocaba/SP*

1. Introduction

DLC (Diamond-Like Carbon) film is an amorphous carbon thin film which contains carbon hybridizations sp^2 and sp^3 related to graphite and diamond, respectively. This combination provides a high hardness and low friction coefficient improving the wear resistance of the material [1]. AISI M2 tool steel is a high-speed steel, utilized as machining, milling and cutting tools, due to its high hardness. The objective of this work is to evaluate the influence of the DLC film on tribological behavior of M2 steel, used as a machining tool.

2. Experimental

The technique utilized to obtain the DLC film was the PECVD by plasma using Pulsed-DC power supply. Before the treatment it was made an ablation treatment with gas mixture of 80% Ar/20% H₂ during 30min. After it was deposited an organosilicon film, to improve the DLC film adhesion, with a gas mixture of 70% HMDSO/30% Ar during 15min. Finally, the DLC film deposition was performed with gas mixture of 90% CH₄/10% Ar, gas flow of 30sccm, 200°C and 500V of tension, at a 2h treatment. The micro-abrasive wear tests by fixed ball were performed in 600s with 4N and 8N load. The material was characterized by Vickers microhardness.

3. Results and Discussions

The wear resistance of the samples with and without treatment is presented at Figure 1. It is observed that the wear resistance was improved with the presence of DLC film, in the tests of 4N and 8N, presenting wear volume of $1,34 \times 10^{-5} \text{ mm}^3$ and $3,25 \times 10^{-5} \text{ mm}^3$ respectively, while the base material presented $2,21 \times 10^{-3} \text{ mm}^3$ and $3,10 \times 10^{-3} \text{ mm}^3$ for the loads of 4N and 8N respectively. This result is explained by the high hardness, 1231 HV, provided by the sp^3 carbon hybridizations, like diamond, while the base material presented 354 HV. Other explanation to this result is presented at Figure 2, that shows low friction coefficient to DLC film compared to base material, explained by the similarity with the graphite due to sp^2 hybridizations, being an excellent solid lubricant. Thus, these results show that the DLC film is an excellent thin film to provide improvement to wear resistance of AISI M2 steel, being an alternative to improve tools useful life.

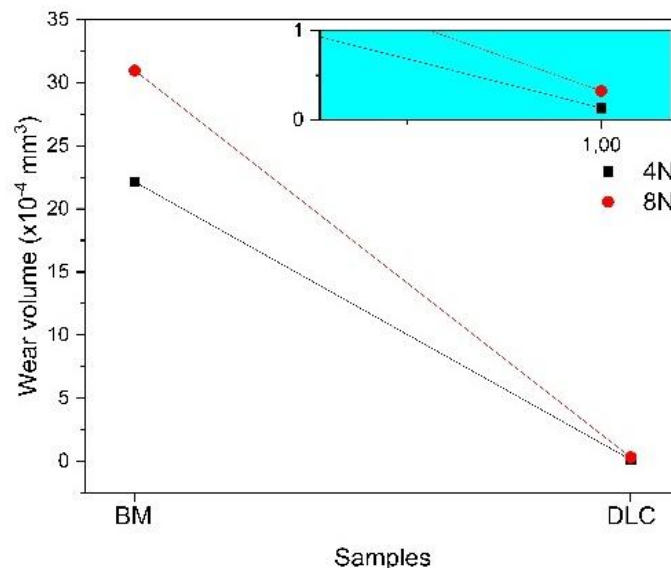


Fig. 1. Wear volume as a function of the base material and DLC film, varying the test load of 4N and 8N.

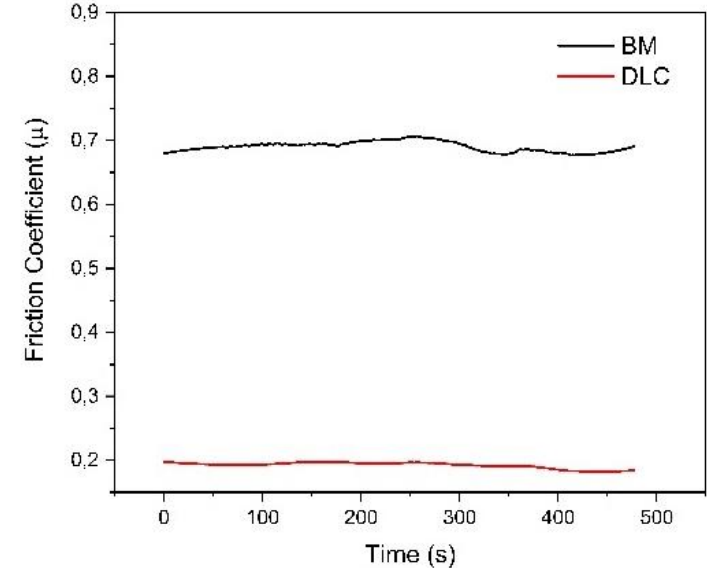


Fig. 2. Friction coefficient as a function of the test time for the base material and DLC Film.

4. References

[1] ROBERTSON, J. Diamond-like amorphous carbon. **Materials Science and Engineering: R: Reports**, v. 37, n. 4–6, p. 129–281, may 24 2002.

Acknowledgments

The authors acknowledge FATEC-SO, UFPI and CAPES (001) for the financial support.

DEPOSITION OF SiO_2 THIN FILMS USING PLASMA ENHANCED ATOMIC LAYER DEPOSITION FOR CORROSION PROTECTION

Danielle Cristina Fernandes da Silva Spigarollo*¹, Davi Henrique Starnini de Camargo², Nilson C. Cruz¹, Carlos Cesar Bof Bufon², Elidiane C. Rangel¹.

¹Universidade Estadual Paulista (Laboratório de Plasmas Tecnológicos), Sorocaba, SP, Brazil

²Centro Nacional de Pesquisa em Energia e Materiais (CNPEM), Campinas, SP, Brasil

1. Introduction

Thin films of SiO_2 have already been deposited by atomic layer deposition [1]. Plasma treatments allows the alteration of the surface without altering the material's volume properties [2], a decrease in temperature, when compared to ALD, and a faster and more uniform deposition, enabling the deposition of different materials. Some precursors have been used for deposition of SiO_2 in ALD process, but tris(dimethylamino) silane (TDMAS) has been reported energetically difficult by this way [3]. So that, in this work, TDMAS was used for the deposition of SiO_x films on carbon steel by PEALD, to evaluate the mechanisms of deposition of this precursor and action against the corrosion of metallic surfaces.

2. Experimental

PEALD of Oxford Instruments – OpAL was utilized with TDMAS and O_2 as an oxidizing agent. The temperature was 150°C with varying the number of cycles from 2632 to 6140. The films were deposited on rectangular 1020 carbon steel substrates (10 mm x 20 mm), which were polished to 1200 grit, cleaned in an ultrasonic bath with ethanol and dried using a thermal dryer. PM-IRRAS spectrum was used for chemical determination of deposited species and Electrochemical impedance spectroscopy in 3,5% NaCl medium was utilized for analysis of films corrosion protection at three different thicknesses 150, 300 and 350 nm.

3. Results and Discussions

Although the presence of a third dimethylsilane group inside precursor is energetically unfavorable to the reaction [3, 4], the Grow per cycle of 0.57 Å/cycle found here is consistent with those reported for SiO_x films [4]. Figure 1 shows the PM-IRRAS spectrum of the samples. It is possible to observe the characteristic bands of the Si-O-Si groups in 1057 cm^{-1} and 1143 cm^{-1} [1]. The band in the range of 670 cm^{-1} may indicate the presence of impurities, like Si-H or Si-CH₃. The last may indicate a residue of the precursor due to the high energy required for complete breakdown of TDMAS [2]. The contribution related to Si-CH₃ group also appears at the peak of 1252 cm^{-1} and 1290 cm^{-1} [2]. Figure 2 presents the Nyquist representations for the as received and coated carbon steel samples. This diagrams indicated an increase in the resistance to polarization with the film deposition [5]. The film deposited via PEALD presented important characteristics of SiO_2 deposition, but the presence of impurities could also be observed. The EIS results indicated possible protection of carbon steel. Further studies are needed to elucidate the process of deposition of SiO_x films via PEALD using TDMAS as a precursor.

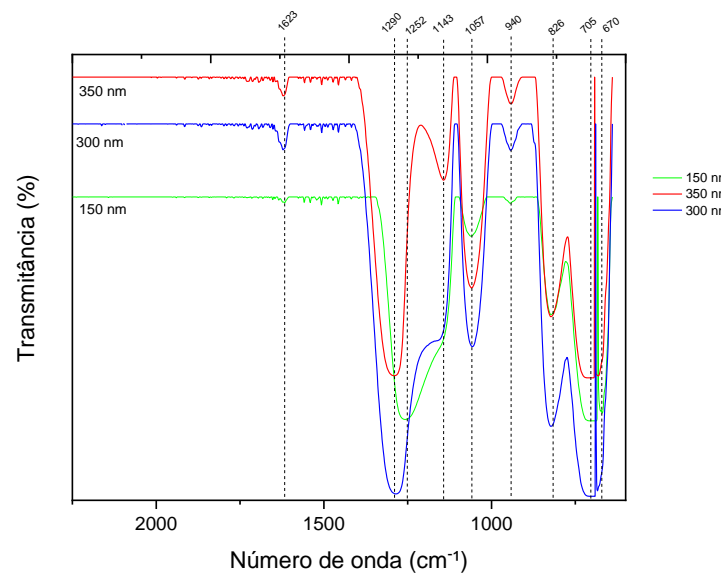


Fig. 1. PM-IRRAS spectra of films deposited via PEALD on carbon steel with 150, 300 and 350 nm

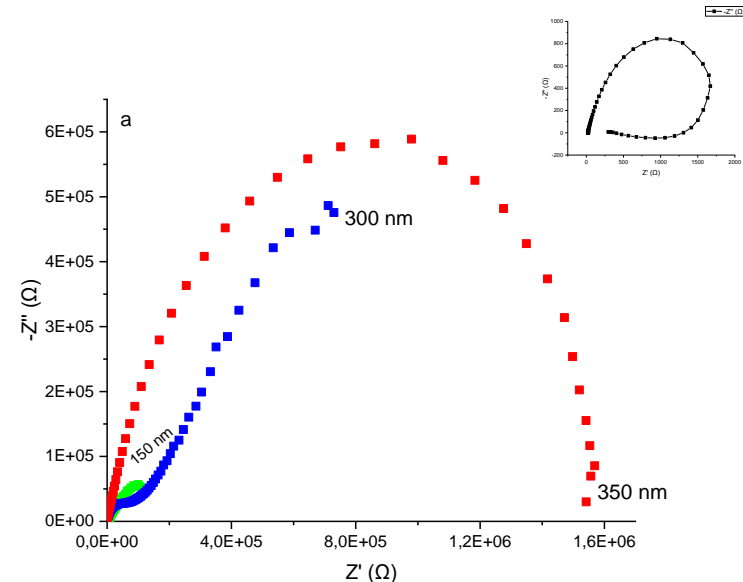


Fig. 2. (a) EIS diagram of SiO_x films deposited on carbon steel in 3.5% NaCl solution; (b) diagram of carbon steel as received in 3.5% NaCl solution

4. References

- [1] B.B. Burton, et al., *The J. of Phy. Chem.*, 113 (2009) 8249-8257.
- [2] H. Yasuda and Y. Iriyama, *Plasma polymerization*, 4th edition Academic Press (1989)
- [3] Y.-C. Jeong, et al., *Applied surface science*, 280 (2013) 207-211.
- [4] G.-Y. Fang, et al., *Chemical Communications*, 51 (2015) 1341-1344.
- [5] F. Hirose, et al., *ECS Transactions*, 19 (2009) 417

DEPOSITION OF REDUCED GRAPHENE OXIDE (rGO) AND FORMATION OF HYBRIDSTRUCTURE WITH THIN FILMS OF TIN DIOXIDE (SnO₂)

Letícia da Silva de Oliveira^{1,*}, Cristina de F. Bueno¹, Luis Vicente de A. Scalvi¹
¹São Paulo State University (UNESP), School of Sciences, Department of Physics, Bauru, Brazil

1. Introduction

Tin dioxide (SnO₂) is a n-type oxide semiconductor [1] with a wide variety of applications, as inoptoelectronics or gas sensors [2]. On the other hand, advanced 2D materials present improved properties when coupled to transparent oxides, as the case of reduced graphene oxide (rGO), with high conductivity [3]. In this communication rGO is deposited on glass substrate by dripping, giving rise to hybrid nanostructures in combination with thin films of SnO₂:2at% Eu, whose surface electrical conductivity can be applied to electronic devices or gas sensors. Electrical measurements show that the presence of rGO on the SnO₂ surface decreases the conductivity in vacuum, due to the surface interaction.

2. Experimental

Eu-doped SnO₂ is obtained by dissolving Eu₂O₃ in HCl, which is added to an aqueous solution of SnCl₄.5H₂O. Dialysis is performed for about 10 days to eliminate Cl⁻ and NH⁺ ions. rGO synthesis is performed according to the method of Abdolhosseinzadeh, with graphite being added to H₂SO₄ stirred at 0°C, followed by KMnO₄ added slowly. After the standard procedure by this method, the precipitate is filtered in vacuum and washed in HCl until neutral pH.

3. Results and Discussions

Figure 1 shows scanning electron microscopy (SEM) of rGO (1 drop) on borosilicate glass, with magnetic stirring of the rGO solution. The formation of rGO structure in this case similar to deposition on SnO₂ (sample SnO₂:2%Eu/rGO). Figure 2(c) shows the carbon mapping on the sample surface, which comes from the rGO. In the bottom of Fig. 1 (SEM) it is observed that the growth of these rGO structures follows the increase in the number of drops, as expected. Figure 2 shows electrical current as a function of the applied bias for SnO₂:2%Eu/rGO. The effect of lower pressure is a decrease in conductivity, and the vacuum expands the electron capture effect of rGO. This is in good agreement with calculations by DFT that show the reactivity of the SnO₂ plane (001), indicating the coupling with rGO, leading to increase in electronic density, which alters the gas adsorption.

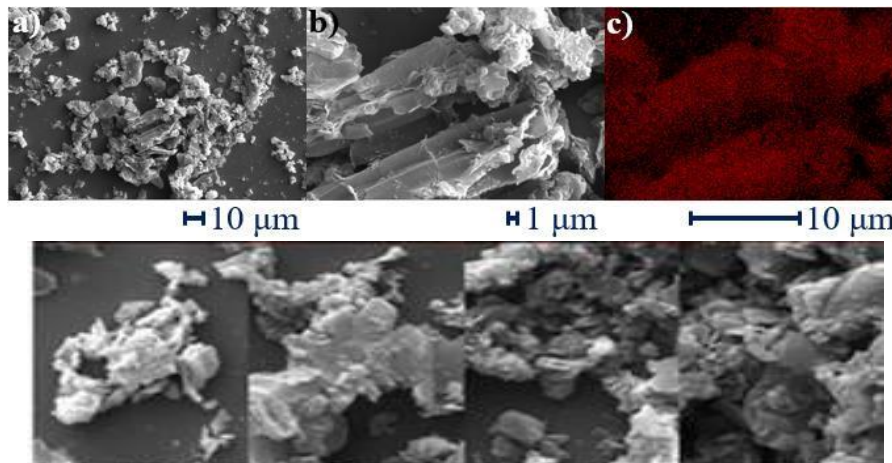


Fig. 1. SEM of rGO deposited on borosilicate glass substrate by dripping (1 drop): (a) magnitude of 2000 X, (b) 10000 X (c) chemical mapping of carbon of the same region of the image with magnitude of 10000X. **Bottom:** SEM with magnitude of 10000X of rGO samples for different drop numbers: 1, 2, 3, 4 from left to right

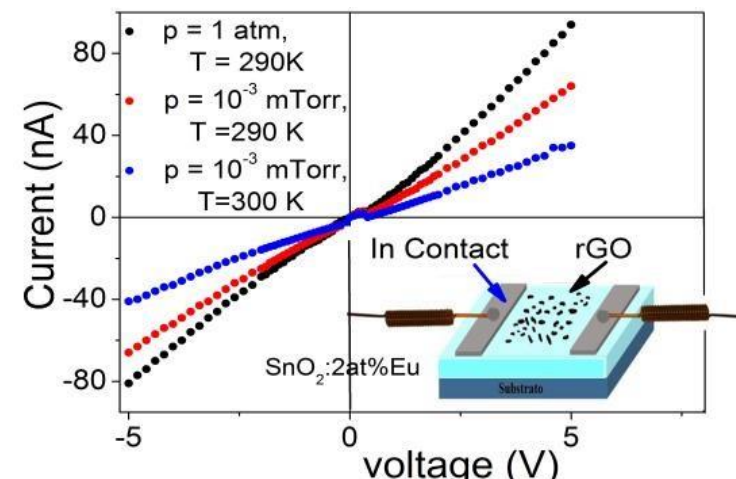


Fig. 2. Electrical current as function of applied voltage of the sample SnO₂:2%Eu/rGO with In contact. **Inset:** diagram showing the structure of the hybrid sample used for electrical characterization

4. References

- [1] S. H. Luo *et al.*, Nanotechnology **17**, 1695-1699, (2006)
- [2] L. Xiong *et al.*, Advanced Functional Materials **28**, 1802757, (2018)
- [3] Y. Wang *et.al.*, Materials Today **21**, 186-192, (2018)

Acknowledgments

The authors thank CNPq and FAPESP by financial support and Renato D. Souza by DFP calculation.

Plasma deposited THFMA-co-MOx coatings for drug delivery

F.V.P. Kodaira^{1*}, E. Makhneva², K.-D. Weltmann², K. Fricke², Kostov. K. G¹

¹São Paulo State University (UNESP), School of Engineering, Guaratinguetá, SP, Brazil.

²Junior Research Group Biosensing Surfaces, Leibniz Institute for Plasma Science and Technology e.V. (INP), Greifswald, Germany.

1. Introduction

Plasma polymerized coatings are very versatile, they have good adhesion on substrates of different shapes and materials, they are highly customizable and can be wear resistant, stable in mildly acidic or basic media, stable or soluble in water, and biocompatible. This versatility makes it suitable for many applications, such as, dielectric, protective, drug releasing, biocompatible or biosensing coatings, among others.

The plasma polymerization process has many advantages over wet chemistry, it can grow films from monomers that do not polymerizes by using conventional processes, the process may occur in one single step, and it generates no harmful wastes. When operating in atmospheric pressure, the process becomes cheaper in comparison with the low-pressure reactors since a vacuum system is not required.

A biocompatible coating capable of retain a substance and further release it when needed can be useful for applications in drug delivery. The usual means of admitting drugs, such as oral or intravenous, require a higher dose than needed due to losses in the body. If you can target the region where the drug is needed, it is possible to make a more efficient delivery, causing less collateral damage to the patient's body, since a smaller dose will be required.

2. Experimental

In this work, the Cold Atmospheric Plasma Polymerization (CAPP) of the coatings was performed by using a non-thermal plasma jet fed by 5W@27.12MHz. A mixture of Tetrahydrofurfuryl Methacrylate (THFMA) and 2-methyl-2-oxazoline (MOx) (T:MOx) with 4:1 ratio was chosen as precursor. The drug releasing tests were carried using Methylene Blue (MB) as the incorporated drug. The coated substrates were immersed in MB solutions for 24h then analyzed by FTIR (C=N peak at 1600 cm⁻¹) and XPS. The release of MB over time was evaluated by UV/Vis spectroscopy. Interleaved layers of T:MOx and MB incorporation were also studied to try to control the release time.

3. Results and Discussions

The FTIR of the polymerized coatings showed characteristic groups like amide, C=O and C-N. It was also taken after the samples were immersed in water, the spectrum had some change in intensity, but all peaks were still present, implying that the sample is stable in water, something important for the drug incorporation process and later applications. The FTIR was also able to detect the characteristic MB peak (at 1600 cm⁻¹) after its incorporation in the films. The presence of Cl and S was detected by XPS after the MB incorporation process, indicating the presence of the drug in the film, confirming the previous FTIR results. The tests with the interleaved layers for the MB releasing showed that adding thicker layers on top after the MB incorporation extended the releasing process.

References

- [1] A. Brooks, S. Woppard, G. Hennigan, T. von Werne, in: Proceedings of the SMTA International Conference, 2012, pp. 1–6.
- [2] V. Jalaber, D. Del Frari, J. De Winter, K. Mehennaoui, S. Planchon, P. Choquet, C. Detrembleur, M. Moreno-Couranjou, *Front Chem* (2019).
- [3] N. Bertrand, J.C. Leroux, *Journal of Controlled Release* 161 (2012) 152–163.
- [4] J. Li, D.J. Mooney, *Nat Rev Mater* (2016).

Acknowledgments

This work was supported by DAAD and CAPES no. 290317/2017-7.

PHOTOELECTROCHEMICAL CHARACTERIZATIONS OF $\text{TiO}_x/\text{SiO}_x$ THIN FILMS DEPOSITED BY PECVD

Rafael Parra Ribeiro^{1*}, Nilson Cristina Cruz¹, and Elidiane Cipriano Rangel¹

¹Science and Technology Institute of Sorocaba (ICTS), São Paulo State University (UNESP), 511 Av. Três de Março, Sorocaba, 18087-180, Brazil

1. Introduction

Cathodic protection is a method in which the metal to be protected is supplied by the application of an external electrical current. When electrical current is supplied by a photoanode, this technique is called photoelectrochemical cathodic protection or photogenerated cathodic protection. Photoelectrochemical cathodic protection technology (PhotoElectrochemical Cathodic, PEC) is a new method, first reported in 1995 in the work of Yu et al. [1], being environmentally friendly and non-polluting [2]. Therefore, this work aimed to evaluate the photoelectrochemical cathodic protection performance of $\text{TiO}_x/\text{SiO}_x$ thin films produced by plasma-assisted chemical vapor deposition (PECVD) on titanium.

2. Experimental

Thin films were deposited onto grade 2 titanium from atmospheres containing titanium tetraisopropoxide (TTIP), hexamethyldisiloxane (HMDSO), Ar and O_2 . The total pressure in the chamber and the deposition time were fixed at 133 Pa and 1800 s, respectively. The proportion of O_2 was varied from 0 to 90%, while the proportion of the mixture TTIP, HMDSO and Ar (carrier gas) was varied in the opposite direction. The plasma was excited by applying 25 W of RF signal (13.56 MHz) to the upper electrode, while the lower electrode (sample holder) remained grounded. The PEC properties were investigated using a conventional three-electrode cell and a potentiostat. Open circuit potential (OCP) and Mott-Schottky plots were analyzed in 0.1 M Na_2SO_4 solution, while electrochemical impedance spectroscopy (EIS) was performed with 0.6 M NaCl solution. Except for the Mott-Schottky plots, the analyzes were carried out in the dark and under UV lighting.

3. Results and Discussions

Under UV light, the OCP curves shifted to more negative potentials, demonstrating that there is an electron flow from the coatings to the substrate. Samples deposited with 0 and 50% O_2 showed greater potential drops than uncoated titanium. The films had a more negative flat band potential (Fig. 2) than uncoated titanium. However, this value was shown to be dependent on the proportion of oxygen used in the plasma atmosphere.

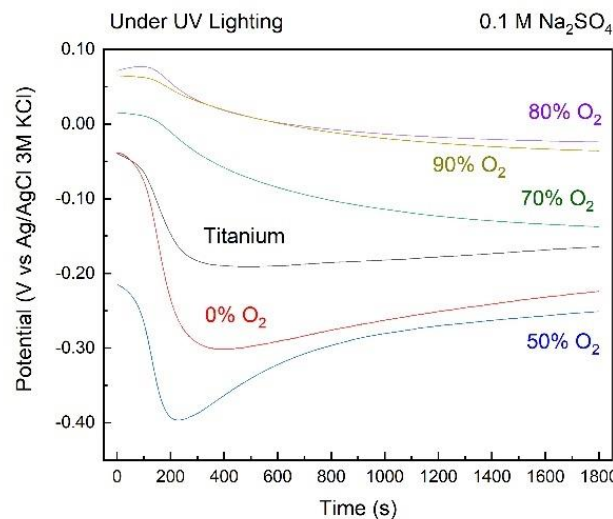


Fig. 1. OCP curves obtained under UV illumination.

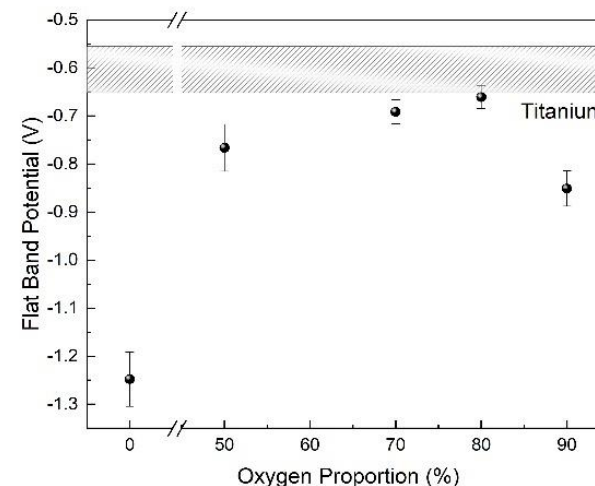


Fig. 2. Flat band potential obtained by Mott-Schottky plots.

4. References

- [1] J. Hu et al., Corros. Sci., **125**, 59–67, (2017).
- [2] Y. Bu J.P. Ao, Green Energy Environ. **2**, 331–362,(2017).

Acknowledgments

Authors would like to thank CAPES (1766917- RPR) and FAPESP (2017/21034-1) for their support.

VARIATION OF PLASMA JET PARAMETERS ACCORDING TO THE DISTANCE TO TARGET

Fellype do Nascimento^{1*} and Konstantin Kostov¹

¹ São Paulo State University – UNESP, Faculty of Engineering in Guaratinguetá, Guaratinguetá, Brazil

1. Introduction

The diversity of applications for atmospheric pressure plasma jets (APPJs) has been grown consistently along the last years. Such applications started with the treatment of materials, and are now in the areas of biology, medicine, dentistry, among others. The positive effects observed in applications that used APPJs have been attributed to the presence of reactive oxygen and nitrogen species (RONS) produced by the plasma jets, together with the low temperature values obtained in this kind of gas discharge [1]. In this work it was studied how the plasma jet parameters behave as a function of the distance between the device outlet and the target surface as well as the corresponding behavior for the production of some RONS.

2. Experimental

The APPJ equipment used in this work is a dielectric barrier discharge device with a long and flexible tube attached to the reactor (see details in [2]). In order to obtain parameters from different portions of the plasma jet, optical emission spectroscopy (OES) was performed at the regions 1 and 2, indicated in Fig.1., as a function of the distance d from the device outlet and the target surface (a metal plate for instance). By using OES, the production of hydroxyl (OH) and nitric oxide (NO) was evaluated through the intensity emission of these species – the greater the intensity, the greater the amount of such species. In addition, the discharge power (P_{dis}) and effective electric current (i_{RMS}) were also measured as a function of d .

3. Results and Discussions

The main results obtained in this work are presented in Fig. 2, from which we can observe that the P_{dis} and i_{RMS} values stay almost constant when d is in the 3 to 9 mm range, before a significant decrease in the values of both parameters for $d = 11$ mm, being that at higher d values the plasma discharges start to fail. Regarding the production of RONS, Fig. 2 shows clearly that the behavior of the intensity emissions from OH and NO molecules as a function of d are quite different at the plasma outlet (region 1) and close to the surface target (region 2). Being that at region 1 both OH and NO emissions remain almost unchanged while at region 2 the production of both species present a growth trend, even with the reduction that occurs in the P_{dis} and i_{RMS} values, from which we can infer that the production of RONS has no direct relationship with the electrical parameters under the conditions studied.

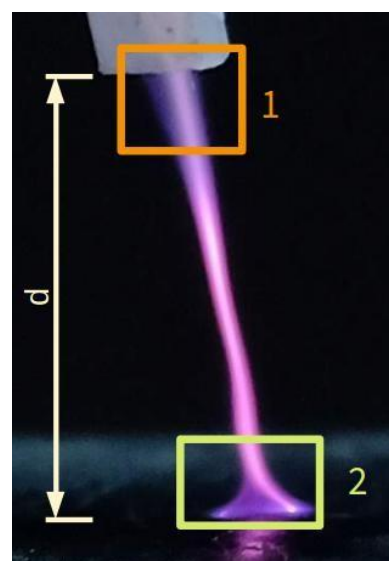


Fig. 1. Plasma jet produced and the different regions observed in spectroscopic measurements

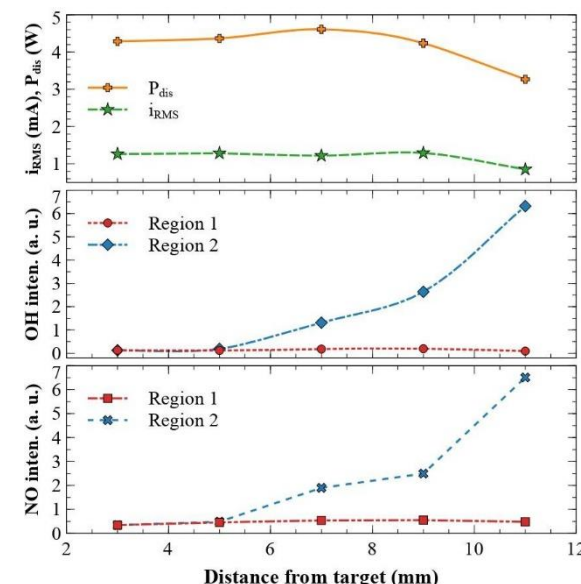


Fig. 2. Discharge power, effective current and intensity emissions of reactive species vs distance

4. References

[1] G. Busco, E. Robert, N. Chettouh-Hammas, *et al*, Free Radical Bio. Med., 161, 290-304, (2020). [2]- K. G. Kostov, *et al*, Plasma Process. Polym., 12, 7 1383 (2015)

Acknowledgments

This work was supported by FAPESP (grants #2019/05856-7 and #2020/09481-5)

GROWTH OF POROUS ZIRCONIA ON BIOMEDICAL Ti-6Al-4V ALLOY BY PLASMA ELECTROLYTIC OXIDATION

Nanuh¹, A.C.; Rangel¹, E.C.; Correa², D.R.N.; Cruz¹, N.C.

¹UNESP – Univ Estadual Paulista, Laboratório de Plasmas Tecnológicos, Sorocaba, Brazil

²IFSP – Câmpus Sorocaba, Advanced Metallic Materials Group, Sorocaba (SP), Brazil

1. Introduction

Titanium and its alloys are extremely used on implantable materials, in special as orthopedic and dental devices, due to their optimal combination of high strength-to-density ratio, relatively low Young modulus, good corrosion resistance and recognized biocompatibility [1]. However, Ti alloys are bioinert materials, lacking bioactive integration with cells and tissues. A possible way to overcome this drawback is by coating the metallic surface with selected oxide layers, such as, zirconia (ZrO_2) coatings, which possesses biocompatible and osteoinductive properties, as well as high wear resistance. In this scenery, Plasma Electrolytic Oxidation (PEO) can be considered as an important tool as it allows the deposition of porous ceramic coatings with adjustable composition and morphology [2,3]. The aim of this study was to produce porous zirconia coatings on the biomedical Ti-6Al-4V alloy by PEO treatment.

2. Experimental

Disk-shaped samples of Ti-6Al-4V (ASTM F136), with dimensions of $\phi 10$ mm x 3 mm, were used as substrate. The electrolyte was composed of 0.08 mol.L⁻¹ of zirconium oxide (ZrO_2) and 0.04 mol.L⁻¹ of potassium hydroxide (KOH). The PEO treatments were performed in a system consisting of a pulsed voltage source (MAO-30), a water-cooled stainless steel tank, and a suspended electrode. The surface treatments were carried out at voltages between 300 V and 500 V. Surface morphology was determined by scanning electron microscopy (SEM). Semi-quantitative chemical analysis was obtained by X-ray energy dispersion spectroscopy (EDS). Surface characteristics were also evaluated by XRD, contact angle and roughness measurements.

3. Results and Discussions

Figure 1 shows the SEM micrograph of the Ti-6Al-4V alloy (a) without coating and (b) after treatment with PEO at 500 V. Comparing the micrographs it is possible to verify that the treatment produced a clear change in the surface topography, with the formation of round structures and pores. In addition, EDS revealed the reduction in the atomic proportion of vanadium (alloy element) in the outermost surface layer. Furthermore, zirconium atoms were detected indicating the incorporation of electrolyte species in the coating. XRD, contact angle and roughness measurements indicated the formation of a coating with suitable properties for use as biomaterials.

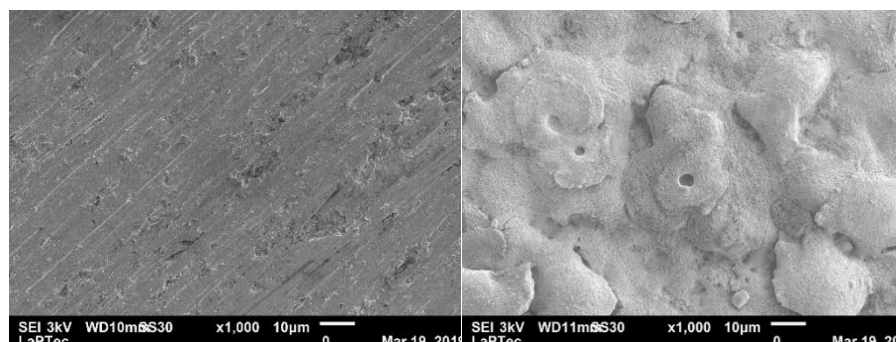


Fig. 1. Scanning electron micrograph of the Ti-6Al-4V alloy surface as-received (left) and after treatment with PEO at 500 V (right).

4. References

- [1] Correa, D.R.N. et al. Surface and Coatings Technology, 344, 373-382 (2018).
- [2] Antonio, R.F. et al. Surface and Coatings Technology, 357, 698-705 (2019).
- [3] Clyne, T. W. et al. International Materials Reviews, 64, 127-162 (2019).

Acknowledgments

The authors thank the Brazilian funding agencies CNPq and FAPESP.

DEPOSITION OF SnO_2 AND ZrO_2 THIN FILMS, FORMING TRANSPARENT HETEROSTRUCTURE FOR USE IN OPTOELECTRONIC DEVICESLucas Prado Fonseca^{1*}, Luis Vicente de A. Scalvi¹¹São Paulo State University (UNESP), School of Sciences, Department of Physics, Bauru, Brazil.

1. Introduction

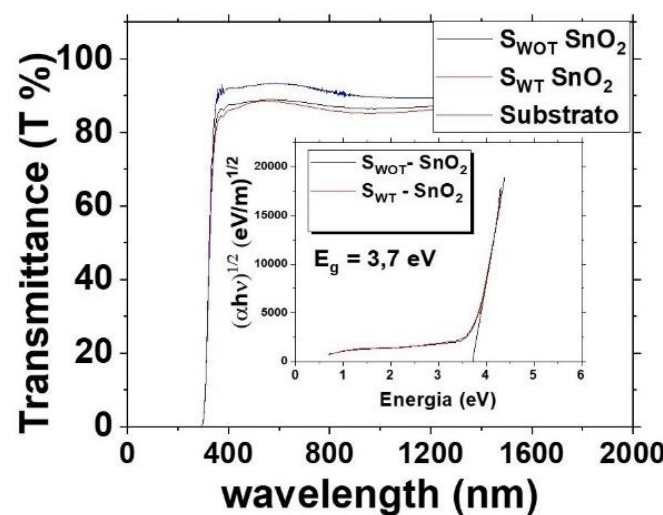
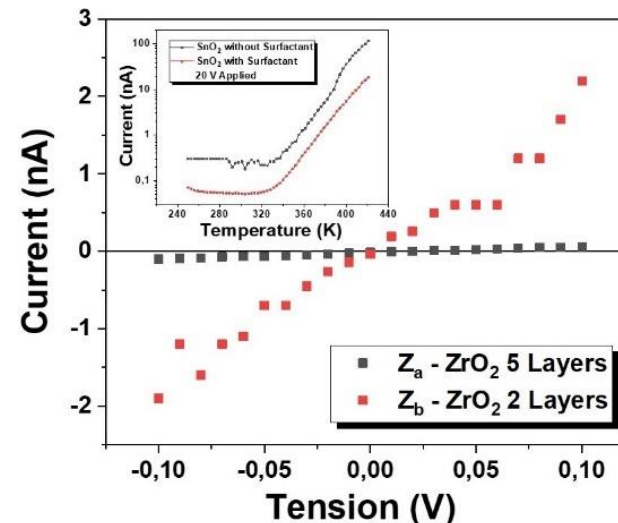
The semiconductor oxide SnO_2 has increasing interest for use in transparent optoelectronic devices due to its high transparency in the visible region of the electromagnetic spectrum, in the form of thin film. It presents good electrical conductivity associated with the presence of oxygen vacancies and interstitial tin atoms, which are electron donors in the matrix [1] making it a naturally n-type semiconductor. The precursor solution of SnO_2 can be chemically more stable with the use of surfactants such as Triton X100 [2]. On the other hand, zirconia, an oxide insulating material used in this work, arouses interest also due to its high transparency, as well as its high mechanical strength and high dielectric constant [3].

2. Experimental

To obtain nanostructured films of SnO_2 and ZrO_2 the sol-gel-dip-coating technique was used, which consists of using a colloidal suspension, where the films are properly deposited by the process of immersion and removal of clean substrates. Films are subjected to intermediate thermal annealing between each layer and a final annealing for solvent evaporation and material crystallization. In the process of obtaining the suspensions, the non-ionic surfactant Triton X100 was used to ensure the stability and homogeneity of the solution [2], thus, in the figures, WT means with triton and WOT, without triton. More recently, to build the heterostructure, polystyrene particles located between ZrO_2 and SnO_2 are being used to ensure thermal protection for the zirconia when subjected to thermal treatment.

3. Results and Discussions

Figure 1 denotes the high transparency of SnO_2 , being approximately 85% in the range of 300 to 2000 nm was obtained, collaborating with the manufacture of completely transparent devices. Through Tauc plot it was possible to estimate the direct gap energy of tin dioxide as approximately 3.6 eV. Figure 2 denotes the decrease in electric current as the thickness of the film obtained from ZrO_2 is increased, an effect related to structural defects, and the electrical insulation, which is of great importance for the optoelectronic purposes of the heterostructure. In the inset of figure 2, the behavior of the electrical current of SnO_2 is verified when the film is subjected to the temperature increase in vacuum (about 10^{-5} mTorr), presenting a transition insulating/semiconductor about 340K, which leads to high activation energy for the defects [2]. The device $\text{SnO}_2/\text{ZrO}_2$ built as a field effect transistor (FET) has shown peculiar I-V behavior.

Fig. 1. Transmittance and gap energy of thin films of SnO_2 .Fig. 2. Current x Tension of ZrO_2 thin films. Inset. Log of current x Temperature of SnO_2 in vacuum.

4. References

- [1] C. Xu, et al. Journal of Applied Physics 111, 6, 063504, 2012.
- [2] L. P. Fonseca et al. Applied Physics A 127, 503, 2021.
- [3] M. U. Jewel et al. RSC Advances 9, 1841-1848, 2019.

Acknowledgments

We thank CNPq (proc. 126234/2020-5) and FAPESP (proc. 2021/04144-3 for financial support.

CHEMICAL STRUCTURE AND PHOTOELECTROCHEMICAL CATHODIC PROTECTION PROPERTIES OF $\text{SiO}_x\text{C}_y\text{H}_z\text{-TiO}_2$ NANOCOMPOSITE FILMS

Lucas Pires Gomes Oliveira^{1*}, Rafael Parra Ribeiro¹, José Roberto Ribeiro Bortoleto¹, Nilson Cristina Cruz¹, and Elidiane Cipriano Rangel¹
¹Science and Technology Institute of Sorocaba (ICTS), São Paulo State University (UNESP), 511 Av. Três de Março, Sorocaba, 18087-180, Brazil

1. Introduction

Plasma deposition techniques are recognized as efficient tools for the production of thin films having diverse functions and applications, in a cost-effective and sustainable way [1-2]. Recently, there has been growing interest in the incorporation of particles in plasma deposited thin films to creation of multifunctional surfaces. In this work a new hybrid methodology based on the plasma enhanced chemical vapor deposition (PECVD) of hexamethyldisiloxane combined to the reactive sputtering of TiO_2 is proposed for the preparation of $\text{SiO}_x\text{C}_y\text{H}_z\text{-TiO}_2$ composite films. Specifically, the effect of the proportion of O_2 in the plasma environment, % O_2 , on the properties of the films was studied.

2. Experimental

The plasmas were generated in a capacitively coupled reactor, with powdered titanium dioxide (TiO_2) spread onto the lower electrode and an atmosphere fed hexamethyldisiloxane (HMDSO), O_2 and Ar, at a working pressure of 6.0 Pa. The plasma was ignited by applying a rf signal (150 W, 13.56 MHz) to the lower electrode, while the upper electrode, to which the substrates were fixed, was earthed. Chemical structure of the films were examined by Polarization modulation-infrared reflection-adsorption spectroscopy (PM-IRRAS). The barrier properties and photoelectrochemical cathodic protection of the films were analyzed using electrochemical impedance spectroscopy (EIS) with and without UV lamp illumination. Wettability was investigated using the sessile drop method, while film thickness and surface roughness were obtained using profilometry. The morphology of the samples was examined using Atomic Force Microscopy (AFM).

3. Results and Discussions

Organosilicon films were obtained with thicknesses between 90 and 400 nm containing C (43-45%), O (13-14%), Si (7-8%) and of $\text{Si-(CH}_3\text{)}_x$, Si-O-Si and CH_3 groups. Agglomerates of TiO_2 (16-83 μm) were detected into the organosilicon matrix with the concentration of particulates growing with the percentage of oxygen in the feed. The corrosion potential values became more positive as the proportion of O_2 increased, indicating an improvement in corrosion resistance compared to carbon steel. Interpretation is proposed in terms of the influence of the oxygen supply on the TiO_2 sputtering rate and in the oxidation of plasma species.

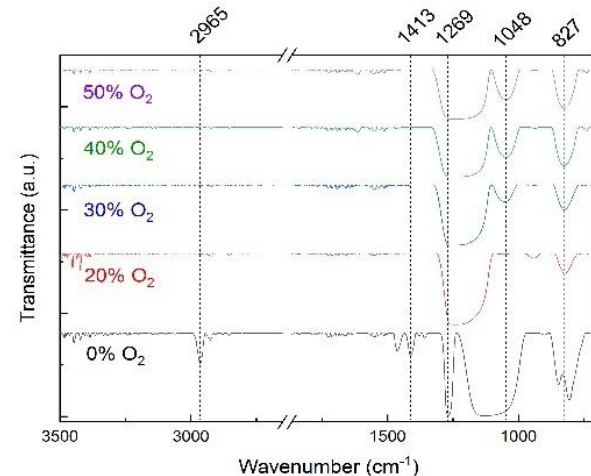


Fig. 1. PM-IRRAS spectra for samples deposited with different proportions of O_2 .

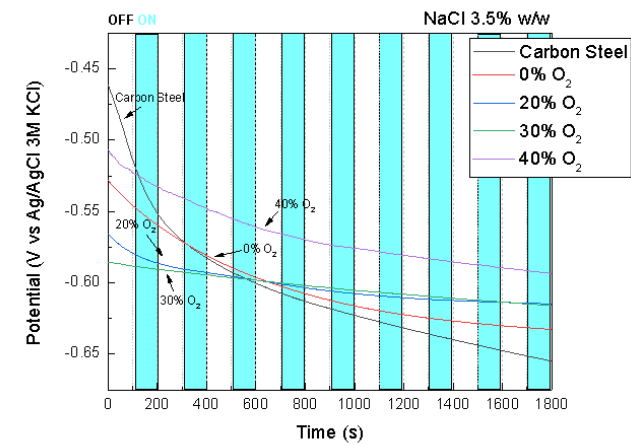


Fig. 2. OCP variations as a function of immersion time, with and without UV illumination.

4. References

[1] Gandhiraman RP, Daniels S, Cameron DC. Plasma Process Polym. 2007;4(Suppl 1):369-73.
[2] Fanelli F, Fracassi F. Plasma Chem Plasma Process. 2014;34(3):473-87.

Acknowledgments

Authors would like to thank FAPESP (Process 2017/21034-1) and CAPES (Processes 1754231/2017 and 1560670/2015).

DEPOSITION OF TANTALUM-BASED OXIDE COATINGS ON AISI 304 STEEL FOR USE AS A BIOMATERIAL

Proença, J. P.^{1,2*}, Correa, D. R. N.²; Cruz¹, N.C.; Rangel¹, E.C.

¹UNESP – Univ Estadual Paulista, Laboratório de Plasmas Tecnológicos, Sorocaba, Brazil

²IFSP – Câmpus Sorocaba, Advanced Metallic Materials Group, Sorocaba (SP), Brazil

1. Introduction

Among the austenitic stainless steels, the AISI 304 has been widely used in the medical and dental fields, due to its high mechanical strength and its biotolerance by the human body. However, its use as implants requires greater corrosion resistance, so that the material does not release ions or debris, causing a rejection of the prosthesis through inflammation or necrosis. One way to increase this corrosion resistance is by adding a surface coating of ceramic oxides, which act against intergranular corrosion [1]. Through the process of plasma electrolytic oxidation (PEO), it is possible to create an oxide layer on the metal surface strongly adhered to. Considering the recent biofunctional properties discovered in tantalum oxide [2,3], such as biocompatibility, bioactivity, and corrosion resistance, its use as coatings in PEO can give 304 stainless steel a greater potential for use as metallic biomaterials.

2. Experimental

The PEO treatment was carried out in a stainless steel reactor with internal water cooling. The samples were placed at a negative potential (anode), while the stainless steel chamber was kept at a positive potential (cathode). The surface treatments were carried out with a pulsed voltage source, with voltages of 200 V, frequency of 1000 Hz, duty cycle of 60%, during 10 min. The electrolyte was varied, consisting of an aqueous solution of 2 g/L, 2.5 g/L, and 3 g/L of potassium hydroxide (KOH), and tantalum hydroxide (TaOH) in the proportions of 10 g/L, 30 g/L, and 50 g/L. The treatments were carried out in triplicate, to ensure good reproducibility of results. Then, morphology, phase proportion, and chemical composition were evaluated by SEM/EDS and XRD measurements.

3. Results and Discussions

During the first minute of treatment, it is possible to see in Fig. 1 a current increase due to the KOH electrolyte. After that, an exponential decrease of the current proves that an oxide layer is formed on the substrate surface, which hinders the passage of current and favors the appearance of micro-arcs. SEM/EDS results indicated that the oxide layer was porous, with some amount of Ta oxide incorporated into the coating. The XRD pattern exhibited just an amorphous phase composition.

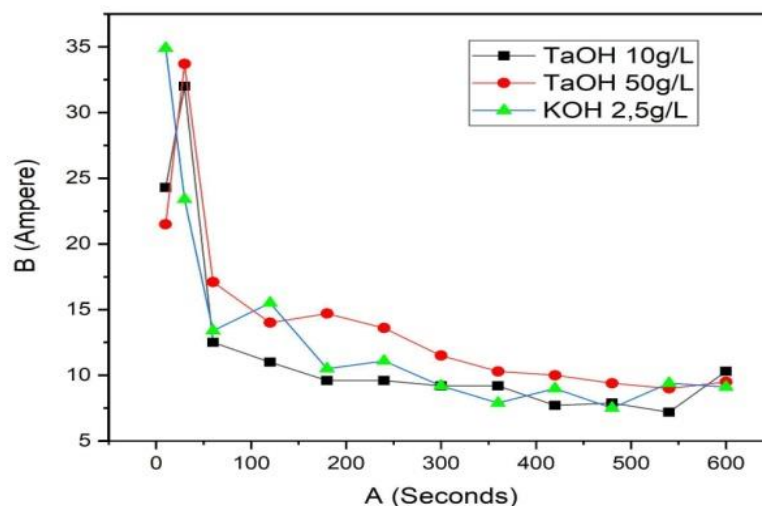


Fig. 1. Graph of current variation (B) over time (A).

4. References

- [1] MANAM, N. S. et al., Journal of Alloys and Compounds, v. 701, p. 698–715, (2017).
- [2] ANTONIO, R. F. Tese (Doutorado) – Universidade Estadual Paulista. Faculdade de Ciências. Bauru, (2016).
- [3] ZELIANG D. et al., Ceramics International, Volume 47, Issue 1, (2021).

Acknowledgments

The authors thank the Brazilian funding agencies CNPq and FAPESP.

THREE-DIMENSIONAL POLYPYRROLE/CARBON FELT COMPOSITE AS A BINDER-FREE SUPERCAPACITOR ELECTRODE

M. G. C. Munhoz^{1,2*}, A. C. Rodrigues², J. T. Matsushima³, J. S. Marcuzzo⁴, G. F. B. Lenz e Silva¹, G. A. Amaral-Labat.² and M. R. Baldan²¹Polytechnic School of the University of São Paulo, São Paulo, SP, Brazil²National Institute of Aerospace Research, São José dos Campos, SP, Brazil³Faculty of Technology Professor Jessen Vidal, São José dos Campos, SP, Brazil⁴JMHP - Consultoria em Materiais, Ltda - Jacareí, SP, Brazil

1. Introduction

Composites of porous carbons materials and polymers are searched compounds for applications as electrodes for supercapacitors, especially due its three-dimensional and conducting morphology [1]. Although, most electrodes use binders, reducing the conductivity [2] and increasing the price of the final product. In this work, a binder-free composite based on activated carbon fiber felt (ACFF) and polypyrrole is proposed.

2. Experimental

The ACFF was surface treated by electrochemical oxidation using a conventional three-electrode system with H_2SO_4 (0.5 M) at a constant potential of 2 V for 300 s [2], originating the ACFF-P. The pyrrole *in-situ* reaction was performed on the samples ACFF and ACFF-P by heating a 0.1 M solution of pyrrole in acetone at 50°C for 1 hour. The electrochemical performance of all samples was evaluated in a Autolab PGSTAT 302N potentiostat/galvanostat.

3. Results and Discussions

Figure 1b shows the surface modification produced by the electrochemical oxidation on ACFF sample (1a). The nanostructured three-dimensional polypyrrole (Ppy) are clearly observed on the treated fiber PPy/ACFF-P (1d), instead of a roughed surface on the Ppy/ACFF (1c).

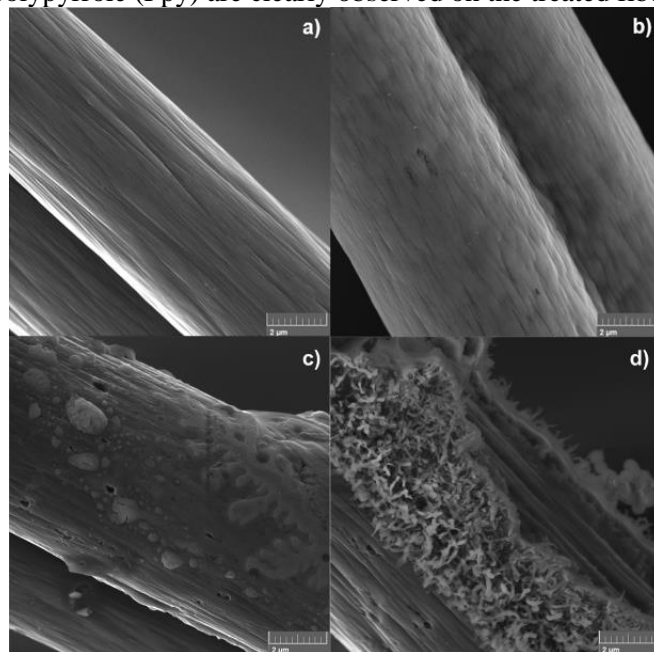


Fig. 1 SEM images of (a) ACFF, (b) ACFF-P, (c) Ppy/ACFF and (d) PPy/ACFF-P.

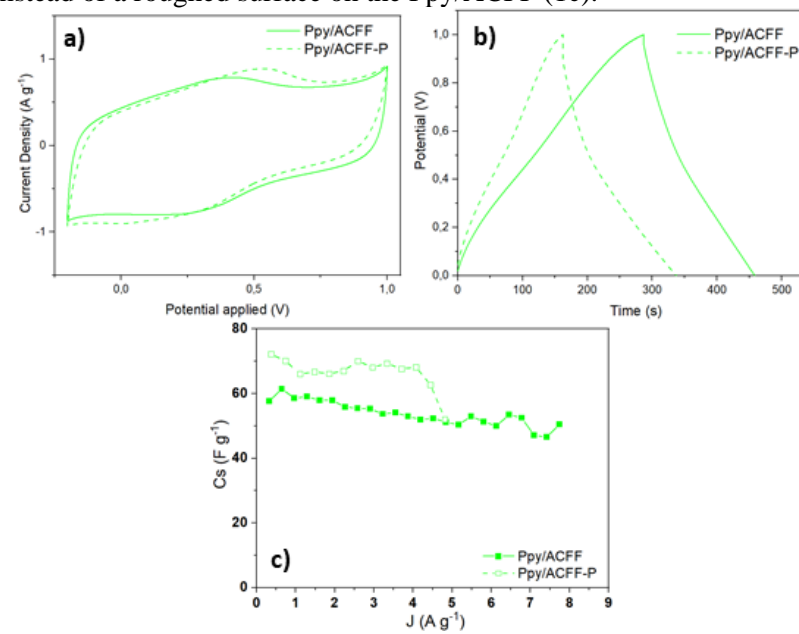


Fig. 2. (a) CV at $10mV s^{-1}$, (b) CDGC and (c) Specific Capacitances of Ppy/ACFF and PPy/ACFF-P in $2M H_2SO_4$.

The CV and CDG curves (Fig. 2a and 2b) presented current peaks associated with reversible faradaic reactions evidenced by the redox pair (0.2 V - 0.6 V). The higher capacitance values (Fig. 2c) of the pre-treated sample (Ppy/ACFF-P) is probably related to the presence of nanostructured polypyrrole on the fiber surface, assisted by the large amount of oxygen groups on the surface, as observed by XPS results.

4. References

[1] M. Mirzaeian, et al., International Journal of Hydrogen Energy, 42 (40), 25565–25587, (2017).
 [2] M. He, Y. Zheng; Q. Du, Materials Letters, 104, 48-52, (2013).

Acknowledgments

This work has been supported by the Coordenação de Aperfeiçoamento de Pessoal de Nível Superior (CAPES) - Brazil, grant number 88887.631486/2021-00.

ASSOCIATION OF ATMOSPHERIC PRESSURE COLD PLASMA AND AMPHOTERICIN B ON *CANDIDA ALBICANS* BIOFILMSLeite, L.D.P¹, Oliveira M. A. C.¹, Nishime T.M. C.², Kostov K.G.³, Koga-Ito C.Y.¹¹Department of Environmental Engineering/ Science Applied to Oral Health Graduate Program, Institute of Science and Technology, São Paulo State University (UNESP), São José dos Campos, Brazil.² Leibniz Institute of Plasma Science and Technology (INP, Greifswald), Greifswald, Germany.³Department of Physics, Faculdade de Engenharia de Guaratinguetá, São Paulo State University (UNESP), Guaratinguetá, Brazil.

1. Introduction

Antifungal resistance represents a great challenge in the medical areas. Amphotericin B is a broad-spectrum antifungal drug against a variety of pathogenic fungi, but its adverse effects limit its clinical use. For this reason, the search for new alternative methods is necessary. The aim of this project is to study the effects of the association of cold atmospheric plasma (CAP) and Amphotericin B on *Candida albicans* biofilms.

2. Experimental

Candida albicans SC 5314 (wide type reference strain) standardized suspension were obtained. Then, 24h *C. albicans* biofilms were formed in 96 wells microplates using RPMI broth + 2% glucose. After incubation, biofilms were exposed to the treatments. The associations between CAP and the Amphotericin B were done according to the following experimental groups: i) amphotericin B followed by CAP (A/CAP), and ii) CAP followed by the amphotericin B (CAP/A). Treatments with CAP and amphotericin B separately were also tested for comparative purposes. The exposure time to CAP and amphotericin B was 2.5 min. For amphotericin B at reductions of 75% (2.5 µg/ml) and 50% (3.75 µg/ml) the minimal inhibitory concentration were used. Helium plasma jet (99.5% purity, 2.0 slm) was excited by using a low-frequency high-voltage signal with 32 kHz frequency and power of 1.0 W. The distance between nozzle and biofilm surface was kept fixed at 1.5 cm. The number of colony forming units was determined by plating method. Non-exposed control was included. The experiments were performed in triplicate in three occasions. Data was compared by One-way ANOVA and post hoc Tukey (5%).

3. Results and Discussions

Both CAP and amphotericin B (2.5 µg/mL and 3.75 µg/mL) reduced significantly the viability of *C. albicans* biofilms. When CAP was associated to amphotericin B at 2.5 µg/mL, no synergic effect was observed. In fact, CAP alone was more effective than when associated with amphotericin B. Similarly, no synergic effect of amphotericin B at 3.75 µg/mL and CAP was detected. The application of CAP alone was more effective against *C. albicans* biofilms than in combination with amphotericin B, suggesting that the application of CAP may be a promising alternative for the treatment of fungal infections.

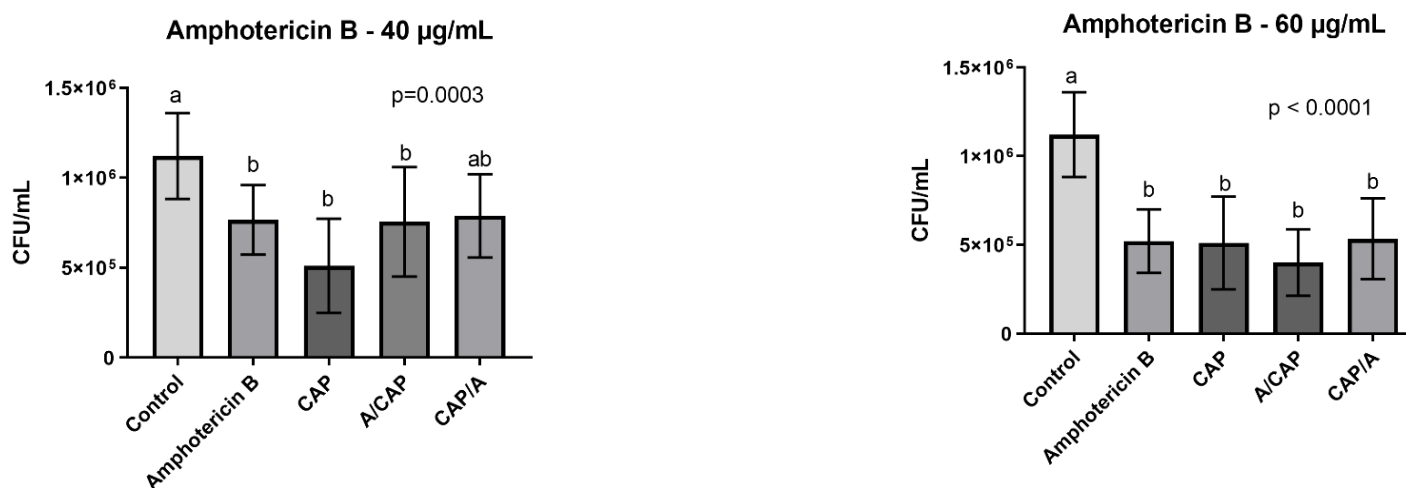


Fig. 1. Viability of *C. albicans* biofilm, expressed in values of colony forming units per milliliter (cfu/ml, mean and standard deviation), treated with CAP (2.5 min), amphotericin B (2.5 µg /ml and 3.75 µg/ml), CAP followed by amphotericin B (CAP / A), amphotericin B followed by CAP (A / CAP) and untreated negative control group.

[1] Quindós, G.; Gil-Alonso, S.; Marcos-Arias, C.; Sevillano, E.; Mateo, E.; Jauregizar, N.; Eraso, E. Therapeutic tools for oral candidiasis: Current and new antifungal drugs. *Med. Oral Patol. Oral Cir. Bucal* 2019, 24, e172–e180.

[2] Borges, A.C.; de Moraes Gouvêa Lima, G.; Mayumi Castaldelli Nishime, T.; Vidal Lacerda Gontijo, A.; Kostov, K.G.; Koga-Ito, C.Y. Amplitude-modulated cold atmospheric pressure plasma jet for treatment of oral candidiasis: In vivo study. *PLoS One* 2018, 13, 1–12, doi:10.1371/journal.pone.0199832.

Acknowledgments

Funding by FAPESP 2019/05856-7 and CNPq (308127/2018-8). This study was financed in part by the Coordenação de Aperfeiçoamento de Pessoal de Nível Superior – Brasil (CAPES) – Finance Code 001.

THE EFFECT OF SYNERGISTIC TREATMENT OF VITAMIN C AND COLD ATMOSPHERIC PLASMA ON THE INHIBITION OF *Candida albicans* BIOFILM

Milhan, N.V.M.*¹, Sampaio, A.G.¹, Vegian M.R.C¹, Mui, T.S.M.², Kostov, K.G.², Koga-Ito, C.Y.¹

¹Department of Environmental Engineering/Oral Biopathology Graduate Program, Institute of Science and Technology, São Paulo State University (UNESP), São José dos Campos, Brazil.

²Department of Physics, Faculdade de Engenharia de Guaratinguetá, São Paulo State University (UNESP), Guaratinguetá, Brazil.

1. Introduction

Candida albicans is commensal but also opportunistic fungus that may cause disease in the presence of predisposing factors, leading to local or invasive candidiasis [1]. A previous study demonstrated that cold atmospheric plasma (CAP) could significantly reduce the viability of *C. albicans* biofilms after 5 minutes of exposure [2]. Interestingly, another study showed that 15 min of pretreatment with vitamin C enhances the bactericidal effect of CAP [3]. The aim of this study was to evaluate if the pretreatment with vitamin C could improve the antifungal effect of CAP against *C. albicans*, which could lead to reduced CAP exposure time.

2. Experimental

Suspension of 10^6 cells/ml of *C. Albicans* (ATCC 18804) in RPMI 1640 medium (2% glucose) was distributed in 96-well microplates (200 μ L/well). After pre-adhesion, the plates were incubated for 24 h at 37°C for the formation of biofilms. The vitamin (Vit) C was prepared in distilled water (dH₂O) at concentrations of 90 and 180 mM and the pretreatment was performed by 15 minutes, followed by CAP exposure. The pretreatment with the vehicle (dH₂O) was also analyzed, followed or not by CAP exposure. Plasma jet was produced by electric discharge in helium (99.5% purity) with 2.0 SLM gas flow rate. CAP was applied at a distance of 1.5 cm for 2.5 min. After treatment of biofilms, serially diluted microorganisms were plated on Sabouraud dextrose agar and incubated at 37°C for 24 h. The results were expressed as colony forming units per mL (CFU/mL), after three independent experiments conducted in triplicate. The data were analyzed by Kruskal-Wallis test, with a significance level of 5%.

3. Results and Discussions

A statistically significant reduction ($p < 0.05$) was observed in the groups in which the pretreatment with vitamin C or distilled water were performed, followed by CAP exposure (Figure 1). The group Vit C 90 mM + CAP presented the lowest number of colonies. The treatment only with vitamin C or distilled water showed no response while the group treated only with CAP for 2.5 min promoted more than one log of reduction, although there was not statistical difference to untreated control group. The findings indicate that the pretreatment with vitamin C could potentiate the effect of CAP against *C. albicans*. However, additional investigations are required once the association between the vehicle and CAP also was positive.

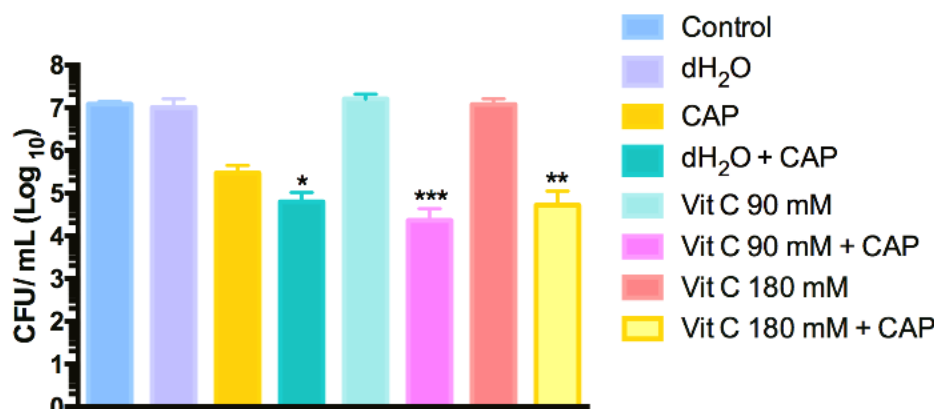


Fig. 1. Colony forming units per mL (CFU/mL) of *Candida albicans* biofilms (* $p < 0.05$; ** $p < 0.01$; *** $p < 0.001$ indicate statistical difference to untreated control group).

4. References

- [1] Pappas P.G., Lionakis MS, Arendrup MC, et.al., Nat Rev Dis Primers, 4:18026, (2018).
- [2] Borges A.C., Lima GMG, Nishime TMC, Gontijo AVL, et.al., One, 13, 6:e0199832, (2018).
- [3] Helgadóttir S, Pandit S, Mokkapati VR, Westerlund F, et. al., Front Cell Infect Microbiol., 7:43, (2017).

Acknowledgments

Funding by FAPESP (São Paulo Research Foundation, 2021/00046-7 and 2019/05856-7) and CNPq (National Council for Scientific and Technological Development, 405653/2016-6 and 308127/2018-8)

Pd ESPECIES DISPERSED IN PAN FILMS AND FIBERS: IMPORTANCE OF EMULSION PRODUCTION METHODS

Ana Neilde Rodrigues da Silva^{1,2*}, Maria Lúcia Pereira a Silva^{1,2}, Esteban Rosim Fachini³, Sebastião Gomesdos Santos Filho²

¹ Faculty of Technology of São Paulo, CPS, Brazil

² School of Engineering, University of São Paulo, Brazil

³ University of Puerto Rico, Rio Piedras, USA

1. Introduction

The production of nanofibers decorated with palladium is a hot spot field in nanotechnology nowadays. The importance of such product relies on palladium properties as catalytic material and nanofibers as an easy way of obtaining high area/volume ratio, a paramount characteristic for catalytic or adsorbent material. Furthermore, electrospinning is an easy way of nanofiber productions and sensors devices and/or miniaturized analytical instruments development [1]. Therefore, this work aims the evaluation of Pd/Polyacrylonitrile (PAN) films and also the surface of electrospun nanofibers.

2. Experimental

6% polymeric emulsions were obtained stirring polyacrylonitrile (PAN) with N,N Dimethylformamide (DMF). 10% w. of PdCl₂ was added at different steps of emulsion preparation. A pure emulsion was also produced for comparison. Films were obtained by casting and nanofibers were electrospun over silicon substrate using a homemade setup. Surface characterization used X Ray photoelectron spectroscopy (XPS).

3. Results and Discussions

It is well known that DMF complexes Pd ions [1] and entangles on PAN molecules during dissolution. Therefore, depending on production method, infrared spectra show PAN molecule along with DMF and Pd/DMF complex. Thus, four different approaches for Pd/PAN emulsions production were analyzed and XPS analyses were carried out to unravel Pd surface mechanisms on fibers and its interactions. For all films and fibers, the flat baseline indicates a clean surface. Carbon peaks are symmetrical and do not show meaningful chemical shift except if competition between Pd complexation and DMF envelopment of PAN molecule is present, which leads to chemical shift on higher binding energy. This phenomenon is less evident on fibers probably due to solvent vaporization during electrospinning. Although Pd peaks in films and fibers are similar, there are quite different spectra depending among the emulsion (Fig. 1). The competition for Pd complexation with DMF molecules resulted in high chemical shift, even in films, which was expected to show less stress due to deposition (Fig. 1D). Emulsions which present Pd atoms already complexed before the addition of PAN reactant, the peaks are consistent with the appearance of Pd(0) and Pd(II) due to PdCl₂ reactant. Therefore, this data seems to indicate that these emulsions present a freer Pd atom if compared to the other options. On such condition, during annealing it will not be expected clusterization of such atoms, ideal condition for catalysis. Since XPS, a surface analysis, shows composition on approximately 5 nm depth, the clear peaks found on the spectra indicate not only high Pd amount on the fiber but also the presence on the surface, which indicates the use of such emulsions on production of catalytic material.

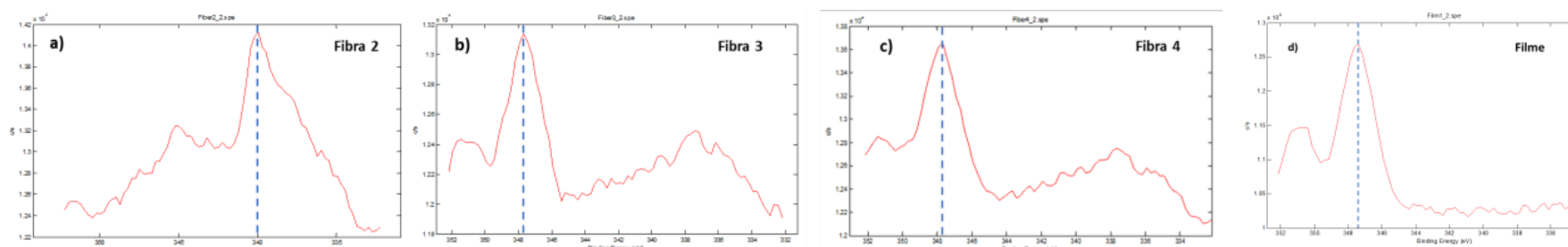


Figure 1: Details of the XPS Spectra of a), b), c) fibers and d) film.

4. References

[1] A. N. R. Silva; M. L. P. Silva, S. S. Gomes Fo., Acad. J. Electronics, Telecom and Comp, to be published.

Acknowledgments.

Fapesp and CNPq for financial support.

STUDY OF POLY (LACTIC ACID) FILMS INCORPORATED WITH ATORVASTATIN

Annie Meireles¹; Yasmin dos Anjos Garcia¹; Debora Baptista Pereira², Roberta Helena Mendonça³, Beatriz Ferreira de Carvalho Patrício⁴,
Helvécio Vinícius Antunes Rocha⁴

¹Undergraduate students from the Department of Chemical Engineering at UFRRJ ²Graduate Student of the Postgraduate Program in Chemical Engineering at UFRRJ ³Professor of the Postgraduate Program in Chemical Engineering at UFRRJ

⁴Micro and Nanotechnology Laboratory at Farmanguinhos - FIOCRUZ

Materials Development Laboratory (LADEMAT) DEQ-UFRRJ - Federal Rural University of Rio de Janeiro.

1. Introduction

Synthetic polymers such as poly-lactic acid (PLA) have been widely used in tissue engineering as they provide good mechanical support and a good biological basis for tissue development [1]. The present study aimed at the synthesis of PLA films incorporated with atorvastatin and its characterization. Recent studies assess that PLA obtained by direct polycondensation of lactic acid results in polymers with low molar mass, but it becomes interesting when applied in controlled drug release systems (SLFs) [2]. The effect of statins such as atorvastatin (ATV) on tissue repair in animals has been investigated in numerous studies, showing their anti-inflammatory and antioxidant actions, on vasodilation, neoangiogenesis, and in the reduction of endothelial dysfunction.

2. Methodology

The production of PLA/ATV films was carried out using the solvent casting technique, where a PLA solution at a concentration of 10% (m/v) was prepared. For this, 5 g of the polymer were solubilized in 50 ml of chloroform. The system was kept under reflux for two hours using a digital magnetic stirrer (LAB1000, model LM-MS-H280Pro). In preparing the PLA/ATV films, 40 mg (F304), 80 mg (F408), 120 mg (F512), and 160 mg (F616) of drug were used. Afterward, the samples were analyzed in a conventional scanning microscope with a tungsten filament (Hitachi model TM3000, IF-UFRRJ).

3. Results and Discussions

With the images, it was possible to observe that with the increase in the concentration of ATV, the dispersion of the drug was not as efficient. From 120 mg, shown in the proportion of 160mg, there are more drug accumulation points, which can occur in unwanted places, which can alter the process of drug release. The solvent casting technique using PLA was easily reproducible and the F304 and F408 films showed more uniform and homogeneous surfaces, evidencing the good interaction between drug and polymer, a necessary effect for application in SLFs.

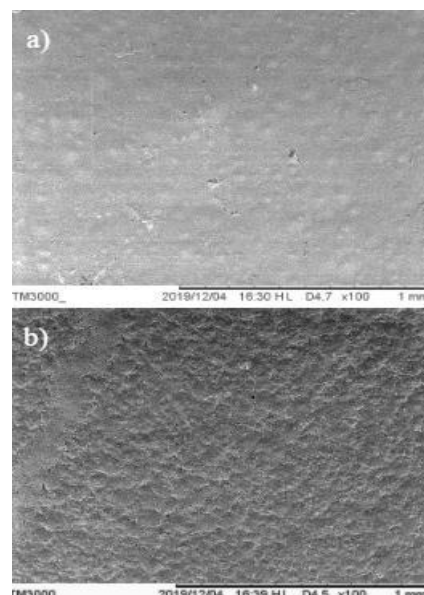


Fig. 1. Scanning electron microscopy images of the surface of the films a) F304; b) F408.

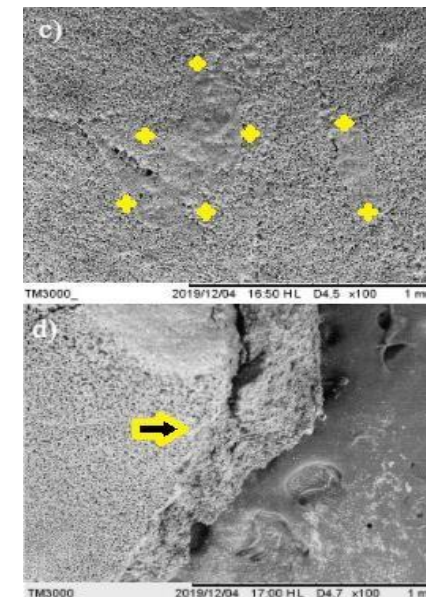


Fig. 2. Scanning electron microscopy images of the surface of the films a) F512; b) F616.

4. References

[1]- GUILAK, Farshid; [et al.]. *Functional tissue engineering*/editors. Springer-Verlag New York, Inc (2003)
[2]- Auras R, Harte B, Selke S. *An overview of polylactides as packaging materials*. *Macromol Biosci* 4(9):835–64(2004).

OPTICAL TRANSMITTANCE OF TiO_2 AND TiN MULTILAYER THIN FILMSAline Medeiros Morais^{1*}, Luís C. Fontana¹, Julio César Sagás¹, A. A. C. Recco¹, Joel Stryhalski²¹*Laboratory of Plasmas, Films and Surfaces - Santa Catarina State University, Joinville, SC, Brazil*²*Federal Institute of Santa Catarina, Jaraguá do Sul, SC, Brazil***1. Introduction**

The application of thin film low-emissivity coated glass in architectural windows has received much attention due to its energy-saving performance. Covering the glass surface with a low-emittance material is possible to block a significant amount of the radiant heat transfer to the intern and, thus, lowering the total heat flow through the glass [1]. The optical requirements of a heat mirror are high transmittance in the visible region, 380–760 nm in wavelength, and high reflectance in the infrared [2].

2. Experimental

Multilayer thin films composed by titanium dioxide (TiO_2) and titanium nitride (TiN) were deposited by magnetron sputtering triode technique on glass substrate. The sputter target was a metallic titanium disc (99.5% purity) and the working gas was a mixture of argon and just one reactive gas: oxygen or nitrogen. The plasma was powered by a pulsed power supply (Pinnacle-Plus/Advanced Energy). Before depositing of the films, the soda-lime glass samples were washed with isopropyl alcohol, in ultrasound.

3. Results and Discussions

The optical characteristics were analyzed by transmittance spectra of films deposited onto glass substrates (Fig. 1). Film thickness and roughness are shown in Table 1. The transmittance spectrum of glass coated with single TiO_2 film show little transmittance variation compared to uncoated glass. Single TiN film coated glass has the greatest variation in the transmittance spectrum. Glass coated with TiN/ TiO_2 /TiN/ TiO_2 multilayer film has a transmittance spectrum intermediate between glass coated with single TiN and TiO_2 film. TiO_2 /TiN/ TiO_2 multilayers films on glass substrate have been investigated because of the optical properties stability and rather manufacturing process using a sputtering deposition [3]. TiO_2 is known to have excellent photocatalytic properties and the top layer maybe expected to work as a photo-catalyst as well as the anti- reflection coating.

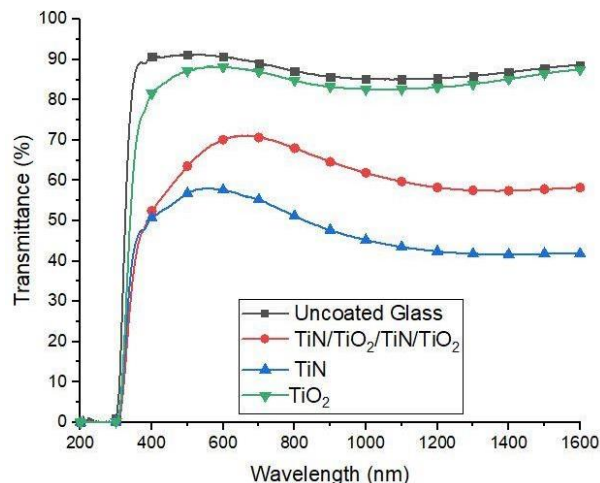


Fig. 1. Transmittance spectra of TiO_2 , TiN, TiN/ TiO_2 /TiN/ TiO_2 films deposited onto glass substrates compared to uncoated glass.

Sample	Thickness (nm)	Roughness RMS (nm)
TiO	$4,0 \pm 0,5$	$0,51 \pm 0,03$
TiN	$4,0 \pm 0,5$	$0,58 \pm 0,03$
TiN/ TiO_2 /TiN/ TiO_2	$7,0 \pm 0,5$	$0,55 \pm 0,03$

Tab. 1. Film thickness measurements through x-ray fluorescence dispersive energy spectroscopy (EDX) and roughness measurements by atomic force microscopy (AFM).

4. References

- [1] M. Yuste, R. E. Galindo, S. Carvalho, J. M. Albella, and O. Sánchez, *Appl. Surf. Sci.*, **258**, 1784–1788, (2011).
- [2] M. Tazawa, M. Okada, K. Yoshimura, and S. Ikezawa, *Sol. Energy Mater. Sol. Cells*, **84**, 159–170, (2004).
- [3] M. Okada, M. Tazawa, P. Jin, Y. Yamada, and K. Yoshimura, *Vacuum*, **80**, 732–735, (2006).

Acknowledgments

The authors knowledge the financial and structural support provided by Santa Catarina State University (UDESC), Brazil, and the Brazilian funding agency CAPES.

SARS-COV-2 DATA ANALYSIS ON FOG COMPUTING ENVIRONMENT

Leandro Colevati dos Santos^{1,2*} Maria Lúcia Pereira da Silva^{1,2}, Sebastião Gomes dos Santos Fo.²

¹*Faculty of Technology of São Paulo, Centro Paula Souza, Brazil*

²*School of Engineering, University of São Paulo, Brazil*

1. Introduction

Last year, with the surge of COVID pandemic, global efforts have been recruited to face the new disease. Among the needs, it was essential to understand the influence of comorbidities for the worsening of the disease. Therefore, the main stakeholders agreed to reveal their data for analysis by the scientific community, as was done by clinical analysis laboratory. However, due to the huge amount of disperse not structure data, some tool should be developed.

Among others, one of the main technologies that have been automated is the use of sensors to measure several parameters; this replacement of manual measurements not only adds precision but also reduces the time to obtain answers, i.e. increases production and facilitates decision-making actions. Nonetheless, such amount of data, lead to different approaches, one of them being fog computing [1]. Therefore, this work aims the use of computational resources for analysis applied specifically applied to the pandemic issue.

2. Experimental

The analyzed data were made available in FAPESP's Shared Database. Several clinical analysis laboratory institutes have taken automated measurements with volunteers who might, or might not, be infected. Most of them started to carry out blood analysis with people infected by the virus to better understand the behavior of the virus in the human body and possible impacts of comorbidities. An advantage of such analysis is the automation of data collection [2]; however, this data may not be adequately available for future or second-order studies, being restricted to reports, spreadsheets or other internal documents. The analyzed universe comes from a file with approximately 6 million clinical exams of various types. The provided tool for analysis was part of the cloud computing structure in enterprise services bus (ESB) structure, already contemplated with file analysis services in several formats and remote communication service with sensors [3]. The provided services were the analysis and decoding of files, storage and query data, but no real-time analysis was performed or required.

3. Results and Discussions

The available data was structured; therefore, the chosen storage service was connected to a SQL-type database. Preliminary data explained that a potentially fatal comorbidity for the infected would be morbid obesity, therefore, a service was designed that, in low latency, would bring a second-order analysis that would be a quick check, if in a group of infected, the high glycemic rate, blood glucose greater than 100, favored contamination. The introduction of a data analysis service at the ESB did not expect a positive or negative response to the hypothesis, but rather a quick response that would allow further analysis or new attempts.

The analysis offered by the ESB showed 365 hyperglycemic infected patients, which means that it is not possible to directly associate the fact that having a blood glucose rate higher than 100 makes the individual more susceptible to infection because the result showed similar values for those who did not.

Hyperglycemic, however, this analysis brought, from the universe of data, the analysis in less than 1 second and only the amount of hyperglycemic infected in approximately 300 milliseconds. Therefore, we can consider that associating measures that generate large amounts of data and that, increasingly, need low latency, can be associated with cloud computing framework for its advantages when compared to cloud computing. Thus, the structured data, measured from clinical laboratories, can offer the possibility of analyzing second-order effects on human health indicators, with low latency and guide new fast decision-making.

4. References

- [1] Santos, L.C. et al, Anais do XXI Engema (2019).
- [2] Silva, C. C. M. et al., Proceedings of ISTI/SIMTEC, 237-241 (2018).
- [3] Santos, L.C. et al, RBAV e-ISSN 1983-4047 (2021).

Acknowledgments

FAPESP and CNPq for data and financial support.

STUDY OF THE INFLUENCE OF TEMPERATURE ON BORIDING Ti6Al4V ALLOY

Felipe Lopes Fonseca da Silva^{1*}, Rafael Roberto Pavani², Otávio Augusto de Moraes Rosa Santos³, Marcos Dorigão Manfrinato⁴ and Luciana Sgarbi Rossino⁵^{1,2,4,5}*Federal University of São Carlos – Sorocaba Campi, Sorocaba, SP, Brazil*^{3,4,5}*Sorocaba Technological College, Sorocaba, SP, Brazil***1. Introduction**

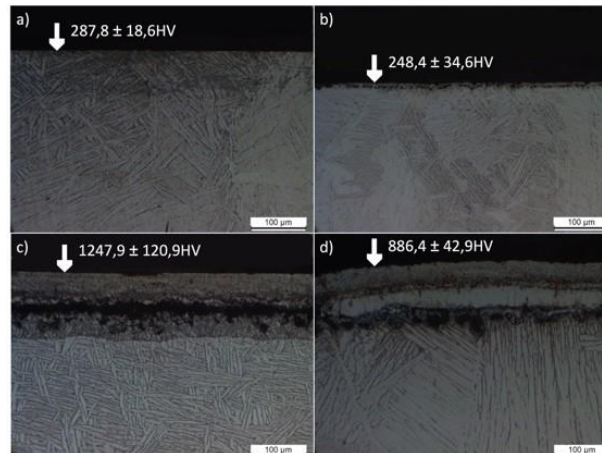
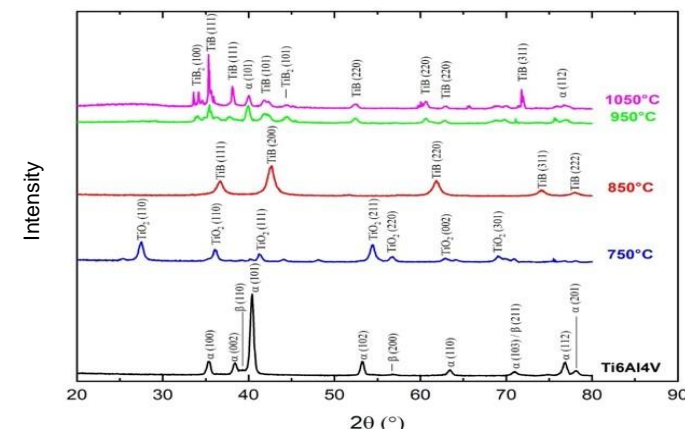
Boriding is a thermochemical treatment aimed at the surface hardening of the material, where boron atoms are introduced through the diffusion process of the element in the substrate. The diffusion process occurs in high temperature, usually between 800 and 1100°C, and with a treatment time of 1 to 12 hours. Diffusion is carried out by transferring the boron found in the boronizing agent to the substrate. Boronizing agents can be provided in solid, powder and paste form, liquid format through molten salts, gaseous format through boron trichloride, diborane and boron trifluoride. The solid boriding process is considered one of the best performance processes in economic, technological, and toxicological terms [1]. The Ti6Al4V Alloy has several applications, mainly in the biomedical and aerospace areas, due to its excellent mechanical properties. But surface treatments are still needed in this alloy, seeking ideal parameters for its application in service [2]. This work aims to obtain the boron layer in the ti6al4v alloy through solid boriding.

2. Experimental

In this work, the Ti6Al4V alloy was cut into cubes (10x10x10mm) and prepared metallographically through sanding and polishing, aiming at a regular surface for the surface treatment. The samples were placed in the oven, inside a crucible, covered with the boronizing agent Ekabor 2A, and the treatment was carried out at 750°C, 850°C, 950°C and 1050°C for 3 hours. The samples were analyzed by metallography under an optical microscope with 200x, surface microhardness with a load of 0,025kgf for the substrate, 750°C and 850°C, and 0,1kgf for 950°C and 1050°C, and x-ray diffraction with Cukα font and $\theta - 2\theta$ sweep mode.

3. Results and Discussions

At 750°C (Figure 1.a) there was no boron diffusion due to the low temperature, confirming with the surface microhardness test, confirmed by the XRD (Figure 2), which did not detect any typical boriding phase formation. The formation of the layer only occurred at temperatures of 850°C (Figure 1.b) extremely thin and not detected in the surface microhardness but found in the XRD with the presence of phases formed by TiB. At 950°C (Figure 1.c) and 1050°C (Figure 1.d) it was possible to identify and perform the measurements of the layer with thickness of $58.929 \pm 2.799\text{ }\mu\text{m}$ and $81.501 \pm 5.883\text{ }\mu\text{m}$, with high microhardness, confirmed in the XRD with the presence of phases of TiB and TiB₂. It was also possible to observe the pores of the diffusion zone, due to the easy binding of oxygen to titanium, preventing the regular adhesion of the layer to the substrate, observed in XRD with the presence of TiO₂.

**Fig. 1. Metallography and Surface Microhardness. a) 750°C, b) 850°C, c) 950°C and d) 1050°C.****Fig. 2. X-ray Diffraction****4. References**

[1] GUNES, I.; ULKER, S.; TAKTAK, S. Kinetics of plasma paste boronized AISI 8620 steel in borax paste mixtures. *Protection of Metals and Physical Chemistry of Surfaces*, [s. l.], v. 49, n. 5, p. 567–573, 2013.

[2] INAGAKI, I., SHIRAI, Y., TAKECHI, T., ARIYASU, N. Application and Features of Titanium for the Aerospace Industry. *Nippon Steel & Sumitomo Metal Technical Report*. n° 106, p. 22-27, 2014.

Acknowledgments

I thank CAPES for the financial assistance and all members of LabTES.

MODELING WITH OPTICAL EXPERIMENTAL PROCEDURES OF THE CHOKED FLOWEFFECT IN VACUUM SYSTEMS

Iris del Carmen Claudino Flores¹, Eduardo Acedo Barbosa², Francisco Tadeu Degasperi³
^{1, 2, 3} Faculdade de Tecnologia de São Paulo

1. Introduction

The refractive index is widely used for analysis of results since it is a basic optical parameter of materials and has great precision, so it is extremely important in several areas of science and technology, mainly due to its non-interfering character. The refractive index of a gas is dependent on its density, so it is possible to measure the pressure of the gas using this parameter [1]. Thus, the current project aims to experimentally study the variation in the refractive index of light that interacts in a gas by the pressure variation (variation of gas density) in a vacuum chamber, seeking to accurately determine the start of the choked flow effect in a gas, or when the throughput is no longer constant, which can be useful in the calibration of equipment that make up vacuum systems.

2. Experimental

The experiment will consist of an optical analysis of the gases that will pass through the vacuum chamber, this method being based on light interference, the interferometer to be built should be sensitive to the refraction index of the gas (Fig. 1), where initially we will use a Michelson interferometer. Then, an experimental relation between the refractive index of a gas and its pressure will be established, which will be later compared with theoretical expressions. During the experiment, the fringes pattern presented in the bulkhead and its variations will be analyzed. The vacuum chamber to be built will be made of AISI 304L stainless steel and will have two visors on the sides through which the interferometer light beam will pass, as shown in figure 2, that shows the arrangement of the vacuum system.

3. Results and Discussions

It is expected to obtain a significant variation in the fringe pattern on the bulkhead, we can then accurately determine the moment when the flow becomes choked, being useful later for the calibration of vacuum systems. The experimental arrangement and the data obtained will also be later used for mathematical modeling for conductance in the vacuum system for different cross-sections of a tube, which, when shown to be effective, can bring advances to vacuum technology, serving as a further development of existing studies on the behavior of gases in a flow process, mainly in relation to the choked flow effect, a vast topic and of great importance mainly for areas that include fluid mechanics.

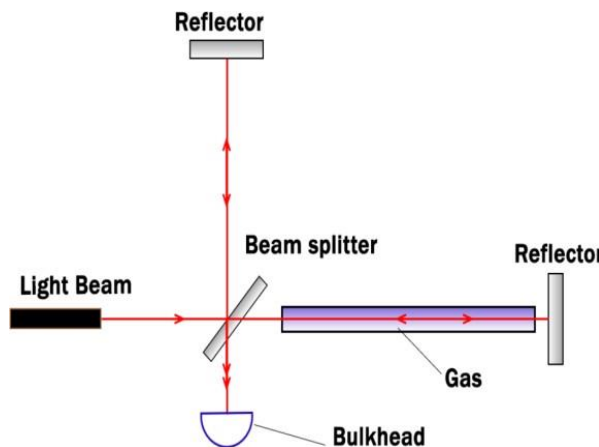


Fig. 1. Optical System Arrangement

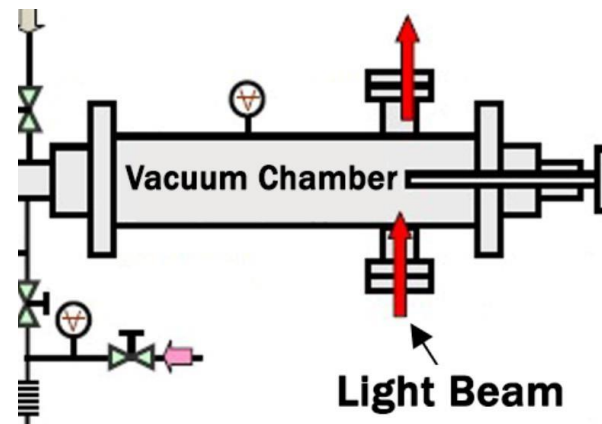


Fig. 2. Vacuum System Arrangement.

5. References

[1] R. G. Cerqueira, Medição e Análise Detalhada da Blocagem de Gás[...]. 2016. 41 f. TCC – Curso de Materiais, Processos e Componentes Eletrônicos. FATEC-SP, 2016.

Acknowledgments

To my teachers and my family for their support and to CNPq for the PIBIC scholarship.

ROLE OF Ar_2^+ AND Ar_2^m IN ARGON PLASMA: A GLOBAL MODEL STUDY

Júlia Karnopp^{1*}, Julio César Sagás², Rodrigo Sávio Pessoa¹

¹Instituto Tecnológico de Aeronáutica – São José dos Campos

²Universiade do Estado de Santa Catarina - Joinville

1. Introduction

Argon plasma is widely used for a range of application in science, industry, medicine, and technology. The inert argon gas has an excellent thermal performance and low cost and is used for plasma generation in laboratory at low and high pressure [1]. The gas pressure affects the plasma chemistry changing the electron temperature, species density, and reaction rates. For low pressure argon plasma the main species present in discharge volume are argon in ground state (Ar), argon ion (Ar^+), and excited (Ar^r , Ar^p) and metastable (Ar^m) atoms. However, as the gas pressure increases, other species become relevant in the plasma chemistry such as the molecular ion or dimer (Ar_2^+) and molecular metastable or excimer (Ar_2^m).

The modelling of the plasma environment is essential to understand the plasma chemistry and the influence of process parameters. In this work, a (zero dimensional) global model [2] for inductively coupled plasma (ICP) of argon was developed for study how the plasma species are influenced by the gas pressure, specifically the species Ar_2^+ and Ar_2^m .

2. Methodology

In this model, eight species were considered, electrons, Ar, Ar^+ , Ar^r , Ar^p , Ar^m , Ar_2^+ and Ar_2^m , and a reaction set with 81 reactions that includes electrons impact reactions, heavy species reactions and three body reactions. The Maxwell-Boltzmann distribution was considered for electrons. The simulations were performed for a pressure range of 2 mTorr to 10 Torr. The software Comsol Multiphysics was used to solve the problem.

3. Results and Discussions

Figure 1 shows the density of species as function of gas pressure. The specie Ar_2^m is produced by three collisions between Ar and the species Ar^r , Ar^p , and Ar^m . Due to the increase in Ar with increasing pressure, Ar_2^m density also increases, since the rate constants and the other species density does not vary significantly. The Ar_2^+ density is initially almost constant and around 0.1 Torr increases with gas pressure. Below 0.1 Torr, Ar_2^+ is produced mainly by the reaction $2\text{Ar}^m \rightarrow e + \text{Ar}_2^+$ whose reaction rate has constant behavior like Ar^m . For pressures greater than 0.1 Torr, the major contribution to the creation of Ar_2^+ is the reaction $2\text{Ar} + \text{Ar}^+ \rightarrow \text{Ar} + \text{Ar}_2^+$, which increases proportionally with Ar and Ar^+ density.

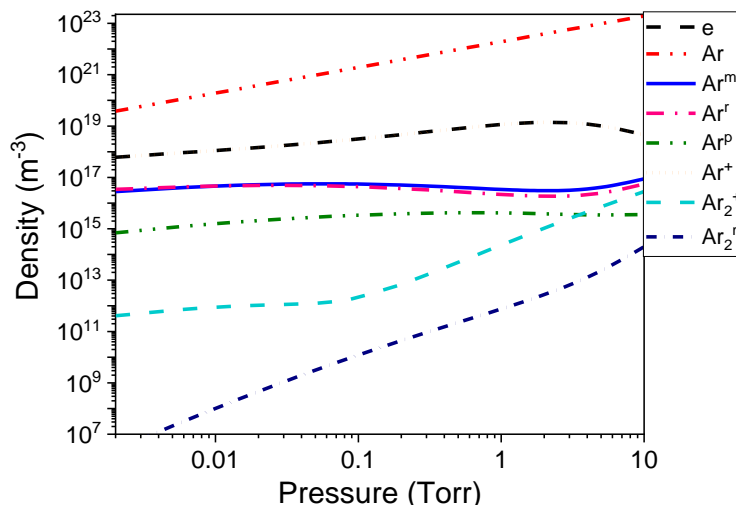


Fig. 1. Density of all species as function of gas pressure.

4. References

[1] R S Pessoa et al. Chemistry Studies of Low Pressure Argon Discharges: Experiments and Simulation. In: Argon: Production, Characteristics and Applications (2013).
 [2] L. L. Alves, A. Bogaerts, V. Guerra, M. M. 2018 Turner, Plasma Sources Sci. Technol. 27 023002

Acknowledgments

Júlia Karnopp thanks CAPES (Finance Code 001) for the scholarship.

DESIGN OF TENSIMETRIC CAPSULES PROTOTYPE FROM DIFFERENT COMPOSITIONS.

Jônatas de O. Sousa^{1*}, Belmira B. Lima-Kuhn¹, Daniel Fonseca de Carvalho², Antonio R. Bigansolli¹¹Departamento de Engenharia Química, Instituto de Tecnologia, UFRRJ, Seropédica.²Departamento de Engenharia, Instituto de Tecnologia, UFRRJ, Seropédica.

1. Introduction

Ceramic materials are composed of inorganic raw materials that are powdered, which after shaping and burning become solid objects with different applications and uses. The main raw material used in the production of ceramics is clay, which is a natural material and is generally made up of hydrated silicates, iron, magnesium and aluminum [1]. The practice of irrigation in Brazil has been done without proper management. The survey of the soil moisture level in the region of greater root absorption has been recommended as a favorable option for soil monitoring. The tensiometer is a device used to measure the tension at which water is held by soil particles [2]. The present work aimed to prepare the formulations and specimens of tensiometric capsules used in various areas with the aim of establishing viable standards for monitoring soil moisture.

2. Experimental procedure

The material used was yellow clay extracted in the municipality of Seropédica. The clay went through a drying process and comminution in the ball mill. The resulting material was sieved and 220 mesh was the chosen particle size. The clay was hydrated with water at room temperature, calculating 8% by weight and mixed with the selected materials presented in the table below, together with the prepared formulations indicating the compositions. To make the specimen, an adapted 10 mL syringe was used. With the aid of a metal rod, the interior part of the specimen was made, which consists of a 4 cm vertical space without material indicated in figure 1.

3. Results and discussion

The result of the porosity test showed a result in percentage that varies between 9.78% and 15%. Sample S₃ showed the least satisfactory result with a loss of 1% of porosity compared to the standard sample S₁. The S₂ sample showed a 5% improvement compared to the standard sample. This last sample cited was composed of corn starch and clay, with corn starch as the main pore-forming source. The clay proved to be efficient in the production of specimens with easy moldability and presented a reddish color at the end of sintering.

Materials	S ₁	S ₂	S ₃	S ₄	S ₅	S ₆
Clay	70	70	70	70	70	70
Potato starch	30	-	15	-	10	-
maize starch	-	30	-	15	-	10
Feldspar	-	-	-	-	10	10
White kaolin	-	-	15	15	10	10

Tab. 1. Proportion of Samples.

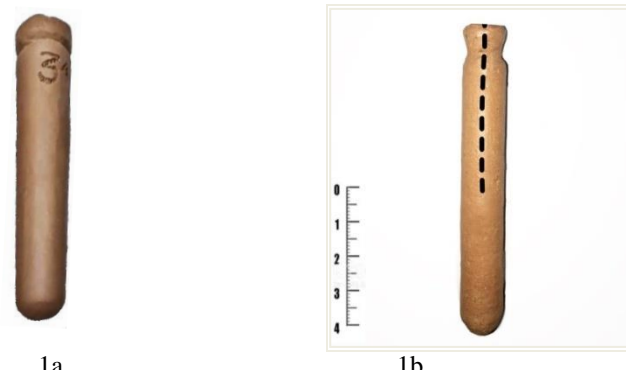


Fig. 1. Sample before (1a) and after sintering (1b).

4. References

[1] SANTOS, P. S; SANTOS, H. S, Ciência e Tecnologia de Argilas, 2 ed., Capítulo 1, São Paulo – BR, Editora Edgard Blucher LTDA, 1989.
 [2] AZEVEDO, J. A.; SILVA, E.M.; Tensiômetro: Dispositivo prático para irrigação. Circular técnica nº 001, ISSN EMBRAPA. Planatilda, DF 1999.

Natália de Macedo do Lago¹, Belmira Benedita de Lima Kühn¹ and Tessie Gouvêa da Cruz Lopes¹¹Universidade Federal Rural do Rio de Janeiro, Seropédica, RJ Brasil

1. Introduction

In this work, the characterization of granite particles that will be used as load in epoxy resin composites was performed, regarding their size and shape parameters using non-destructive tests. From the images captured by optical microscopy, a characterization methodology was proposed based on image processing and analysis associated with statistical methods. The images obtained were analyzed and processed with the aid of the public software ImageJ.

2. Experimental

To obtain the granite particles, a stone lent by Marmoraria Jardim LTDA (Cruzeiro-SP) was used as raw material. The stone was manually fragmented using a hammer to facilitate the grinding process. The particles were observed under the microscope and the images were captured using an attached digital camera. The images obtained, were processed and analyzed using the public software ImageJ. The images were segmented in order to separate the objects of interest (granite particles). For this, they were segmented using thresolding (ImageJ program) with the levels that highlighted the particles. With the plugin "Analyzer Particle" size (area, Feret diameter) and shape (circularity, aspect ratio and shape factor) parameters were extracted.

3. Results and Discussions

Images were characterized (Figure 1 [(a) - (b)]) for processing and analysis of the parameters to be extracted. Based on the size and shape related parameters that were calculated (Figure 2) the results indicate a heterogeneity in the distribution of the results, indicating that the particles are not asymmetric and spherical, but tend to be oval possessing maximum roundness, i.e. they have no indentations (Figure 3).

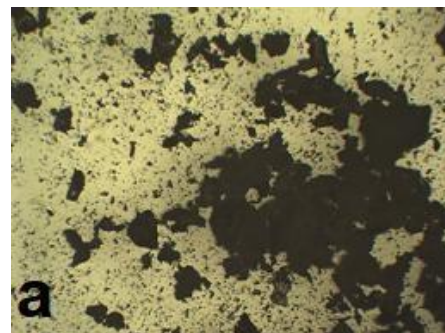


Fig. 1. (a) Granite particles obtained by optical microscopy.

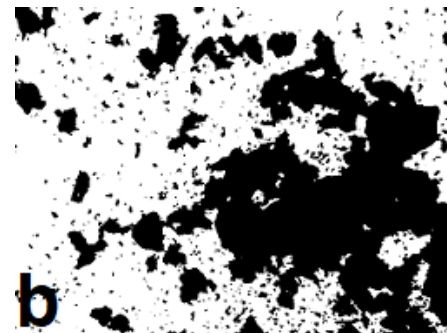


Fig.1 (b) Segmented image and group of aggregated particles.

Parameters	Average	Standard Deviation	Maximum	Minimum
Area (μm^2)	100	180	100	10
Feret Diameter (μm)	40	110	85	10
Circularity (CIRC)	0,84	0,16	1	0,29
Aspect Ratio (AR)	1,59	0,51	1,94	1
Roundness (A)	0,67	0,17	0,98	0,11

Fig 2. Results of the granite particle characterizationparameters.

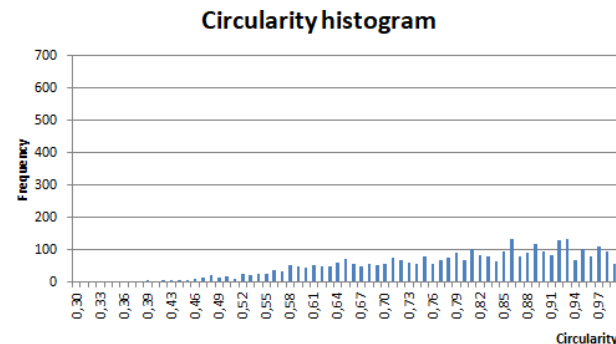


Fig. 3. Circularity histogram of the granite powderparticles.

4. References

- [1] Atkinson, H. V. & Shi, G. Characterization of inclusions in clean steels: a review including the statistics of extremes methods. *Progress in Materials Science* 48:457–520, (2003).
- [2] Pawar, M. J., Patnaik, A. & Nagar, R. Investigation on mechanical and thermo-mechanical properties of granite powder filled treated jute fiber reinforced epoxy composite. *Polymer Composites*. (2015).

MORPHOLOGICAL CHARACTERIZATION USING PROCESSING AND IMAGE ANALYSIS TECHNIQUES ON BENTONITE CLAY PARTICLES MODIFIED BY CHEMICAL ACTIVATION

Tessie Gouvêa da Cruz Lopes^{1*}, Lucas Santos Almeida², Renata Nunes Oliveira¹ and Antonio Renato Bigansolli¹¹Universidade Federal Rural do Rio de Janeiro, Seropédica, RJBrasil²Ex alunoUniversidade Federal Rural do Rio de Janeiro, Seropédica, RJBrasil**1. Introduction**

In this work, the morphological characterization of bentonite particles after acid activation treatment was performed. Using images obtained by SEM, morphological parameters were calculated using image analysis and processing techniques.

2. Experimental

The activation process was carried out with the addition of 100 ml of 6M HCl on the samples (In natura sample) and mechanical agitation was carried out in a magnetic stirrer for 30 minutes (Sample NAC30min) and 1 hour (Sample NAC1h). They were cooled to room temperature and then washed with distilled water until reaching the range $5 < \text{pH} < 6$. Then they were subjected to drying for 36 hours. After drying, they were disaggregated and submitted to characterization tests by SEM and the images obtained were processed to extract morphological parameters from the particles.

3. Results and Discussions

Based on the results (Table 1), it is observed that the particles had different average sizes as a result of particle fractionation. Roundness values indicate elongated particles for different treatment times.

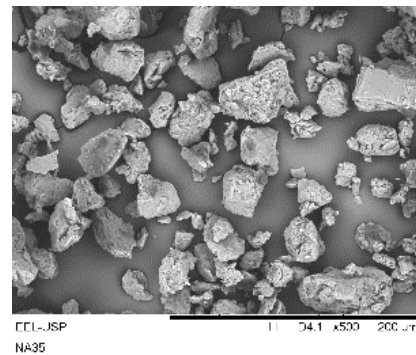
**Fig. 1. Sample of in natura bentonite.**

Image of bentonite particles characterized by SEM before HCl treatment.

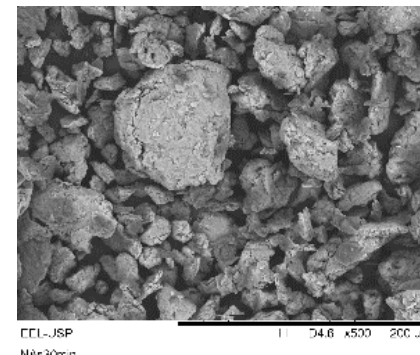
**Fig. 2. Bentonite sample treated for 30min.**

Image of bentonite particles characterized by SEM after treatment with HCl for 30min.

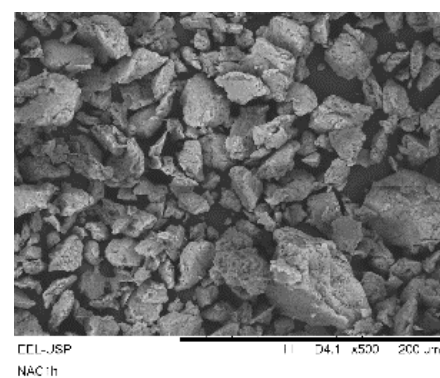
**Fig. 3. Sample of bentonite treated for 1h.**

Image of bentonite particles characterized by SEM after treatment with HCl for 1h.

Samples	Feret Diameter	Circularity
<i>In natura</i>	33,981	0.682
<i>Treatment 30min</i>	22.433	0,669
<i>Treatment 1h</i>	6.502	0.633

Fig. 4. Morphological characterization result.

Table 1 presents the results for the size and shape parameters of bentonite particles.

4. References

- [1] Almeida, L.S.A, Preparação e caracterização de argilas bentonitas por ativação química, Trabalho Conclusão de Curso, (2017).
- [2] Igathinathane, C et al, Shape identification and particles size distribution from basic shapeparameters using ImageJ, Computers and Electronics in Agriculture (2008).

Acknowledgments

To the School of Engineering of Lorena - USP, Department of Chemistry, and to the Catalysis Laboratory at UFRRJ for the sample characterization tests.

MANUFACTURING AND METROLOGICAL CHARACTERIZATION OF REFERENCE SPECIMENS FOR INDIRECT CALIBRATION OF CHARPY IMPACT TEST MACHINES

Frank Omena de Moura^{1,2}, Carlos Alberto Fabrício Jr.¹, Antônio Carlos M. Garcia¹, Manuel Antônio P. Castanho¹, João Roberto Moro²

¹*Instituto de Pesquisas Tecnológicas de São Paulo*

²*Instituto Federal de Educação, Ciência e Tecnologia de São Paulo*

1. Introduction

The Charpy impact test is the most used when determining the toughness of metallic materials when dynamically requested. Its achievement requires the use of machines and measuring instruments calibrated, in order to obtain reliability and metrological traceability.

Charpy impact testing machines are calibrated using two methods: direct and indirect. The direct method consists of the physical evaluation of the machine, from the measurement of the components and verification of its functioning. The indirect method consists of the machine's functional evaluation through the performance of impact tests, using certified reference specimens, which are manufactured with a pre-assigned nominal energy [1].

These certified reference Charpy specimens are currently provided only by a few international research institutions, among them the *National Institute of Standards and Technology* (NIST) and *Institute for Reference Materials and Measurements* (IRMM).

The purpose of this article is to externalize the development of the methodology and procedure for the fabrication and metrological characterization of reference Charpy specimens, which is being implemented in the Laboratório de Metrologia Mecânica of the business unit in Tecnologias Regulatórias e Metrológicas of the Instituto de Pesquisas Tecnológicas de São Paulo (LMM-TRM-IPT), seeking to meet the technical standards relevant to the production of this reference material and quality. Thus, expanding the laboratory's scope of action and making IPT the supplier of this reference material in Brazil.

2. Procedure

Based on research on methodologies applied by international institutes, like the ones mentioned above, for the manufacture of reference Charpy specimens, as well as methodologies studied in Brazil and related research, the main steps in the manufacturing process to be established in the LMM were defined. Studies were also carried out on the relevant standards that define the criteria for the manufacture of these reference materials, their evaluation and the infrastructure required by their producer.

After defining the steps of the manufacturing process, some sub-steps of metrological evaluations were inserted among them, such as, dimensional evaluations of all devices used, chemical analysis of the material used, dimensional evaluations of specimens after each machining step, metallographic and hardness evaluations after heat treatments and computed tomography evaluation of the finished product, with the objective of guaranteeing the homogeneity and quality of the specimens and the reproducibility in the manufacturing process.

The specimens are being manufactured by conventional mechanical machining and heat treatments carried out in laboratory ovens. The material used is Villares Metals V300MQA.

All steps of the manufacturing process and metrological evaluations meanwhile the production of specimens are being carried out by laboratories belonging to the IPT infrastructure. The attribution of nominal energies will be carried out in the Instituto Nacional de Metrologia Qualidade e Tecnologia (Inmetro).

3. Expected results

This project intends to institute a consistent methodology and manufacturing process, which enable the production of specimens that meet the regulatory requirements and the necessary quality standards and thus provide traceability to the calibrations of Charpy impact testing machines, meeting the needs of the national industrial sector and contributing to the development of the testing and calibration sectors in the country.

4. References

- [1] Metallic materials - Charpy pendulum impact test. Part 2: Verification of testing machines. ISO 148-2 (2016).
- [2] Metallic materials - Charpy pendulum impact test. Part 3: Preparation and characterization of Charpy V-notch test pieces for indirect verification of pendulum impact machines. ISO 148-3 (2016).

ZINC OXIDE FUNCTIONALIZATION BY RADIO-FREQUENCY PLASMA

Larissa Aline Klok, Teresa Tromm Steffen*, Luis César Fontana, Daniela Becker.
Center for Technological Sciences, UDESC, Joinville, Santa Catarina, Brazil

1. Introduction

Lactic polyacid/zinc oxide (PLA/ZnO) nanocomposite is a promising material to produce scaffolds, used in bone regeneration. In the way to prevent PLA degradation by ZnO presence, this nanoparticle can be surface modified [1]. So on, this work proposes ZnO surface treatment by plasma, using two functionalization agents: lactic acid (LA) and maleic anhydride (MA).

2. Experimental

The solid ZnO was manually mixed with LA and MA in a mass proportion of 20:80 (ZnO:LA) and 90:10 (ZnO:MA). Each of the samples was treated by CCP RF-plasma, in a reactor adapted from [2], with samples occupying half of vacuum chamber volume. Time of treatment was set as 30 minutes, with the power supply at 35 W. After treatment, samples were washed with methanol (in case of MA) and distilled water (for LA) to remove unreacted molecules, following a method described by Steffen et al. [2].

3. Results and Discussions

By XPS results (Fig. 1) it was identified that, in comparison to ZnO, treated samples present an increase in oxygen contribution related to zinc (O:Zn ratio), which indicates nanoparticles functionalization. The carbon contribution in ZnO sample comes from contamination, while in treated samples come also from functional groups. O 1s deconvolutions (Fig. 1, 2 and 3) show contribution of zinc oxide (~530.9 eV), carbonyl groups (~531.9 eV), ester oxygen groups (~532.6 eV) and carboxyl groups (~533.9 eV) [2,3]. For treated samples, the major increase regards to carbonyl groups, provided from the functionalization agents.

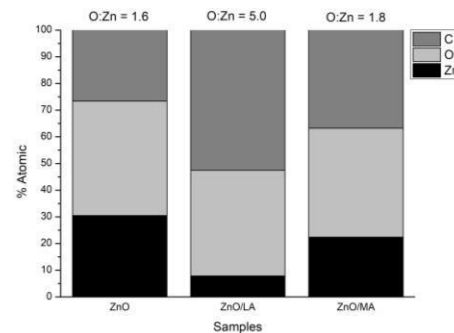


Fig. 1. Samples composition pointing out the ZnO functionalization by the increase in O:Zn ratio

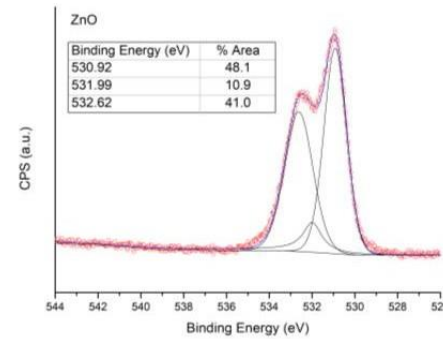


Fig. 2. XPS O 1s deconvolution for ZnO sample

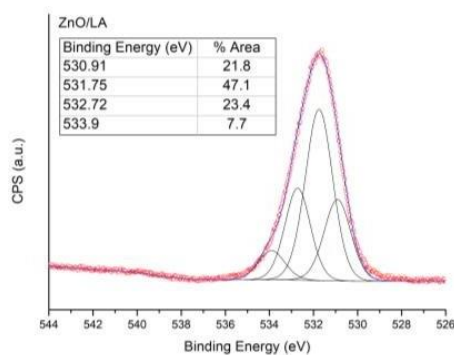


Fig. 3. XPS O 1s deconvolution for ZnO/LA sample

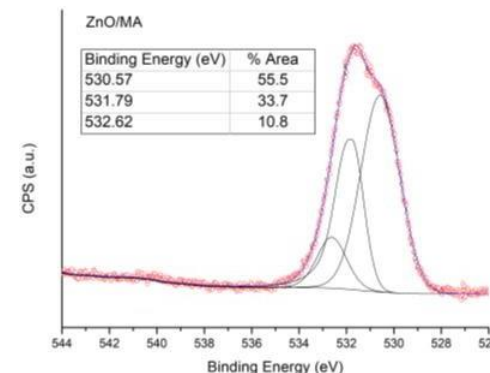


Fig. 4. XPS O 1s deconvolution for ZnO/MA sample

4. References

- [1] I. Armentano, et al. Polym. Degrad. Stab, 95, 2126-2146, (2010).
- [2] T. T. Steffen, et al. Appl. Surf. Sci, 491, 405-410, (2019).
- [3] S. B. Amor, et al Appl. Surf. Sci, 255, 5052-5061, (2009).

Acknowledgments

This work was supported in part by FAPESC project 2020TR1450. The authors are also thankful for the Multi-User Facility infrastructure from Santa Catarina State University's Technological Sciences Center.

EFFECTS OF TUBE LENGTH ON THE LEAKAGE CURRENT OF A TRANSFERRED COLD ATMOSPHERIC PRESSURE PLASMA JET

Kleber Alexandre Petroski^{1*}, Fellype do Nascimento¹, and Konstantin Georgiev Kostov¹

¹São Paulo State University (UNESP), School of Engineering, Guaratinguetá-SP

1. Introduction

Cold atmospheric pressure plasma jets (CAPJs) have been investigated with focus in biological and clinical treatments during the last decades because of their biological effects, which are mainly related to reactive species and UV photons generated within plasma jets. One of the ways to produce CAPJ is using the jet transfer technique, which is made by placing an electrical conductor inside a flexible plastic tube that transfers the potential and the working gas from a first discharge, which is generated in a dielectric barrier discharge (DBD) reactor. Then, a CAPJ is obtained at the end tip of the tube. Among the advantages of this configuration, compared to the non-transferred configuration, are a larger distance between the high voltage source and the target, and also an easier manipulation of the plasma plume at the output of the tube, which can be operated even by holding the tube with naked hands. In this work, the leakage current through the tube was investigated by wrapping partially the tube with an Al foil which was connected to an electrical circuit that simulates the impedance of the human body (referred as human box hereafter).

2. Experimental

A homemade device which works using the jet transfer technique and operated with a sinusoidal voltage of 14 kV p-p in burst mode with a period of 1.7 ms and 15 oscillation cycles was employed to produce the CAPJ. The CAPJ was produced using a He flow rate of 2.5 l/min and was directed to a metallic target and the measurements of electrical currents were performed, with two Rogowski coils and a resistor. One of the Rogowski coils was positioned in a way to measure the current that flows through the Al foil, the other one was centered with the long tube to measure the current that flows through it at different positions and the resistor was placed after the target. The target was positioned 5 mm away from the tube output. Tubes of 50, 100 and 150 cm in length were used. To simulate contact with a human body, a section of the tube was wrapped with a 10 cm long Al foil connected to the human box and positioned from 20 to 30 cm away from the DBD reactor.

3. Results and Discussions

Figure 1 shows the root mean square values of the electrical currents (i_{RMS}) that flow through the Al foil/human box when tubes of different lengths are employed. From Fig. 1, It can be observed that the lower the tube length, the higher the i_{RMS} values obtained. These observations indicate that the longer the tube, the lower is the leakage current. On the other hand, as it is presented in figure 2, for longer tubes there are higher currents flowing through the target. These data indicate that when longer tubes are used, the efficiency of the system to deliver current to the target increases. However, more investigations are needed in order to fully confirm this.

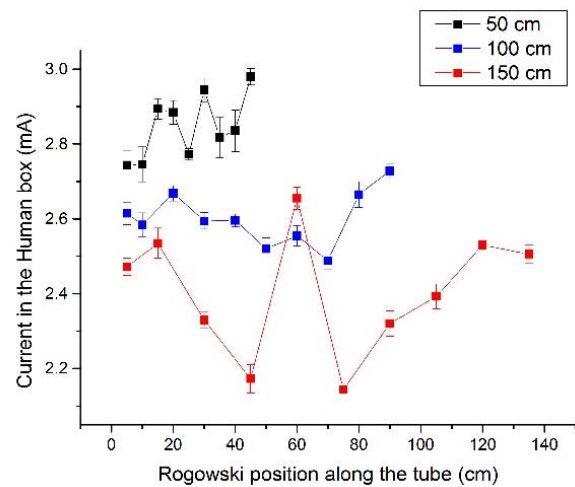


Fig. 1. Currents measured in the human box while moving a Rogowski coil along the tube.

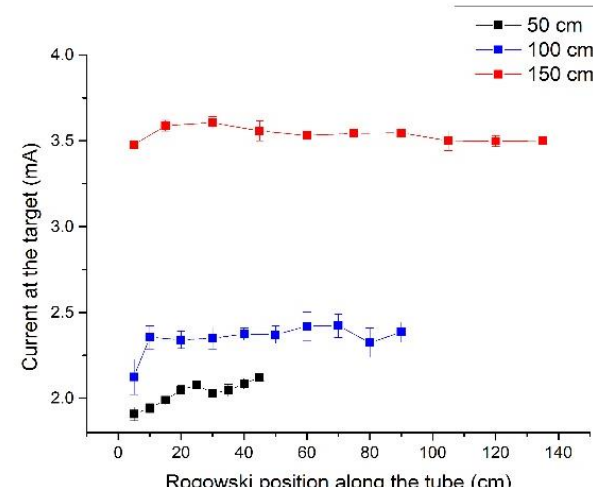


Fig. 2. Currents measured at the target while moving a Rogowski coil along the tube.

Acknowledgments

The authors would like to thank CAPES and FAPESP for their financial support.

OBTAINING AND CHARACTERIZATION OF GRANITE-EPOXY COMPOSITES WITH 44% AND 54% GRANITE

Marcello Luiz da Silva dos Anjos¹, Antônio Renato Bigansolli¹, Belmira Benedita de Lima Kühn^{1*}

¹Department of chemical engineering, Federal Rural University of Rio de Janeiro (UFRRJ), Rio de Janeiro, RJ, Brazil

1. Introduction

The processing of ornamental stones by the industry after its extraction from nature generates a high amount of waste and these must be used for sustainable purposes, such as obtaining new products with a glimpse of new materials. As for the resin, it has presented a growing and high cost worldwide production, being employed in the application of surface coating and electronic applications, but the variety of properties allow the application in various sectors such as construction, aerospace and others [1-2]. In order to minimize the impacts caused by granite extraction, as well as to improve the properties of epoxy resin, the present work evaluated the impact resistance of polymer composites formed by a granite reinforced epoxy resin matrix.

2. Experimental

The granite was fragmented by a hammer mill and milled in a high energy mill. After high energy grinding the granite powder was characterized by dry sieving, laser diffraction and infrared spectrometry (FTIR). The composites were obtained with 44 wt.% and 54 wt.% from two granite samples, sample A in which the particulate was retained in the 270 # sieve after high energy milling (fine particles) and sample B in which the particulate was retained in the 20 # sieve after grinding in the hammer mill (coarse particles). Finally, a mechanical impact test was performed.

3. Results and Discussions

For the sample obtained after high energy milling, more than 90% of the sample has particle size smaller than 112 μm , Fig. 1, and the infrared spectrum indicates the presence of quartz and biotite.

The granite-epoxy composites presented test of impact resistance in the range of 1.5 kJ/m^2 to 3.0 kJ/m^2 . Fig. 2 show absorbed energy for each granite-epoxy composite in the test of impact. The sample B present higher absorbed energy than the sample A. In this case, the sample B was obtained with particles larger. Thus, it can be concluded that composites with particles larger incorporated in the epoxy, for this percentage range of granular material, was obtained higher absorbed energy and consequently higher values of tri-axial impact resistance.

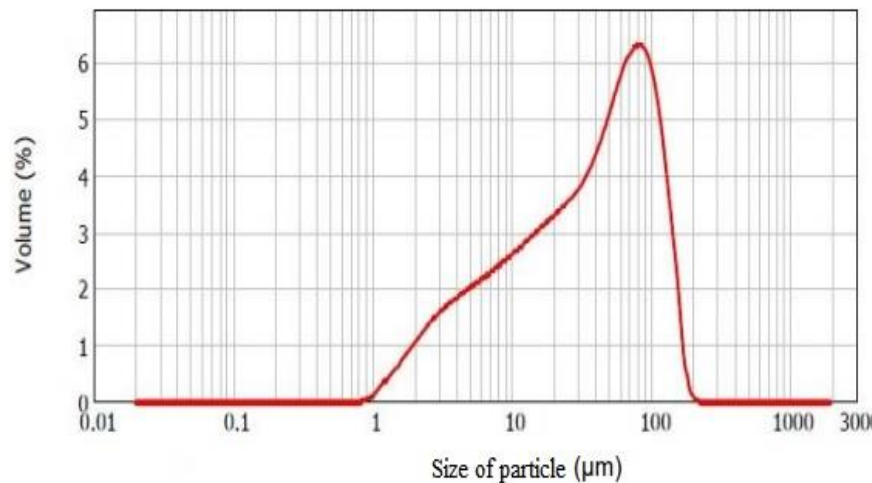


Fig. 1. Particle size distribution by laser diffraction.

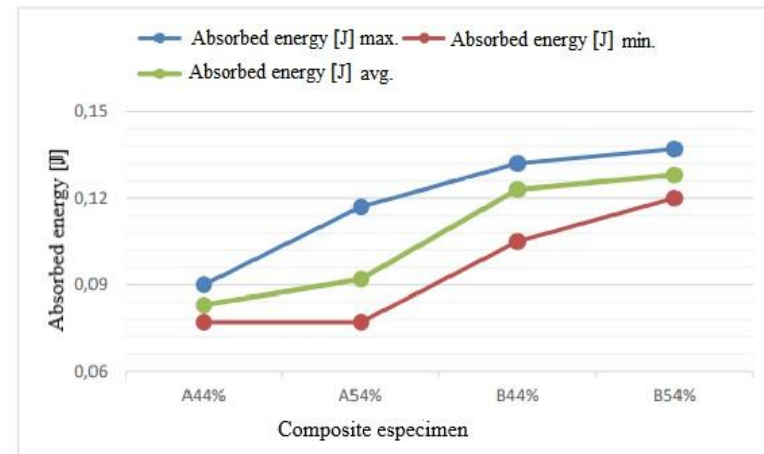


Fig. 2. Maximum, minimum and average values of absorbed energy.

4. References

- [1] França, M. P, Basic concepts of epoxy resins, science to composite technology, (2019).
- [2] Gonçalves, J. A. V, Composites based on epoxy resin reinforced with fiber from coconut. (2010).

CONTROL AND DATA ACQUISITION SYSTEM TO STUDY DIALECTRIC BREAKDOWN IN LOW PRESSURE DC PLASMA REACTOR WITH PARALLELS ELECTRODES

Bernardo Vieira Magaldi¹, Rodrigo. S. Pessoa¹, Mateus Pereira Cesare¹, Afonso André Ribeiro¹, Cristiane Aparecida Martins¹ and Argemiro. S. da Silva Sobrinho¹
¹Departamento de Engenharia Mecânica Aeronáutica - Instituto Tecnológico de Aeronáutica - Plasma and Processes Laboratory - São José dos Campos (SP), BR

1. Introduction

The electric discharge on electrodes presenting a potential difference between them occurs at a well-defined combination of gas pressure, the distance between these two surfaces and the submitted voltage, as described by Paschen's law [1]. Understanding when the discharge occurs under the conditions of the application is essential for designing and adjusting devices for a reactor or instrument, as well as, for understanding the electrical discharge processes that occur in the process. The Paschen curves measured for atmospheric air and argon will be presented and the results compared with the voltages found in the literature [2]. Possible implications for the treatment of the data obtained on the theory of dielectric rupture of gas, given below, will also be discussed.

2. Theory

A methodology designed for the LabVIEW® software interface was planned to allow the control and reading of fundamental data in a simplified manner. Where the direct (voltage and pressure) and indirect (gas type, electrode distance, reactor geometry etc.) controllable parameters would be chosen for each desired study type, as shown in the schematic diagram of Figure 1.

3. Results and Discussions

From the values of the rupture voltage (V_b) of the argon atmosphere and atmospheric air discharge obtained by the LabVIEW® software, the graphs presented in Figure 2 were plotted, which provide the values related to the rupture voltage study as a function of the pd product on Argon atmosphere and atmospheric air, respectively.

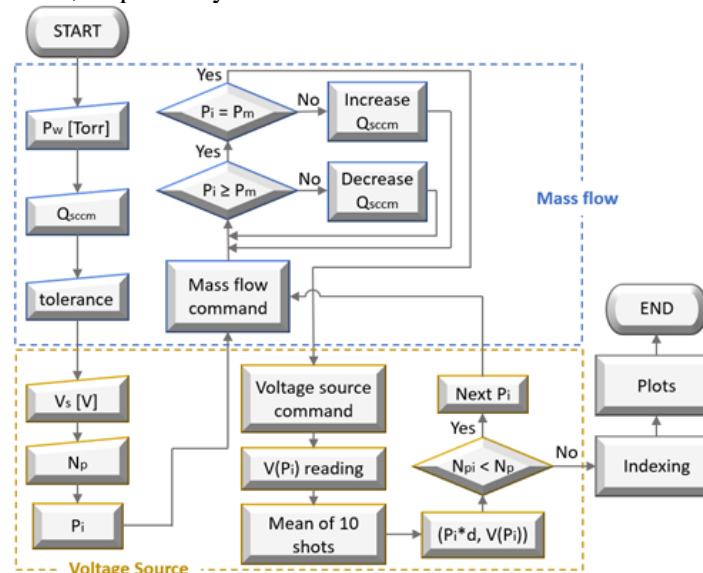


Fig. 1. Methodological diagram of the system.

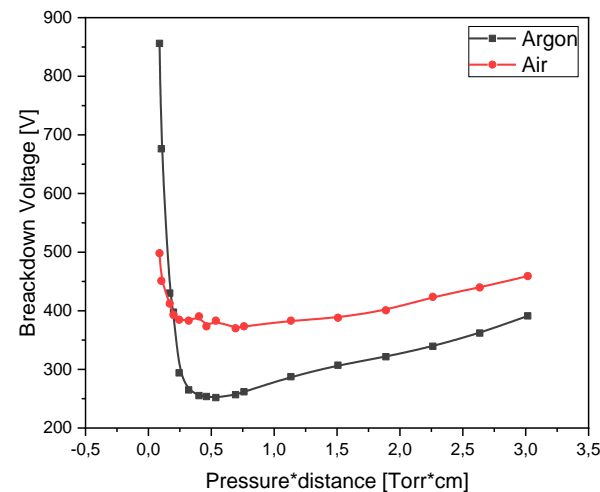


Fig. 2. Argon and Air rupture voltage as a function of product pressure by distance.

LabVIEW® peripheral device data acquisition and control system is capable for managing and measuring the dielectric rupture parameters of argon and atmospheric gas, using the NI USB 6008 acquisition board, and the limitations encountered have been overcome. It is necessary to adjust their respective parameters for each of the two gases tested, but without impairing the validation of the proposed method. Through the analysis of Paschen curves for the configuration with argon gases and atmospheric air, it is observed that the rupture potential for argon gas is lower than for atmospheric air, although the ionization potential of atmospheric air is lower about argon.

4. References

[1] Conrads, H.; Schmidt, M. Plasma generation and plasma sources. *Plasma Sources Science and Technology*, vol.9, n.4, p.441-454, Sept. (2000).
[2] Lieberman, M. A.; Lichtenberg, A. J. *Principles of Plasma Discharges and Materials Processing*. 2nd ed. New Jersey: Wiley-Interscience, 757p., (2005).

Acknowledgments

Coordenação de Aperfeiçoamento de Pessoal de Nível Superior

OBTENÇÃO DAS VARIÁVEIS TÉRMICAS DE SOLIDIFICAÇÃO DA LIGA UNS C65500

Eduardo Palmeira^{1*}, Maurício S. Nascimento¹, Rogério Teram^{1,3}, Vinicius T. dos Santos^{2,3}, Marcio R. da Silva², Jan Vatavuk³, Antonio A. Couto³, Givanildo A. dos Santos^{1,3}

¹ Programa de Pós Graduação em Engenharia Mecânica, Instituto Federal de Educação, Ciência e Tecnologia de São Paulo (IFSP), São Paulo, SP, Brasil.

² Termomecanica São Paulo S.A. – TM -Centro Educacional da Fundação Salvador Arena – CEFSASão Bernardo do Campo, SP, Brasil

³Programa de Pós-graduação em Engenharia de Materiais e Nanotecnologia, Universidade Presbiteriana Mackenzie (UPM), São Paulo, SP, Brasil

1. Introdução

A maioria dos processos de fabricação que envolvem materiais metálicos, excluindo-se os processos de metalurgia do pó, tem alguma etapa envolvendo solidificação [1, 2]. O objetivo deste trabalho é determinar experimentalmente as variáveis térmicas de solidificação da liga UNS C65500 obtidas após a solidificação unidirecional ascendente do lingote e a influência destas variáveis na microestrutura resultante.

2. Experimental

A liga foi solidificada em uma lingoteira de aço inoxidável AISI 304 montada em um dispositivo de resfriamento unidirecional ascendente. O calor foi extraído direcionalmente através de refrigeração por água na chapa base fabricada em grafite. A microestrutura foi analisada por meio de microscopia óptica (MO). As variáveis térmicas de solidificação velocidade de deslocamento da isoterma liquidus (V_L), taxa de resfriamento (T_R) e gradiente térmico (G_L) foram avaliadas em função da distância da superfície de extração de calor.

3. Resultados e Discussões

Observamos que maiores taxas de resfriamento e velocidades de deslocamento da isoterma *liquidus* são obtidas nas posições mais próximas da base de extração de calor. Isso propicia microestrutura mais refinada em posição mais próxima dessa base do que em posição mais distante, conforme Figuras 1(a) e 1(b), respectivamente.

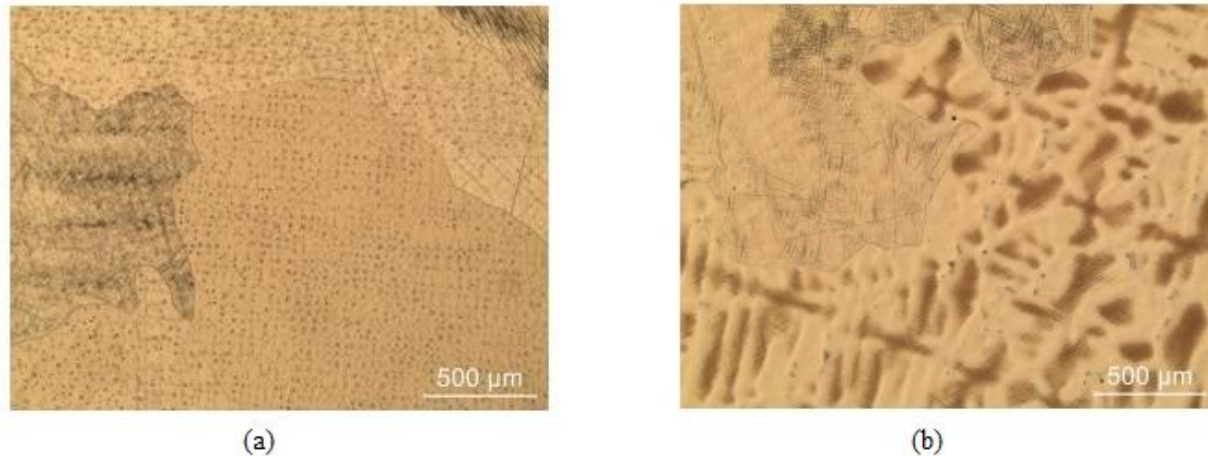


Fig. 1. Microestrutura em relação à distância da base de extração de calor: (a) posição mais próxima e (b) posição mais distante.

4. Referências

- [1] Nascimento M S, dos Santos G A, Teram R, dos Santos V T, da Silva M R, Couto A A. Effects of thermal variables of solidification on the microstructure, hardness, and microhardness of Cu-Al-Ni-Fe alloys. *Materials* (Basel). 2019;12(8).
- [2] Santos G A, Goulart P.R., Couto A.A., et al., “Primary dendrite arm spacing effects upon mechanical properties of an Al-3w%Cu-1w%Li alloy”, In: Öchsner, A., Altenbach, H. (eds), *Properties and characterization of modern materials*, Springer, 2017.

Agradecimentos

Os autores são gratos à CAPES, ao Instituto Federal de Educação Ciência e Tecnologia de São Paulo – IFSP; à Universidade Presbiteriana Mackenzie; e à Termomecanica São Paulo S.A. pelo apoio às atividades de pesquisa desenvolvidas.

TRIBOCORROSION STUDY ON TITANIUM ALLOYS – DYNAMICAL FRICTION COEFFICIENT (COF) AND OPEN CIRCUIT POTENTIAL (OCP)

Enzo L. Galindo^{1*}, Carlos A. F. Pintão¹, Israel R. Rodrigues¹, Renan E. L. Lopes¹, Giovana C. Cardoso¹

¹UNESP – Universidade Estadual Paulista “Júlio de Mesquita Filho”, Bauru, SP, Brazil

1. Introduction

Medical devices, especially dental and orthopedics, are subject to mechanical efforts that cause wear, such as the mastication movement in a dental prosthesis or the rotation in a hip implant, which leads to a loss of the biomaterial. In the human body, such devices are in a corrosive medium: the body fluids. The simultaneous phenomenon of wear and corrosion that gives an irreversible material loss is known as tribocorrosion [1]. In biomedical research, there is a concern with the particles liberated by tribocorrosion, which can prejudice health and lead to undesirable surgeries [1]. Thus, this work was elaborated to contribute with the study of biomaterials with tribocorrosion testing on titanium alloys, through a tribometer developed by *Laboratório de Caracterização Física e Reológica, UNESP, Bauru*.

2. Experimental

A rotary tribometer, ball (fixed) on disk (rotating) type was used, with alumina spheres of 6 or 10 mm diameter. We used the configurations C1 - alumina sphere of 6 mm with 1,55 N of applied load and C2 - 10 mm sphere with 2,50 N load. Artificial Saliva was used as electrolytes at room temperature, and a reference electrode of Ag/AgCl was employed. The testing was done with the samples: Titanium commercially pure grade 2 (TiCp); Ti10MoXZr X = 30, 40 and 50 (%wt); Ti5MoXNb, X = 10, 20 and 30 (%wt). The procedure for the experiment is to sand the sample until #1200 granulation and polish with alumina suspension (0.3 μ m) one day before; wait for OCP stabilization in the electrolyte; make 30 minutes of sliding friction, at 2 rad/s; wait for the worn material repassivation. We acquired the OCP curves with a digital multimeter and the COF curves by a force sensor's friction between sample and sphere.

3. Results and Discussions

We realized the experiments to TiCp and Ti6Al4V samples, testing the conditions C1 and C2. The curve form are in Fig. 1, where the OCP and COF are plotted versus time. The experiments in C1 and C2 gave close results, but the COF values were bigger, and the OCP gaps were lower in C2 than C1, where pressure impressed is lower. So, the pressure can slightly vary the COF but certainly influence the OCP [3]. The system validation is verified since the tribocorrosion system enables reproducible testing and Ti6Al4V results are close to the literature [2-3]. Ti-Mo-Zr and Ti-Mo-Nb alloys were tested only in C1. Fig. 2. shows the comparative graph between OCP curves of the Ti-Mo-Zr system, TiCp, and Ti6Al4V, where one see that Ti10Mo40Zr alloy presented the fastest repassivation while the Ti6Al4V showed the minor OCP gap.

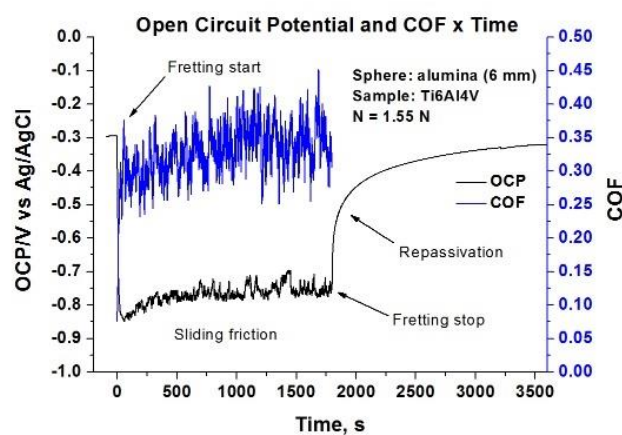


Fig. 1. Ti6Al4V test.

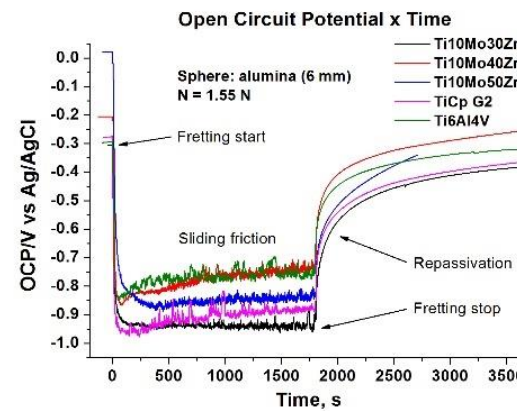


Fig. 2. OCP comparative Ti10MoXZr, TiCp, and Ti6Al4V

4. References

- [1] M. T. Mathew *et al.*, Wear, **271**, 2651-2659, (2011).
- [2] M. P. Licausi *et al.*, Journ. of the Mech. Behav. of Biomed. Mat., **20**, I37-I48 (2013).
- [3] M. Bucuimeanu *et al.*, Tribology International, **107**, 77-84 (2017).

Acknowledgments

Firstly, the author would like to thank God, the financial support by Pró-Reitoria de Pesquisa (PROPe) - UNESP, the collaborators by the samples, the advisor, and Mr. Wiliams Govedise by technical support.

ESTUDO DAS VARIÁVEIS TÉRMICAS DE SOLIDIFICAÇÃO DA LIGA UNS C19400

Anderson B. Gonzaga^{1*}, Maurício S. Nascimento¹, Rogério Teram^{1,4}, Vinicius T. dos Santos^{2,3,4}, Marcio R. da Silva^{2,3}, Jan Vatavuk⁴, Antonio A. Couto⁴, Givanildo A. dos Santos^{1,4}

¹Programa de Pós Graduação em Engenharia Mecânica, Instituto Federal de Educação, Ciência e Tecnologia de São Paulo (IFSP), São Paulo, SP, Brasil

²Termomecanica São Paulo S.A. – TM, São Bernardo do Campo, SP, Brasil

³Centro Educacional da Fundação Salvador Arena – CEFSA, São Bernardo do Campo, SP, Brasil

⁴Programa de Pós-graduação em Engenharia de Materiais e Nanotecnologia, Universidade Presbiteriana Mackenzie (UPM), São Paulo, SP, Brasil

1. Introdução

As características da liga metálica dependem da microestrutura, das heterogeneidades de composição química, da forma e tamanho e distribuição das inclusões, das porosidades formadas etc [1, 2]. O objetivo deste trabalho é determinar experimentalmente as variáveis térmicas de solidificação da liga UNS C19400 obtidas após a solidificação unidirecional ascendente do lingote e a influência destas variáveis na microestrutura resultante. A liga cobre-ferro UNS C19400 é composta principalmente por no mínimo 97% de Cu e entre 2,1% e 2,6% de Fe, com valores em massa.

2. Experimental

A liga de cobre foi solidificada em uma lingoteira de aço inoxidável AISI 304 montada em um dispositivo de resfriamento unidirecional ascendente. O calor foi extraído direcionalmente através de refrigeração por água na chapa base de grafite. A microestrutura foi analisada por meio de microscopia óptica (MO). As variáveis térmicas de solidificação como velocidade de deslocamento da isotermaliquidus (V_L), taxa de resfriamento (T_R) e gradiente térmico (G_L) foram avaliadas em função da distância da superfície de extração de calor.

3. Resultados e Discussões

Notamos que os tempos de obtenção da isotermaliquidus são menores nas posições mais próximas da base de extração de calor, conforme mostrado na Figura 1. Isso propicia maiores valores de taxa de resfriamento e de velocidade de deslocamento da isotermaliquidus nas posições iniciais, o que resulta em microestrutura mais refinada para essas posições em comparação com posições mais distantes.

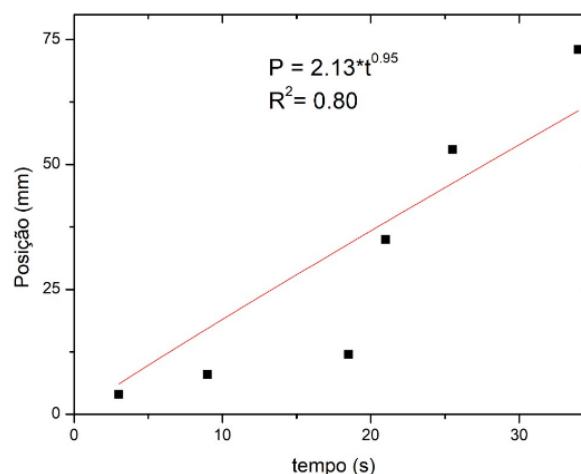


Fig. 1. Posição em função do tempo de passagem da isotermaliquidus

4. Referências

- [1] Nascimento M S, dos Santos G. A, Teram R, dos Santos V T, da Silva M R, Couto A A. Effects of thermal variables of solidification on the microstructure, hardness, and microhardness of Cu-Al-Ni-Fe alloys. *Materials* (Basel). 2019;12(8).
- [2] Santos G.A, Goulart P.R., Couto A.A., et al., “Primary dendrite arm spacing effects upon mechanical properties of an Al-3w%Cu-1w%Li alloy”, In: Öchsner, A., Altenbach, H. (eds), *Properties and characterization of modern materials*, Springer, 2017.

Agradecimentos

Os autores são gratos à CAPES, ao Instituto Federal de Educação Ciência e Tecnologia de São Paulo – IFSP; à Universidade Presbiteriana Mackenzie; e à Termomecanica São Paulo S.A. pelo apoio às atividades de pesquisa desenvolvidas.

STUDY OF WEAR AND CORROSION RESISTANCE OF DLC FILM DEPOSITED ON ALUMINUM 7050-T7451 ALLOY

César Augusto Antônio Junior^{2*}, Marcos Dorigão Manfrinato^{1,2}, Luciana Sgarbi Rossino^{1,2}

¹*Sorocaba Technology College FATEC*

²*São Carlos Federal University UFSCAR – Sorocaba Campus*

1. Introduction

DLC films are amorphous carbon materials which present excellent properties like, chemical inertia, high wear and corrosion resistance, low friction coefficient, among others [1]. In order to reduce the DLC film tension improve the substrate adhesion, it is used organosilicon interlayers based on hexamethyldisiloxane (HMDSO). The main objective of this work is to study the DLC film deposition on 7050-T7451 aluminum alloy focusing on attainment of a better adhesion coating on substrate and verify the corrosion and wear resistance behavior of the obtained film.

2. Experimental

Aluminum 7075-T451 alloy, polished and washed, was utilized and surface treatments by the PECVD technique using pulsed-DC power supply. It was performed plasma ablation cleaning with 50% Ar/50% H₂ gas mixture for 2h. In sequence it was deposited an organosilicon interlayer (C.org) with $9,75 \times 10^{-2}$ torr gas pressure, with a gas mixture of 70% HMDSO/30%Ar during 15min. The DLC film deposition was performed with 90%CH₄/10%Ar, totalizing $3,15 \times 10^{-1}$ torr. A study about the effect of treatment tension and time was prepared, varying the tension in 500 V (DLC500V-2h and DLC500V-4h), 650 V (DLC650V-2h and DLC650V-4h) and the interposition of the interlayer with DLC film (DLC500V-2h+C.org and DLC650V-2h+C.org). The samples were characterized by metallographic assay using a scanning electron microscope (SEM), to analyze the films chemical composition and thickness, micro-abrasive wear test by fixed ball and cyclic polarization corrosion test.

3. Results and Discussions

At the metallographic analysis it was observed the formation of uniform DLC films characterized by the carbon presence, and also the silicon from interlayer C.org between DLC film and substrate. Higher film thickness was obtained by longer treatment time and higher tension, due to deposition rate increase. The wear resistance of treated materials was higher when compared to the untreated material. The treatments DLC500V-2h+C.org and DLC650V-2h+C.org have shown lower wear resistance than the others treated samples, due to overlay deposition of C.org on DLC film. The corrosion test result, observed at Figure 1 (a) and (b), shows that the deposited films presented higher corrosion resistance when compared to base material. The treatment DLC500V-2h shown the highest corrosion resistance, because of high corrosion potential (E_{corr}), low corrosion current (i_{corr}) and superior pit potential (E_{pit}). The short time treatment presented better corrosion resistance if compared to long time treatments. The deposition of C.org layer on DLC film demonstrate intermediate corrosion behavior when compared to DLC films, and the tension variation at these treatments improved the corrosion resistance of the samples. It is observed that for lower deposition voltage, the corrosion potential decreases, while higher deposition voltages, present higher i_{corr} values, indicating higher corrosion speed.

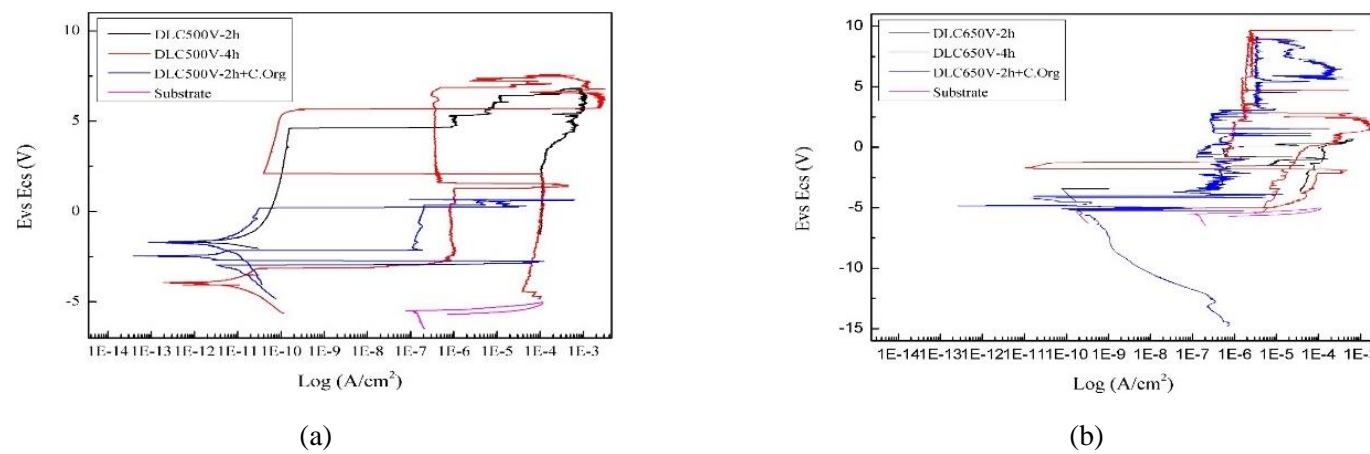


Fig.1. Cyclic polarization curves of DLC film deposited with fixed voltage 500 V (a) and 650 V

4. References

[1] Robertson, J. Diamond-like amorphous carbon. Materials Science and Engineering (2002).

Acknowledgments

The author thanks FAPESP (nº 2019/12192-8) and FATEC-SO for provide the laboratory.

RESISTANCE TO CORROSION OF ABNT 106 ELECTRIC STEEL OXIDIZED BY BIPOLAR PULSE PLASMA

Gabriele Emidio^{1,*}, Paula Fin¹, Carla Dalmolin¹, Roberta Ruschel Campedelli¹, Julio César Sagás¹, Abel André Cândido Recco¹ e Luis Cesar Fontana¹¹Universidade do Estado de Santa Catarina

1. Introduction

ABNT 1006 low carbon steel samples used in the cores of electric motors were treated by plasma oxidation using an asymmetric pulsed bipolar voltage source (ABiPPs). The objective is to obtain a corrosion resistant surface through the formation of an oxide layer on the surface of the plates. Furthermore, these insulating oxide layers can minimize power losses due to the mitigation of Foucault currents. When the plasma is fed by an ABiPPS source, intercalated bombardments of electrons and ions occur on the surface in short periods ($T \leq 1\mu s$) ensuring the support and stability of the plasma, as the accumulation of static charges on the insulating surface is neutralized at each inversion of pulse polarity. Furthermore, the use of the ABiPPS source increases the plasma ionization rate, since the surface is sequentially bombarded by ions and electrons [1, 2]. The samples were treated in two electrode settings: 1- floating potential (FP), in which the sample is electrically isolated and immersed in the luminescent region of the plasma; 2- cathode potential (CP), in which the sample is negatively polarized and acts as the discharge cathode.

2. Experimental

Samples with a thickness of 0.6mm went through a sanding process in different granulometries (100, 220, 320, 400, 600 and 1200) and were ultrasound cleaned with acetone. Subsequently, the plates were oxidized in pulsed bipolar plasma, with the following parameters: treatment time of 2.0 h; temperature of 350°C; 0.5 Torr pressure; O₂ working gas (99.9%) and O₂/Air (20%/80%). The samples were characterized by scanning electron microscopy (SEM) and X-ray spectroscopy (XRS). Corrosion resistance was analyzed through the potentiodynamic polarization (PP) test using a cell with 3 electrodes: working electrode (), reference electrode () of calomel and a counter electrode () of platinum, in a solution of 3.5 % KCl. The voltage was stabilized in open circuit potential (OCP) for 180s and then the polarization curves were drawn with a sweep speed of 1.0 mV/s and a potential range varying from -100mV to 100mV.

3. Results and Discussions

The results of electrochemical corrosion measurements show that plasma oxidation improves the corrosion resistance of ABNT 1006 steel. The best corrosion resistance potential was obtained from the FP configuration with O₂ working gas (Fig 1). SEM measurements show that layer peeling can occur in some regions. Corrosion occurs by pit, from defects in the oxide layers. XRS results, after the corrosion test, show the presence of iron and potassium oxides as corrosion products.

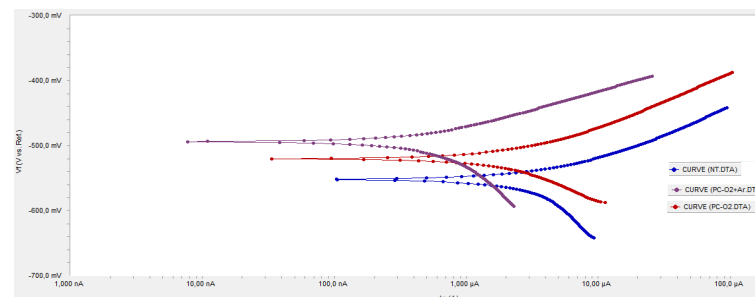


Fig. 1. Potentiodynamic polarization - Cathode potential

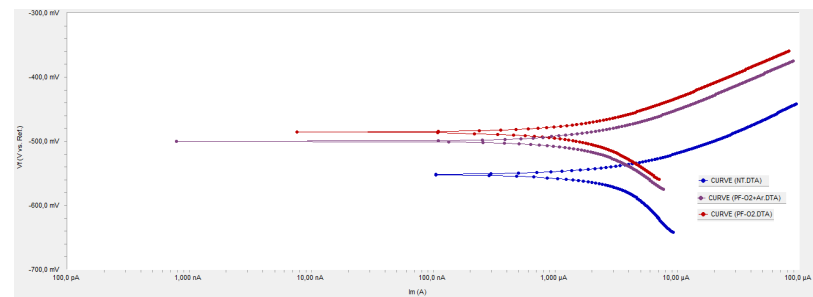


Fig. 2. Potentiodynamic polarization - Floating potential

4. References

[1] FONTANA, Luis César. Nitretação Iônica em Aços Baixo Carbono. 1991. 95 f.
 [2] SCHOLTZ, Juliano Sadi; FONTANA, Luis Cesar; MEZAROBA, Marcello. Asymmetric Bipolar Plasma Power Supply to Increase the Secondary Electrons Emission in Capacitive Coupling Plasmas. Ieee Transactions On Plasma Science, [s.l.], v. 46, n. 8, p.2999-3007, ago. 2018.

Acknowledgments

FAPESC and UDESC

WEAR RESISTANCE OF 8640 STEEL NITRIDED AND TEMPERED SIMULTANEOUSLY

Karine Stefany Coan^{1*}, César Augusto Antônio Junior², Larissa Solona de Almeida², Miguel Rubira Danelon², Marcos Dorigão Manfrinato^{1,2}, Luciana Sgarbi Rossino^{1,2}

¹Sorocaba Technology College FATEC

²São Carlos Federal University UFSCAR – Sorocaba Campus

1. Introduction

SAE 8640 is a medium carbon and low alloy steel being applied in mechanical components of general use such as axles, bearings, bushings, gears, and may even substitute SAE 1045 steel in more severe exposures. To enable its application in service, this steel can be submitted to quenching and tempering heat treatment processes, as well as plasma nitriding surface treatment, acquiring better performance in service due to the increase of wear resistance through the increase of material hardness. The objective of this work was to study the effect of tempering temperature on the properties of the treated material and the nitriding temperature on the hardness and wear resistance of 8640 steel only tempered both on the surface and on the substrate studied.

2. Experimental

In this work, SAE 8640 steel specimens were used in the dimensions of 31mm diameter and 20mm thickness, with a microhardness of 215HV. Two series of treatments were performed, in which tempered samples were quenched in a conventional furnace at temperatures of 250°C, 350°C, 450°C and 550°C for 5 hours, while tempered samples were simultaneously nitrided and quenched in a plasma reactor at temperatures of 250°C, 350°C, 450°C and 550°C. The nitriding treatments were performed in a plasma reactor with a DC-pulsed source for 5 hours with 80% N₂ + 20% H₂. Plasma ablation cleaning was performed for 1 hour using 80% Ar + 20% H₂ prior to the nitriding.

3. Results and Discussions

In Fig. 1 it is possible to observe that all the treated materials presented higher wear resistance compared to the untreated material, due to the increase in surface hardness promoted by the heat treatment and formation of the nitrided layer. Although the quenched and tempered material presented higher wear resistance compared to the quenched and tempered material, it is observed that the wear behavior was similar for both treatments. It is noted that for the samples that were only quenched, the highest wear resistance was obtained at a temperature of 350°C; for the quenched and nitrided samples, it was observed that the highest wear resistance was obtained for the sample nitrided at 550°C, whose metallography is shown in Fig. 2, obtaining a thicker layer. For the hardened and nitrided samples, it was noted that the sample nitrided at 250°C caused a significant increase in wear resistance, achieved by the formation of a thin composite layer with high surface hardness. The layer formation at this temperature was possible due to the martensitic phase that is metastable, requiring less energy to form iron nitrides.

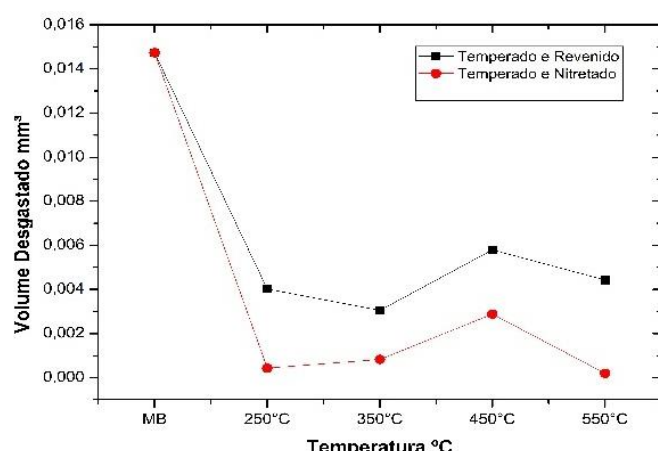


Fig. 1- Wearing volume

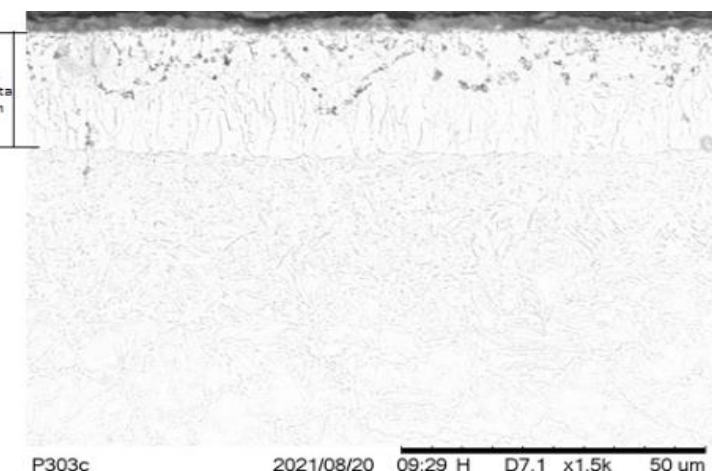


Fig. 2- Nitrided Layer 550°C

4. References

[1] Cruz, D.; Souza, B.A.; Campos, L.A.P.; Almeida, L.S.; Moreto, J.A.; Manfrinato, M.D.; Cruz, N.C.; Rossino, L. S. Design, construction, and commissioning of a reactor for ionic 21 plasma nitriding treatment in P20 steel. Rev. Bras. Apl. Vac., Campinas, Vol. 37, N°3, pp. 102-113, Set. – Dez., 2018.

Acknowledgments

I thank CNPq for the scholarship.

OBTAINING HYBRID COMPOSITE OF EPOXY RESIN AND SODA-CAL GLASS

Jônatas de O. Sousa^{1*}, Belmira B. Lima-Kuhn¹, Alexandre M do Nascimento², Antonio R. Bigansolli¹

¹Departamento de Engenharia Química, Instituto de Tecnologia, UFRRJ, Seropédica,

²Departamento de Produtos Florestais, Instituto de Engenharia Florestal, UFRRJ, Seroédica.

1. Introduction

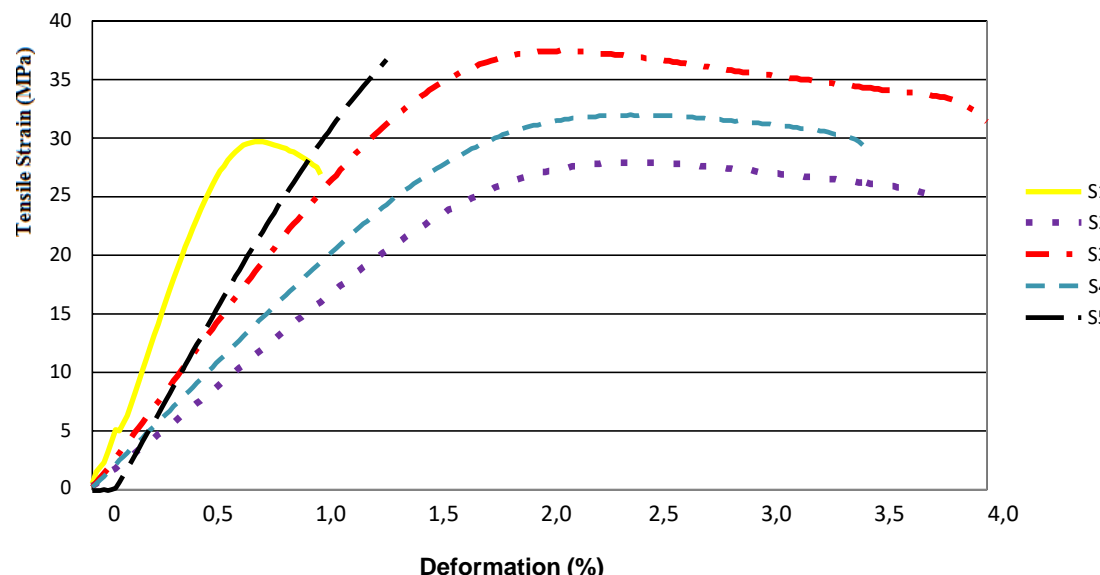
Epoxy resin is a material used in several areas, both in daily domestic work and in the industrial field in civil construction, chemical, and electronics. There are now several companies dedicated to the development and formulation of epoxy-based products with characteristics according to need [1]. In recent decades, glass has been studied due to its properties, with applications in several areas such as optical fiber [2]. Based on this, microparticles generated from glass bottles were added to the epoxy resin in order to investigate the changes in the resin characteristics giving rise to a composite.

2. Experimental procedure

The glass used in this research came from the fragmentation of amber bottles, used in the beverage industries. The glass was subjected to comminution in a high energy mill model PM 100 from Retch, until obtaining an average size of 2,083 μ m. The epoxy resin used was liquid Araldite GY 279 BR, formulated on the basis of Bisphenol A and the curing agent Aradur 2963BR. Five compositions were made with the addition of glass particles: S1, S2, S3, S4 and S5 containing respectively 0%, 3%, 5%, 10% and 20%, the samples (S) and the tensile tests and flexion were performed according to the respective standards: ASTM D3039 and ASTM D790. Microscopy analyzes were also performed. Analyzes were performed in triplicate.

3. Results and discussion

It was observed that the addition of glass microparticles to the epoxy resin significantly influenced the results. The analysis of the tensile tests showed that samples from group C (addition of 5% of glass) had the best results with a 7% improvement in mechanical strength compared to group A, as they are more resistant to crack formation in the polymer matrix [3]. In the flexion tests, sample C also obtained a better result, as shown in graph 1. In the analysis of microscopy, agglomerates of glass particles can be observed.



Graph 1: Fracture stress and strain results to fracture.

4. References

- [1] LÓPEZ, D. A. R.; AZEVEDO, C. A. P. Avaliação da utilização de vidro cominuido como material agregado ao concreto. ULBRA. Canoas, 2003.
- [2] ALVES, O. L.; GIMENEZ, I. F.; MAZILI, I. O. "Vidros". *Química Nova na Escola*, Edição especial. p.9-20, 2001.
- [3] MENDES, T. M. *Influência do coeficiente de atrito entre os agregados e da viscosidade da matriz no comportamento reológico de suspensões concentradas heterogêneas*. Dissertação (Mestrado em Engenharia Civil) Escola Politécnica, Universidade de São Paulo. SP, p. 29. 2008

PREPARATION AND CHEMICAL, MICROSTRUCTURAL AND MECHANICAL CHARACTERIZATION OF AS-CAST Ti-5Mo-XNb ALLOYS

Giovana Collombaro Cardoso^{1*}, Gerson Santos de Almeida², Dante Oliver Guim Corrêa¹, Willian Fernando Zambuzzi², Carlos Roberto Grandini¹¹UNESP - Univ Estadual Paulista, Laboratório de Anelasticidade e Biomateriais, 17.033-360, Bauru, SP, Brazil²UNESP - Univ Estadual Paulista, Instituto de Biociências, 18.618-689, Botucatu, SP, Brazil**1. Introduction**

Cp-Ti and other Ti-based alloys are widely used as biomaterials due to their excellent properties, such as low elastic modulus, good resistance to corrosion, high mechanical strength, and excellent biocompatibility [1]. One of the most used metallic biomaterials is the Ti-6Al-4V alloy. However, some studies showed that V is cytotoxic, and Al ions can cause neurological disorders [2,3]. Thereby, new Ti alloys with non-cytotoxic β -stabilizing elements are being developed [4]. Thus, in this work, Ti-5Mo-xNb ($x = 0, 10, 20, 30$ % wt) alloys were prepared and studied to evaluate the effect of Nb on their microstructure and Vickers microhardness.

2. Experimental

The alloys were produced by arc-furnace, in an inert and controlled argon atmosphere, and a water-cooled copper crucible. Then, the chemical composition of the ingots was evaluated by Energy Dispersive Spectroscopy (EDS), and the densities values were measured by Archimedes' method. Structural and microstructural analyses were made by x-ray diffraction (XRD), optical (OM), and scanning electron (MEV) microscopy images. Finally, Vickers microhardness values of the samples were measured, and the biological *in vitro* tests were performed by MTT and violet crystal analysis.

3. Results and Discussions

The chemical composition of the produced alloys remained close to the nominal values, and the measured density values of the samples were close to the theoretically calculated values. With the addition of Nb, it is possible to observe that the densities of the alloys increase, due to the higher density of this element, compared with Ti. Figure 1 shows the OM images, and these results corroborate with the x-ray diffractograms and MEV images: for Ti-5Mo and Ti-5Mo-10Nb alloys, peaks related to α' , α'' and β phases appear, and in the images, fine and coarser acicular needles are identified, in addition to grain boundaries; for Ti-5Mo-20Nb and Ti-5Mo-30Nb alloys the images have grain boundaries characteristic of the β phase, while the diffractograms show α'' and β peaks for the alloy with 20Nb and only β peaks for the alloy with 30Nb. Finally, MTT and crystal violet tests showed that the alloys do not harm cell viability and promote cell adhesion. Thus, it is concluded that the addition of Nb in the alloys increases the amount of β phase, and, in *in-vitro* tests, the alloys were not cytotoxic.

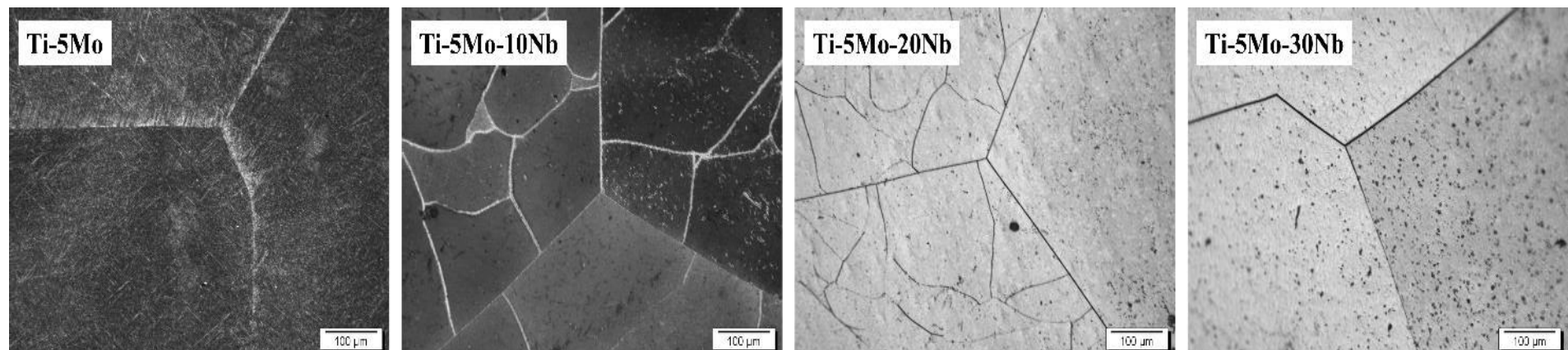


Figure 1 - Optical micrographs of the as-cast Ti-5Mo-xNb system alloys, with 200x magnification

4. References

- [1] Ehtemam-Haghghi, *et al.* Journal of Alloys and Compounds, **787**, 570 – 577, (2019)
- [2] H. M. Silva, *et al.*, Materials Science and Engineering: C **24**, 679 (2004).
- [3] P. Li, *et al.*, Journal of Alloys and Compounds **815** (2020).
- [4] A. Cremasco, *et al.*, Materials Science and Engineering: C **31**, 833 (2011)

Acknowledgments

The authors thank CAPES, CNPq, and FAPESP for financial support, PosMat, and the laboratory's colleagues collaborating with the research.

EVALUATION OF THE SURFACE FREE ENERGY OF EPOXY/GRANITE COMPOSITES THROUGH CONTACT ANGLE.

J. L. Siqueira-Costa-Neto¹, A. R. Bigansolli¹, B. B. Lima-Kühn^{1,*}¹UFRRJ – Universidade Federal Rural do Rio de Janeiro. Rodovia BR 465, Km 7, Seropédica, RJ, 23851-970, Brazil.**1. Introduction**

In order to reduce the environmental impact caused by inadequate waste disposal, it has been proposed to incorporate remnants of ornamental stones into a polymer resin to produce artificial stone. Among the properties of composites, surface energy is an important feature because this energy directly affects the adhesion, adsorption and wettability of the soils, and one way to measure it is the contact angle [2]. In this work, composites of granite waste as filler in epoxy resin were obtained to determine the surface free energy using the theory developed by Owens and Wendt [2].

2. Experimental

Bisphenol A diglycidyl ether epoxy resin (DGEBA) polymer and Aradur 2963 curing agent were used to prepare the composite in the proportions specified by the manufacturer to obtain the best mechanical performance. The granite powders were weighed and mixed manually with Aradur 2963 and Araldite GY 279 BR in a beaker for 30 minutes using a glass stirring rod. Finally, the mixture (containing 0 wt%, 30 wt%, 50 wt% and 60 wt% granite) was poured into molds. The prepared composites were cured at room temperature. The contact angle between the water and the compounds was measured using the droplet method, in which a droplet of liquid is applied to the surface of the compound being evaluated. Finally, the theory developed by Owens and Wendt [2] was used to determine the surface free energy.

3. Results and Discussions

The measured contact angles for water droplets, the dispersive and polar components of the surface free energy values calculated using Equation 1, and the surface free energy values are summarised in Table 1.

$$\gamma_{LV}(1+\cos\theta)=2(\gamma^d \gamma^d)^{1/2} + 2(\gamma^p \gamma^p)^{1/2} \quad (1)$$

It can be observed that as the contact angle increases, the surface free energy decreases, indicating the larger amount of nonpolar groups in samples with higher granite content.

Table 1 - Contact angle values measured for water droplets and dispersive and polar components of surface free energy and surface free energy.

Granite(% wt)	Contact angle (°)	Surface free energy (mN.m ⁻¹)		
		polar components γ_{sp}	dispersive components γ_{sd}	absolute γ_{LV}
0%	47.59	13.05	57.48	70.53
30%	58.11	11.91	44.71	56.62
50 %	60.09	11.68	42.33	54.01
60%	75.61	9.720	24.99	34.71

4. References

[1] R. A. Carvalho, Estudo da molhabilidade de vidrado composto de resíduo de rochas ornamentais em cerâmica vermelha. MSc. Thesis, UFES, Brazil (2017).
 [2] C.M.S Vicente, P.S. André; R.A.S. Ferreira, Simple measurement of surface free energy using a webcam. Revista Brasileira de Ensino de Física, v. 34, n. 3, 3312 (2012).

Acknowledgments

The authors gratefully acknowledge the financial support of CNPQ by PIBIC from UFRRJ.

MODELING COMPLEX PRE-VACUUM SYSTEMS

Kevin Machado Sanches Secco¹, Gabriel Geidson Johanson de Sousa², Francisco Tadeu Degasper³

^{1, 3}Faculdade de Tecnologia de São Paulo - FATEC-SP - CEETEPS

²Centro Tecnológico da Marinha - SP - CTMSP

1. Introduction

This work aims to mathematically model the pressure pumping as a function of time for a vacuum arrangement with two isovolumetric vacuum chambers. The chambers are connected by a pipe and connected to two individual pumps, with different pumping speeds. The pumps in question are rotary vane mechanics.

2. Theory

The theoretical part of this research is basically supported by the kinetic theory of gases and the fundamental equation of the gas pumping process. In this research, Scilab is also used, scientific software for algebraic treatment of the equation.

The definition used for vacuum is as follows: A given volume is said to be in a vacuum when the density of particles in it is lower than that found in the atmosphere at normal pressures and temperatures [1].

The experimental part consists of assembling the arrangement and obtaining the pressure variation through sensors, and later comparing the experimental data with what was theoretically predicted.

3. Results and Discussions

Due to COVID-19, experimental activities were not possible as the laboratory was not available for use. However, the theoretical part is well elaborated and corresponding to real expectations. Below, there is a simulation of two cases, in the first one we have two chambers with different initial pressures, it is expected that the curves reach an equilibrium point and attenuate. In the second case, there are two chambers with different pressures and disconnected from the pumps, it is expected that the pressures reach the equilibrium point in the simple arithmetic mean of the initial pressures.

The results create promising expectations for experimentation, so far, they have been shown to be reliable, which increases the confidence in an existing model to deal with new related problems.

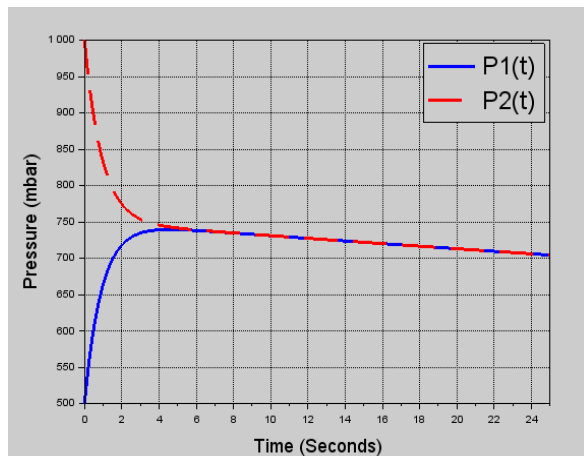


Fig. 1. System pumping with different initial pressures

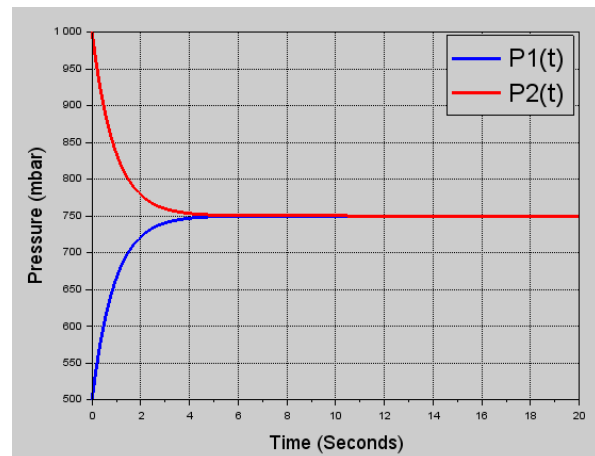


Fig. 2. Vacuum chambers with different initial pressures and disconnected from the pumps.

4. References

- [1] Moutinho, Augusto M. C.; Silva, Maria Eugenia S. Fronteira E; Cunha, Maria Aurea c. M. Isidoro da. Tecnologia de vácuo. 1. Ed. Lisboa: universidade nova Lisboa, 1980. P. 200
- [2] Trabalho de Conclusão de curso – Análise, modelagem e medição de sistemas complexos de pré-vácuo bombeados no regime viscoso laminar de escoamento – tcc do curdo de MPCE. Gabriel Geidson Johanson de Sousa. 2016.
- [3] Degasper, F.T., Modelagem e Análise Detalhadas de Sistemas de Vácuo. Dissertação (Mestrado em Engenharia Elétrica), FEEC – Unicamp, Campinas, SP, 2002

CHARACTERIZATION OF MAVIC® AKSIUM (700C) BICYCLE WHEEL RIM

F. A. Silvestre-Filho¹, J. L. Siqueira-Costa-Neto¹, A. R. Bigansolli¹, B. B. Lima-Kühn^{1,*}¹UFRRJ – Universidade Federal Rural do Rio de Janeiro. Rodovia BR 465, Km 7, Seropédica, RJ, 23851-970, Brazil.**1. Introduction**

The matrix of means of transport is diverse, being composed of cars, buses, trains, etc. Whereas so-called sustainable transport is growing and gaining more space in the current economic scenario; among them the cycling industry that has generated approximately 388,000 direct jobs in Europe, more than the steel industry and the three largest automotive companies in the United States, made up of companies: Ford, General Motors and Chrysler that combined generate about 510 thousand jobs. In Brazil, through using of e-bikes where, through a web-connected application, it is possible to rent a bicycle anywhere in the city. This new technology has been democratizing its use and modifying the way people are moving in the great metropolis of Rio de Janeiro and São Paulo. Whereas initiatives through public safety campaigns with the cyclist and projects to increase infrastructure such as the creation of new roads, could boost the industry and economy linked to cycling.

2. Experimental

The present work has the objective of characterizing the hardness of the AKSIUM model of the bicycle wheel rim manufactured by the company MAVIC from the 6061 T6 aluminum alloy and compare it with the commercially pure aluminum alloy manufactured and cataloged by CBA. Samples were obtained by manual cutting of the rim in non-standard sizes. Where they were then prepared metallographically for characterization by microhardness. For characterization by X-ray diffraction (XRD), the sample was filed to produce powder. The measurements were carried out at room temperature using Ni-filtered Cu-K α radiation in an diffractometer (Rigaku model Miniflex II) and the measurement conditions were $5^\circ < 2\theta < 90^\circ$, 0.05° step. The phases were identified based on Villars and Calvert crystallographic data [1] and the Powder Cell software [2].

3. Results and Discussions

The X-ray diffraction results show only aluminum peaks, indicating that the sample is made of an aluminum alloy. As well as the result of 79.83 VH found for the Vickers microhardness, corresponding to 69.85 HB, indicates that the characterized sample presents hardness values similar to those presented by aluminum alloys of the 6061 series, we can conclude that the Mavic® Aksium (700C) bicycle wheel rim can be made of 6061 aluminum alloy.

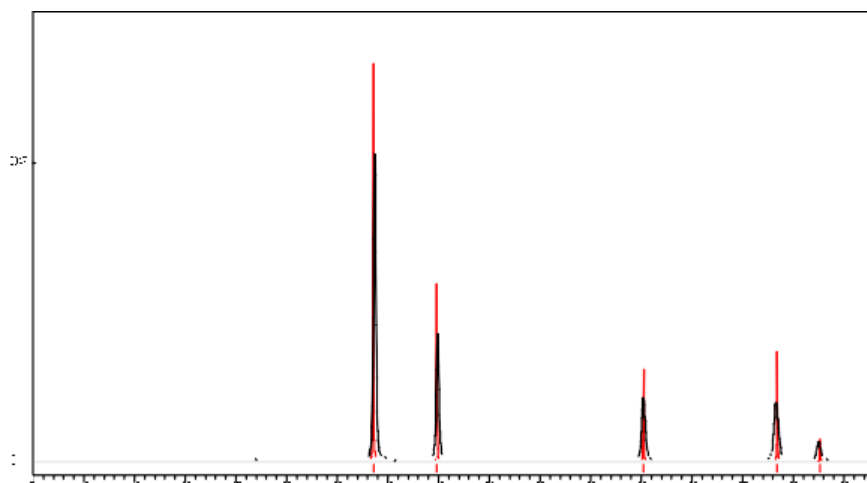


Fig. 1: X-ray diffractogram of the aluminum alloy of the bicycle wheel rim.

4. References

- [1] P. Villars, L.D. Calvert. Pearson's Handbook of Crystallographic Data for Intermetallic Phases. 2nd edition, Ed. Metals Park: ASM International, (1991).
- [2] W. Kraus, G. Nolze. PowderCell (2.3). Berlim: Fed. I. Res. Test, 1999.

ANTIBIOFILM EFFECT OF HELIUM ATMOSPHERIC COLD PLASMA ON *PSEUDOMONAS AERUGINOSA* MATURE BIOFILMS FORMED ON SILICONE SURFACES

Diego Morais da Silva^{1*}, Mariana R. C. Vegian¹, Taiana S. M. Mui¹, Daniel Legendre², Fabio Aoki³, Paulo Cardoso⁴, Konstantin G. Kostov¹, Cristiane Y. Koga-Ito¹

¹São Paulo State University (Unesp)

²Fundação Adib Jatene, ³Universidade Federal de São Paulo, ⁴InCor, São Paulo University

1. Introduction

Silicone is used in several types of prostheses and catheters that are susceptible to microbial biofilm formation. These biofilms can lead to clinical complications and can be a reservoir of microorganisms causing systemic infections. Cold atmospheric plasma (CAP) has been studied as an alternative in biofilm control, due to the reactive species with antimicrobial activity [1]. Then, the hypothesis of this study is that CAP could act as an alternative treatment in the control of *P. aeruginosa* mature biofilms on medical grade silicone surfaces.

2. Experimental

The biofilm was prepared with standardized suspensions of *P. aeruginosa* (ATCC 27853) containing 1×10^7 CFU/ml, from an overnight culture in BHI agar at 37°C. The biofilm was grown on the surface of 2D silicon specimens (8 mm Ø x 1 mm) that were previously sterilized using UV light for 10 min each side. Then, 2.0 mL of BHI supplemented with 0.2% of glucose and 200 µL of *P. aeruginosa* inoculum were added in each well containing the silicone specimens placed in 12-well plates. The biofilms were incubated for 48 h at 37 °C under agitation (120 rpm) and the culture medium was refreshed after 24h. After, the silicone specimens were washed with saline sterile solution and treated for 5 min with cold plasma jet under the following conditions: 31.7 kHz of frequency, tension amplitude of 12.3 kV, 2.0 SLM He gas flow and work distance of 0.5 cm. Then the biofilms were recovered from the specimens by sonication (pulse: 10 s and amplitude of 50%). Finally, the suspensions were serially diluted and plated in BHI agar for the determination of viable cell counts (CFU/mL). The experiments were performed in triplicate. Biofilms formed under the same conditions but not exposed to CAP were used for comparative purposes. Data obtained were analyzed by Mann-Whitney test ($p < 0.05$).

3. Results and Discussions

The results obtained after the biofilm treatment are shown in Figure 1. According to the graphic, CAP reduced significantly ($p < 0.05$) the number of *P. aeruginosa* viable cells when compared to the control group without exposure (~1.8 log). Thus, CAP demonstrates promising antimicrobial activities against *P. aeruginosa* biofilm on silicone materials widely used in hospital environment. The reduction in biofilm viability obtained by using this protocol was more effective than using the same exposure time but with lower working distance (~1 cm) [2].

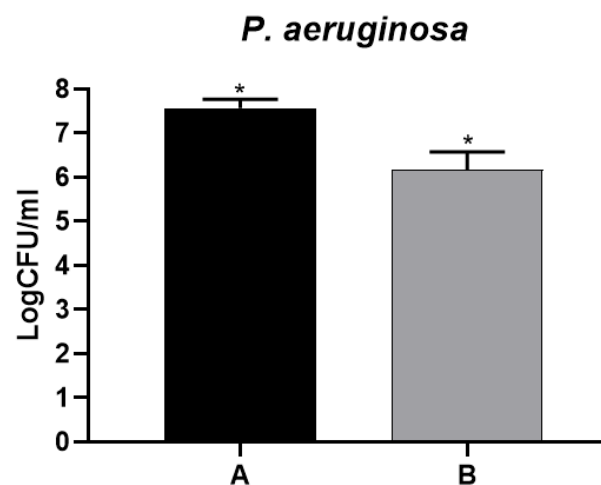


Fig. 1. Antibiofilm efficacy of He- cold atmospheric plasma on *Pseudomonas aeruginosa* (B) when compared to control group (A), expressed in Log CFU/ml. (*) indicates significant difference (Mann-Whitney test, $p < 0.05$).

4. References

- [1] Kostov, K.G. et. al Study of cold atmospheric plasma jet at the end of flexible plastic tube for microbial decontamination. *Plasma Processes and Polymers*, 2015 12(12), p.1383-1391.
- [2] Oliveira, M.A.C.D. et. al Inhibitory Effect of Cold Atmospheric Plasma on Chronic Wound-Related Multispecies Biofilms. *Applied Sciences*, 11(12), p.5441.

Acknowledgments

Funding by FAPESP (2019/05856-7, 2021/02680-5) and CNPq (308127/2018-8).

THERMAL ATOMIC LAYER DEPOSITION OF ALUMINA USING PLASMA-ACTIVATED WATER AS OXIDANT

João Pedro Magalhães Chaves^{1*}, William Chiappim Júnior¹, André Henrique Rabello. Ferreira², Argemiro Soares da Silva Sobrinho², Rodrigo Sávio Pessoa¹

¹Laboratório de Plasmas e Processos (LPP)- Instituto Tecnológico de Aeronáutica – São José dos Campos

²Departamento de Física e Química - Universidade Estadual Paulista “Júlio Mesquita Filho” - Guaratinguetá

1. Introduction

The atomic layer deposition (ALD) of metallic oxides, mainly alumina (Al_2O_3), when performed in thermal mode, uses deionized water (DI) as oxidizing precursor and trimethylaluminum (TMA) as a metallic precursor. However, the growth rate per cycle (GPC) of thin Al_2O_3 films for the precursors mentioned above is limited to 0.1 nm/cycle [1]. To increase the GPC, the plasma-enhanced ALD process (PEALD) is commonly used where DI water is replaced by O_2 plasma as an oxidizer [2]. In this process, which uses TMA and O_2 plasma, there is an increase in the GPC of the alumina to 0.12 nm/cycle, i.e., a gain of 20% compared to thermal ALD. This gain is due to the radicals generated in the plasma, such as electrons, ions, and species of neutral gases that allow greater efficiency in generating active sites for future reactions, promoting greater GPC [3]. PEALD uses a plasma generated in a plasma source that uses electrical energy to ionize and dissociate the introduced gas, usually O_2 , for oxide growth, significantly increasing equipment and film production costs. The present work presents a cheap alternative to increase the GPC of alumina by 17%. We used a gliding arc plasma and compressed air to activate DI water. After activation, plasma-activated water (PAW) is carried out into the oxidizing precursor source of thermal ALD and the PAW increases the GPC of alumina.

2. Methodology

PAW was prepared by a forward vortex flow reactor (FVFR) type with air compressed flow of 5 L min^{-1} , and plasma power of 8.6 W [4]. It was used 40 mL of DI at 0.3 cm of the plasma, and the activation times were 10, 30, and 60 min. It was obtained PAWs with pH of 3.6, 3.1, and 2.7, respectively. After the water activation, the PAWs were put on into a recipient and introduced in the line of oxidant precursor in thermal ALD. The ALD pulse times were 0.15-30-0.3-30 s, respectively, TMA, N_2 purge, PAW, and another N_2 purge. The number of cycles was fixed at 1000 cycles and the substrate was the Si (100). PAW was characterized by a pHmeter and UV-Vis spectrophotometry. Alumina thin films growth was characterized *in-situ* by mass spectrometry and *ex-situ* by an optical profilometer, FT-IR, EDS, and FEG-SEM.

3. Results and Discussions

Through optical profilometry analysis, the GPC of all films was determined, including the control sample, which was DI water with pH = 6.7, and of all activated waters, where we have the following GPCs: 0.0090 (control), 0.105, 0.109, 0.107 nm/cycle, respectively, pH 6.7, 3.6, 3.1, and 2.7. This result demonstrates the ability of PAW to improve the growth rate of films grown by thermal ALD when replacing DI water. This behavior is due to the existence of reactive oxygen and nitrogen species (RONS) generated in the activation of water by plasma, which in the present work increased by 17% the GPC of the samples that used PAW compared to the control sample that used DI water. The following RONS were identified through the UV-Vis spectra: HNO_2 , NO_2 , NO_3 , H_2O_2 , and O_3 , which probably contributed to activating the sites on the Si (100) substrate and thus improved the rate of growth of the films. The morphological analysis of the EDS proved the formation of alumina, and the FEG-SEM showed the existence of crystallites in the shape of the alumina thin films. Photos taken by smartphones prove the uniformity of the films grown using PAW (single color films). In contrast to DI, water was used, where the films show a non-uniformity in the films (multi-color films).

4. References

- [1] Puurunen R.L, J. Appl. Phys. 97, 121323 (2005 a,b);
- [2] Chiappim, W.; et al. Effect of Plasma-Enhanced Atomic Layer Deposition on Oxygen Overabundance and Its Influence on the Morphological, Optical, Structural, and Mechanical Properties of Al-Doped TiO_2 Coating. *Micromachines* 2021, 12, 588. <https://doi.org/10.3390/mi12060588>
- [3] George S. M., Chemical Reviews, 2010, Vol. 110, No. 1(2009)
- [4] Chiappim, W.; et al Antimicrobial Effect of Plasma-Activated Tap Water on *Staphylococcus aureus*, *Escherichia coli*, and *Candida albicans*. *Water* 2021, 13, 1480. <https://doi.org/10.3390/w13111480>

Acknowledgments

João Pedro M. Chaves thanks CAPES by the scholarship and W. Chiappim thanks the individual grant financed by FAPESP grant nº. 20/10450-7.

VALIDATION OF THE NUMERICAL MODEL USING THERMAL BARRIER COATING IN SHAPE MEMORY ALLOY

Brito A. A. R.^{1*}, Costa F. J.², Passaro A.³ and Lima M. S. F.³

¹*Instituto Tecnológico de Aeronáutica – PG-CTE, São José dos Campos - SP*

²*BRENG Engenharia e Tecnologia Ltda, São José dos Campos - SP*

³*Instituto de Estudos Avançados- São José dos Campos – SP*

1. Introduction

In the mid-1960s, high-performance composite materials were introduced definitely into the industry, especially in the aerospace sector. Through the American Naval Laboratory, an equiatomic Nickel-Titanium alloy was discovered in which it demonstrated shape memory effects when exposed to stress or heat. [1]. In order not to suffer any type of ablation when exposed to high temperatures, it is necessary to apply thermal barrier coatings, called TBC (Thermal Barrier Coatings) and make a better analysis of alloy's behavior to validate the numerical model (Auricchio), made by operating ANSYS software.

2. Theory

The Nickel-Titanium alloy, commonly called Nitinol, has characteristics such as superelasticity and Shape Memory Effect (SME), and can return to a previously defined shape at suitable temperatures. In pre-defined paper and considering some bibliographic reviews, the need for specific techniques with the purpose of avoiding alloy ablation is evident. Therefore, in this paper in which the alloy will be exposed to high temperatures, the use of TBC coating is necessary. The TBC system is subdivided by the thermal protection segment (thermal insulation) and chemical protection composed of Bond Coat (BC) and Thermally Grown Oxide (TGO), as shown in figure 1[4]. Its thickness and typing depend on operating conditions [2]. The model used in ANSYS software to represent SME is based on the model proposed by Auricchio [3], which proposes to analyze in detail the pseudoelastic behavior of the alloy phase transaction when submitted to a numerical analysis very close to the experimental results.

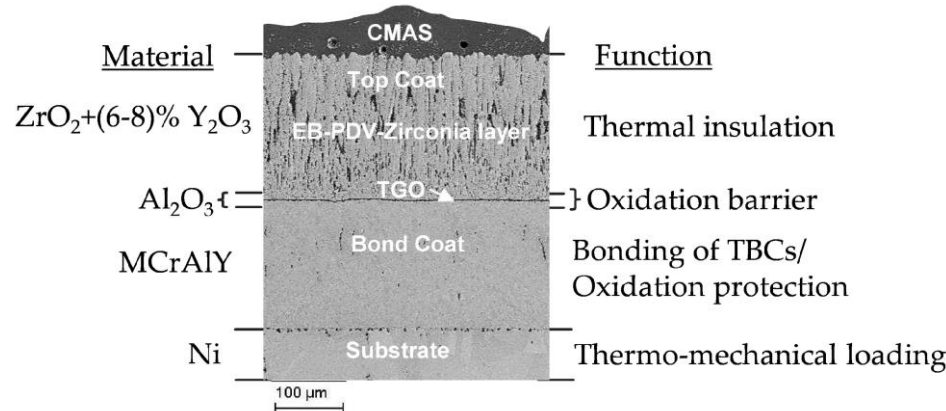


Fig. 1. Layout of the TBC System interconnected on a metallic substrate.

3. Results and Discussions

I've arrived to the conclusion that experimental test results are indispensable to serve as a basis for the parameters necessary for validating the numerical methodology using the Auricchio model through ANSYS software.

4. References

- [1] Brito A. A. R.; Costa F. J.; Passaro A.; Lima M. S. F. "Modeling of shape-memory alloys in scramjet engine applications", rbav.v40, (2020)
- [2] Teleginski, V. "Deposição de revestimentos com laser de CO₂ para proteção térmica de palhetas de turbinas aeronáuticas e industriais". 85f. (2016).
- [3] Silva, P. C. S.; Grassi, E. N. D.; Savi, M. A.; Araújo, C. J.; Santos, N. C. "Simulação numérica do comportamento superelástico de mini molas de niti usando ansys." (2014).
- [4] Kabir, M.R.; Sirigiri, A.K.; Naraparaju, R.; Schulz, U. "Flow Kinetics of Molten Silicates through Thermal Barrier Coating: A Numerical Study". Coatings, (2019).

Acknowledgments

The first author thanks the company Breng Engenharia e Tecnologia Ltda and the Institute for Advanced Studies for providing support to the research project.

EFFICACY ANTIBACTERIAL OF PLASMA ACTIVATED DEIONIZED WATER

Aline da Graça Sampaio^{1*}, William Chiappim², Rodrigo Savio Pessoa², and Cristiane Y. Koga-Ito¹

¹São Paulo State University (Unesp)

²Aeronautics Institute of Technology (ITA)

1. Introduction

Escherichia coli is a Gram-negative pathogen causative of several problems in public health worldwide and, in some occasions, can be related to mortality [1]. Plasma activated water (PAW) has been cited as a promising antimicrobial tool on different microorganisms [2-3]. However, there is still need to standardize the protocols of PAW obtaining and characterization. Therefore, this study aimed to evaluate the kinetic of inhibition of *E. coli* after exposure to PAW obtained with a standardized protocol. Also, PAW was characterized.

2. Experimental

Deionized water (DW) was activated by plasma by indirect application (5 mm from the surface) of a gliding arc reactor with compressed air generated by a compressor with a flow of 5 L/min for 60 min in 40 ml of DW. The pH of deionized water and PADW was measured with a pHmeter. The concentrations of oxygen and nitrogen reactive species (RONS) in PADW were measured by a UV-Vis spectrophotometer at 190 and 1200 nm, using as baseline the curve for DW. The antibacterial activity of PADW on *E. coli* was evaluated at different exposure times (1 min to 1 h). 1 mL of the suspension was prepared in physiologic solution (0.9%) and exposed to 4 mL of PADW pH 2.5. An aliquot of final suspension was serially diluted and plated in BHI agar. After incubation for 37 °C for 24 h, the reduction in bacterial counts was determined. Results were expressed in values of colony forming units (CFU/mL). In order to evaluate the effect of acidic conditions on the microorganism, sterile deionized water pH 2.5 obtained with the addition of nitric acid was tested. Experiments were done in quadruplicate in 2 independent occasions.

3. Results and Discussions

Figure 1 shows the kinetics of *E. coli* inactivation after exposure to PADW. The antimicrobial effect was observed after 5 min with reduction of 5 log. Figure 2 shows the reduction of pH after activation of DW, from 7.3 to 2.5. In Figure 2, the RONS generated by activation can be observed, being 30% of HNO₂ e 42% de NO₃⁻ with low concentration of O₃ and similar concentrations of NO²⁻ e H₂O₂. The result in Figure 1 suggests that the antibacterial effect is not related to low pH, but to the RONS in PADW.

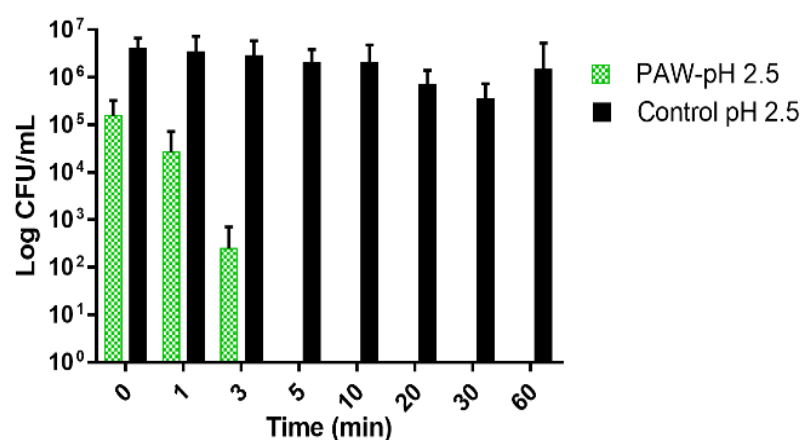


Fig. 1. Inactivation kinetics of *E. coli* after exposition to PADW-pH 2.5.

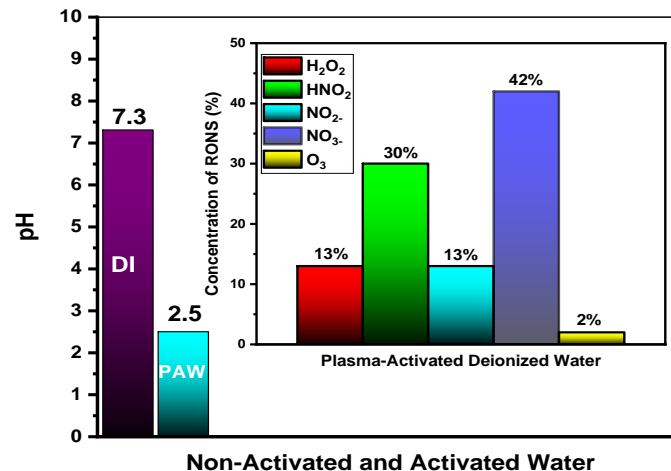


Fig. 2. pH and percentual concentrations of RONS.

4. References

- [1] Jang J, Hur H-G, Sadowsky MJ, Byappanahalli MN, Yan T, Ishii S, J Appl Microbiol, (2017).
- [2] Kamgang-Youbi G., Herry J. M., Meylheuc T., Brisset J.L., Bellon-Fontaine M. N., Doubla A., Naïtali M, L. Appl Microbiol, (2009).
- [3] Naitali, M., Kamgang-Youbi, G., Herry, J.-M., Bellon-Fontaine, M.-N., & Brisset, J.-L., Appl Env Microbiol, (2010).

Acknowledgments

Funding by FAPESP (2019/05856-7, 2021/02680-5) and CNPq (308127/2018-8). W. Chiappim thanks the individual grant financed by FAPESP grant n° 2019/25652-7.

CHARACTERIZATION OF THE Ti-10Mo-40Zr ALLOY FOR BIOMEDICAL APPLICATIONS

Renan Eduardo de Lima Lopes^{1*}, Israel Ramos Rodrigues¹, Gerson Santos de Almeida², Dante Oliver GuimCorrêa¹, Willian Fernando Zambuzzi², Carlos Roberto Grandini¹

¹ UNESP – Universidade Estadual Paulista, Faculdade de Ciências, Lab. Anelasticidade e Biomateriais, 17.033-360, Bauru, SP, Brazil

²UNESP - Universidade Estadual Paulista, Instituto de Biociências, 18.618-689, Botucatu, SP, Brazil

1. Introduction

Due to the large population growth and to the increase in life expectancy in the 21st century, the number of people needing prostheses or orthoses has increased significantly. It is estimated that the investment in biomaterials in 2020 in Latin America was 7.28 billion dollars, with a forecast of 13.01 billion by 2025 [1]. Biomaterials must have certain general and specific application characteristics, good compatibility, osseointegration, no toxicity, good corrosion resistance and low modulus of elasticity. Ti alloys have such characteristics, specifically Ti-Mo- Zr ternary alloy.

2. Experimental

The characterization was divided into four parts, after melting (#0), after the first 12-hour heat treatment (T1), after hot-rolling (#1) and after quenching (T2). X-ray diffraction, electron dispersion spectroscopy (EDS), optical microscopy (OM), scanning electron microscopy (SEM), elasticity modulus and biological analysis were performed.

3. Results and Discussions

After melting, the ingot presented silver color, which shows that the ingot was not contaminated with impurities. Alloy density was 5,71 g/cm³, higher than cp-Ti, which is due to the addition of more dense elements like Zr and o. Regarding the X-ray diffraction (Figure 1) it shows that the crystalline structure is characteristic of β phase. Results of biological analysis (Figure 2) show that the alloy has an excellent adhesion of cells and despite the result of cell viability being under the control group, the alloy has no toxicity. The results show that the alloy has good characteristics for biomedical applications, having an elastic modulus of 66.25 MPa, thus avoiding the stress shielding effect.

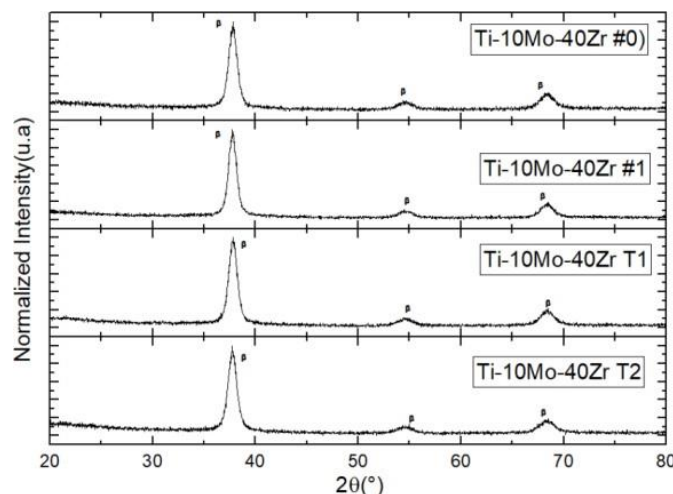


Fig. 1. X-ray diffraction of the studied alloy

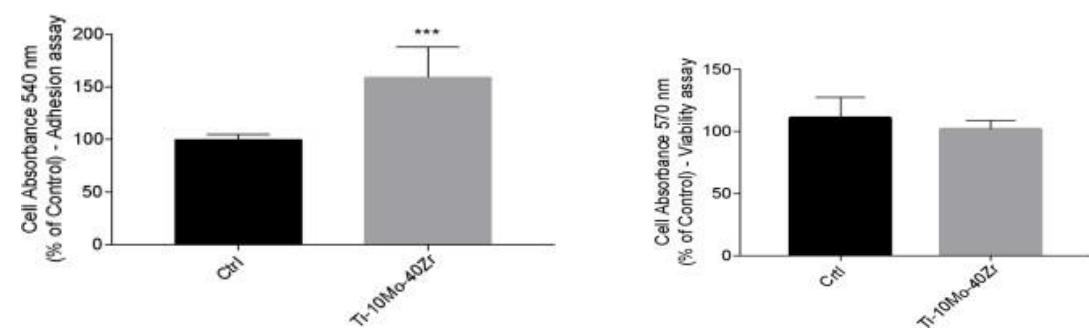


Fig. 2. Biological Analysis - (a)Adhesion Essay. (b)Viability Essay of the studied alloy

4. References

- [1] <https://www.marketdataforecast.com/market-reports/latin-america-biomaterials-market>
- [2] Kuroda, P.A.B.; Buzalaf, M.A.R.; Grandini, C.R. Materials Science and Engineering C 67 (2016) 511-515.).
- [3] Ho, W.F. et al. Materials Science and Engineering C 32 (2012) 517-522.

Acknowledgments

The authors would like to thank CNPq and FAPESP for their financial support.

DEVELOPMENT OF PLASMA BORIDING TREATMENT WITH PASTE INCARBON STEEL AND STAINLESS STEEL

Otávio Augusto de Morais Rosa Santos^{1*}, Felipe Lopes Fonseca da Silva², Rafael Roberto Pavani³, Andrieli Marques dos Santos⁴, Larissa Solano de Almeida⁵,Marcos Dorigão Manfrinato⁶ and Luciana Sgarbi Rossino⁷^{1,4,6,7}*Sorocaba Technological College, Sorocaba, SP, Brazil*^{2,3,5,6,7}*Federal University of São Carlos – Sorocaba Campi, Sorocaba, SP, Brazil***1. Introduction**

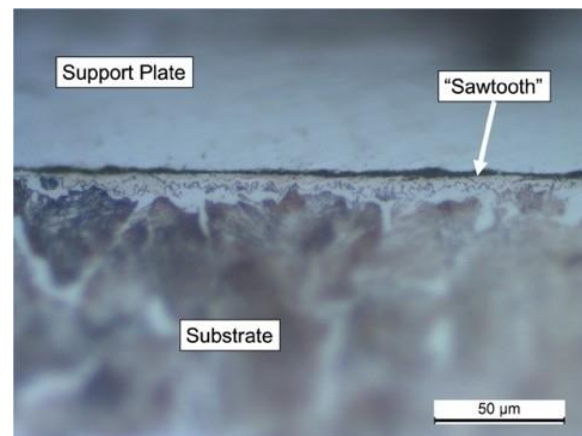
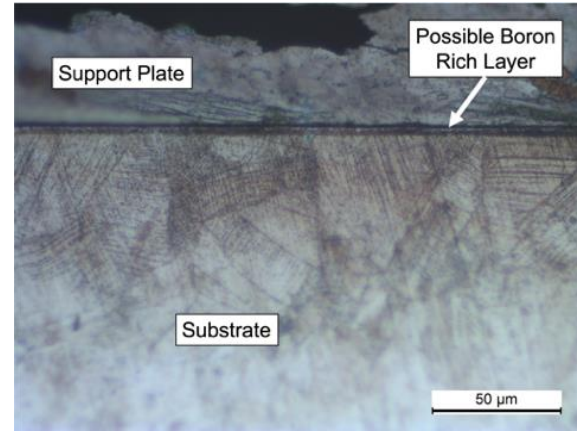
The thermochemical process of plasma boriding is an innovative technology that has been gaining attention in the research and development area. The interest in this process is due to the significant improvement of important properties in the industrial and aerospace areas, such as wear, corrosion, and increased hardness [1]. Among the various methods of this technology, the plasma method is one of the most efficient when it comes to improving the surface properties of the material, however, the gases used as borating agents in this process, such as B₂H₆ (diborane), BCl₃ (boron trichloride) and BF₃ (boron trifluoride) are toxic, corrosive and explosive, making it a dangerous and unfeasible process without the proper equipment [2]. Aiming at the use of this process, but in a less aggressive and dangerous way, the objective of this work is to develop and implement the boron slurry plasma boriding process and analyze the layer formation and diffusion of the boron element in the substrate.

2. Experimental

The samples of 1020 carbon steel and 304 stainless steel were sanded, polished and cleaned, and then covered with the boron paste, which contains in its mixture the borating agent powder Ekabor 2, tetraborate and alcohol fluids. After preparation, the samples were placed in the plasma reactor and surface treated using a DC-power supply was carried out at 850°C for 2 hours, using 40% H₂, 40% N₂ and 20% Ar with a gas flow of 500 sccm. The effectiveness of the treatment was verified by microhardness and metallography characterizations, that were performed to verify and validate the brief diffusion of boron in the substrate.

3. Results and Discussions

It is possible to observe in Figures 1 and 2 the presence of an even broken layer formed on the substrate. For 1020 carbon steel (Figure 1), in the region where the diffusion zone would occur, the typical microstructure of the boron diffusion principle in the material is visible, with the presence of "sawtooth", usually found in carbon steels when they are boron formed layer. For 304 stainless steel (Figure 2), a dark region was observed through metallography. The surface microhardness of the 1020 carbon steel sample was of 1707HV and the 304 stainless steel sample of 622HV, proving the surface hardening through the plasma boriding treatment. It is possible to conclude that the plasma paste boriding treatment was possible in low time combining solid paste and plasma to improve the hardness of two different metals.

**Fig. 1. Metallography of boriding 1020 steel.****Fig. 2. Metallography of boriding 304 stainless steel.****4. References**

- [1] CABEO, E. R. et al. Plasma-assisted boriding of industrial components in a pulsed d.c. glowdischarge. *Surface and Coatings Technology*, [s. l.], v. 116–119, p. 229–233, 1999
- [2] KEDDAM, M. et al. Characterization and Diffusion Kinetics of the Plasma Paste Borided AISI440C Steel. *Transactions of the Indian Institute of Metals*, [s. l.], v. 70, n. 5, p. 1377–1385, 2017.

Acknowledgments

We would like to acknowledge Fapesp (2021/05995-7) and Capes (code001).

EFFECT OF STERILIZATION PLASMS ON PROPERTIES PHYSICOCHEMICALS OF RESPIRATORS N95

R. K. Issaka, E. C. Rangel, R. P. Ribeiro, N. C. Cruz, T. Passeti, M. L. Santos.

Control and Automation Engineering, UNESP – Institute of Science and Technology of Sorocaba, SP, Brazil.

1. Introduction

The emergence of SARS-CoV-2 coronavirus impacted the entire world and brought with it a sudden increase in demand for N95 respirators, high price issues and the lack of this device were notorious. In order to improve the use of masks, their reuse by means of sterilization has become an ecologically and economically alternative.

Plasma sterilization [1] is characterized by its low consumption of materials and energy, making it a promising way to decontaminate and sterilize masks, but further studies are needed in the area. Relevant results on the behavior of masks under plasma can be found in this text, demonstrating the potential in this form of treatment.

2. Experimental

Tissue samples from the N95 masks were placed on the grounded and on the driven (13.56 MHz, 100 W) electrode of the cold plasma reactor. The pressure was stabilized at 1.86×10^{-2} Torr by introduction of citric acid solution vapor diluted with different gases (O_2 , Ar, N_2). Treatments were performed for 10 min. Infrared spectroscopy, energy dispersive spectroscopy, contact angle, scanning electron microscopy were respectively used to evaluate the chemical structure, chemical composition, surface energy and morphology of the samples.

3. Results and Discussions

The mask is composed by an innermost white tissue, characterized as polypropylene (Fig. 1) and by the outermost blue tissue, identified as polystyrene (Fig. 1). After the analysis, it was noted that only slight morphological changes were detected in the tissue fibers and the modification depended on the dilution gases (Ar, N_2 , O_2) (Fig. 2) inserted. Furthermore, the surface energy of the white hydrophobic tissue changed slightly after the treatments, maintaining its hydrophobic nature, while in the blue hydrophobic tissue the surface energy increased a lot, making the mask surface super hydrophilic.

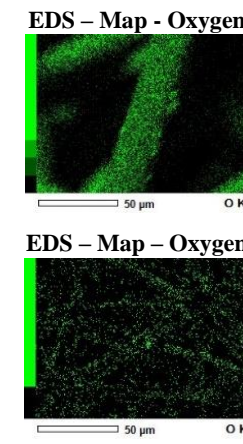
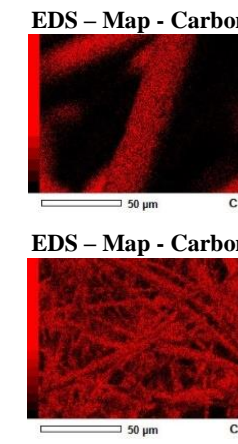
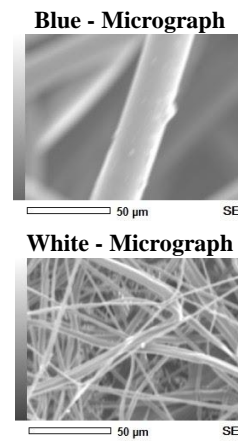
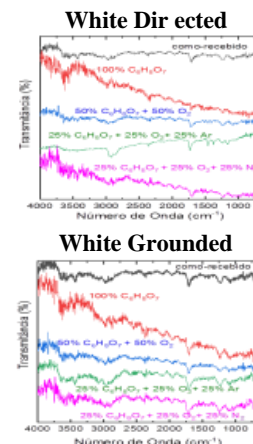
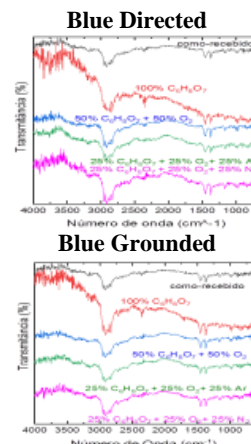


Fig. 1 Infrared spectroscopy graphs of both tissues from N95 masks

Fig. 2. Compositional map of the external and internal fabrics of the N95 mask

4. Conclusions

The results demonstrate that the process used did not affect the usability of the masks as it did not substantially harm the treated tissues. Furthermore, it was noted that the use of citric acid solution vapor in higher concentrations is preferable due to its less aggressive characteristics, however further studies are needed to confirm that the treatment is sterilizing.

5. References

[1] CAMPOS de Souza, J.H; Estudos de esterilização por plasma a pressão atmosférica. 23–27, (2012)

Acknowledgments

Special thanks to the Sorocaba Technological Plasma Laboratory team, the Sorocaba Institute of Science and Technology and everyone who made this project possible.

STUDY OF THICKNESS VARIATION ON Ti80-Nb20-BASED ALLOY FILMS DEPOSITED BY DCMS ON AISI 316L SUBSTRATE FOR BIOMEDICAL APPLICATIONS.

Katherine Martinez-Orozco^{1*}, Raira Apolinario², Pedro Tavares Avila², Haroldo Cavalcanti Pinto², and Pedro Augusto de Paula Nascente¹

¹*Federal University of São Carlos, Department of Materials Engineering, Graduate Program in Materials Science and Engineering.*

²*University of São Paulo, São Carlos, Department of Materials Engineering.*

1. Introduction

Ti-based alloys are one of the best options for biomedical applications. Ti exhibits excellent strength/density ratio, superior corrosion resistance, biocompatibility, and promotes the osteointegration process with implants. The direct current magnetron sputtering is a PVD process that is employed to deposit coatings with excellent features. Coatings with good adhesion, wear, and corrosion resistance, among other desirable properties are obtained by means of DCMS [1]. Recently, our group has reported on the deposition and characterization of Ti-Nb, Ti-Nb-Zr, and Ti-Nb-Mg alloy thin films [2, 3]. These films, which were deposited by DCMS, present a body-centered cubic structure (β phase); this phase has lower elastic modulus and is more suitable for biomedical applications. The main objective of the present work is to explore thicker Ti-Nb coatings in order to assess their influence on the mechanical properties.

2. Experimental

$Ti_{80}Nb_{20}$ alloy coatings were deposited by DCMS on 316L stainless steel substrates, with rectangular shape and an area of 20 x 15 mm. The first deposition (coating #1) was performed at 400°C applying a bias voltage of -180V, the second deposition (coating #2), at 250°C and bias voltage of -150V. For both coatings, the deposition time was one hour. The microstructural and chemical characterization were performed by scanning electron microscopy (SEM) coupled with energy dispersive spectroscopy (EDS); and the mechanical properties were evaluated by nanoindentation tests.

3. Results and Discussions

Coatings having 3.96 and 5.90 μ m were obtained after the first and second deposition, respectively, as shown in figures 1 and 2. Coating #1 presents a hardness value of 674.09 HV, while coating #2 average hardness is 846.11 HV.

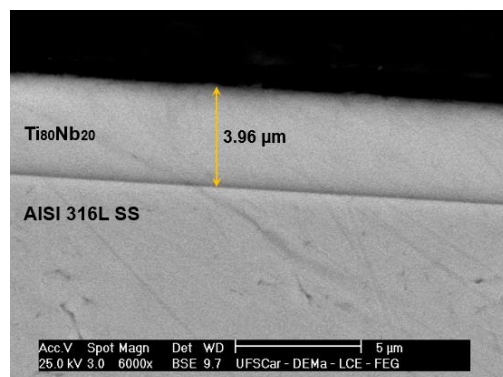


Fig. 1. SEM micrograph for the $Ti_{80}Nb_{20}$ coating #1.

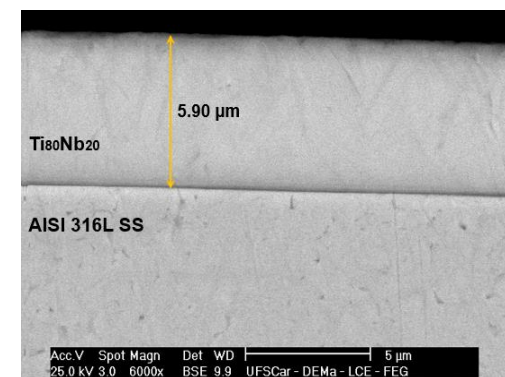


Fig. 2. SEM micrograph for the $Ti_{80}Nb_{20}$ coating #2.

4. References

- [1] D.M. Mattox, Deposition (PVD) Processing, 2009.
- [2] E.D. Gonzalez, C.R.M. Afonso, P.A.P. Nascente, Thin Solid Films 661 (2018) 92–97.
- [3] E.D. Gonzalez, N.K. Fukumasu, A.L. Gobbi, C.R.M. Afonso, P.A.P. Nascente, Surf. Coat. Technol. 400 (2020) 126070.

Acknowledgments

This work was supported by the Brazilian agencies FAPESP (process 2017/25983-9), CNPq (process 302450/2017-3), Coordenação de Aperfeiçoamento de Pessoal de Nível Superior – Brazil (CAPES) – Finance Code 001.

STRUCTURAL AND MICROSTRUCTURAL CHARACTERIZATION OF Ti-25Ta-Nb SYSTEM

Fernanda de Freitas Quadros* and Carlos Roberto Grandini
UNESP – Univ. Estadual Paulista, Laboratório de Anelasticidade e Biomateriais, Bauru, SP, Brazil

1. Introduction

Titanium alloys are widely used as biomaterials as they add good corrosion resistance, low modulus of elasticity, in addition to biocompatibility. When adding other elements to titanium alloys, such as tantalum and niobium, there is a modification of the mechanical properties and a change in the allotropic transformation temperature of titanium¹. Tantalum and niobium are excellent β -stabilizers; when added to titanium alloys, they improve corrosion resistance, aid in the material's biocompatibility, and reduce its elastic modulus². This work aims to analyze the influence of the substitutional element niobium on the crystal structure and microstructure of the Ti-25Ta-xNb system (x = 10, 20, 30 and 40% in weight).

2. Experimental

After pickling, precursors such as titanium, tantalum and niobium were melted in an argon controlled atmosphere arc-voltaic furnace. The chemical characterization was carried out through specification measurements by Archimedes' principle and chemical microanalysis by EDS. Structural and microstructural analysis was performed using X-ray diffractograms and, optical and electronic micrographs.

3. Results and Discussions

EDS measurements and alloy density values indicate that the samples show good stoichiometry, respecting ASTM 2066 standard. The addition of niobium causes an increase in density, as the atomic number of niobium is higher than the atomic number of titanium.

Table 1: EDS measurements

Ligas	Ti (%p)	Ta (%p)	Nb (%p)
Ti-25Ta-10Nb	63.29 \pm 0,2	26.27 \pm 0,2	10.44 \pm 0,2
Ti-25Ta-20Nb	54.08 \pm 0,2	25.78 \pm 0,2	20.15 \pm 0,2
Ti-25Ta-30Nb	43.04 \pm 0,2	25.58 \pm 0,2	31.38 \pm 0,2
Ti-25Ta-40Nb	35.06 \pm 0,2	24.97 \pm 0,2	39.96 \pm 0,2

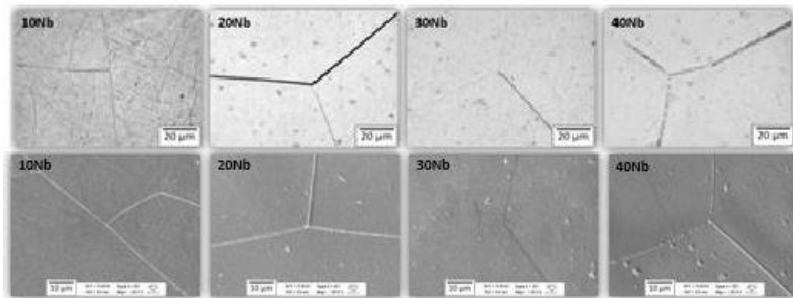


Fig. 2: Optical micrographs of alloys Ti-25Ta-xNb

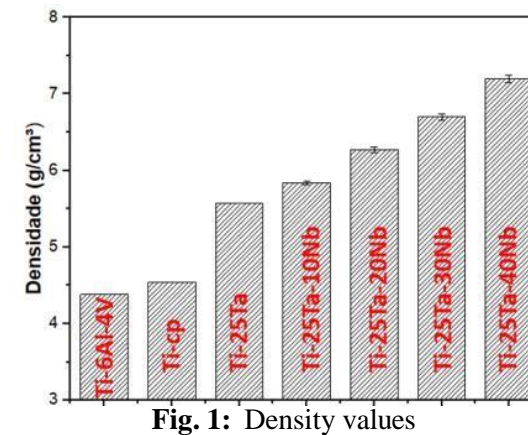


Fig. 1: Density values

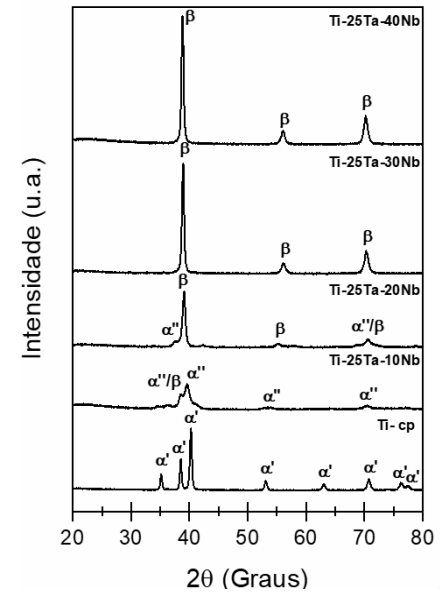


Fig. 3: X-ray diffractograms

4. References

[1] L.-Y. Chen, Y.-W. Cui, and L.-C. Zhang, Metals 10, 1139 (2020).
 [2] F. F. Quadros, P. A. B. Kuroda, K. S. J. Sousa, T. A. G. Donato, and C. R. Grandini, Journal of Materials Research and Technology 8, 4108 (2019).

Acknowledgments

The authors thank CNPq and FAPESP for financial support.

AN STUDY OF THE ROUGHNESS ON METALLIC GLASSES USING ATOMIC FORCE MICROSCOPY

Cícero J. R. Lustosa^{1*}, Paulo Wilmar Marques² and Odila Florêncio³¹Presbyterian Mackenzie University, Engineering School, São Paulo, SP ²Federal University of São Carlos, Department of Physics, São Carlos, SP ³Federal University of São Carlos, Campus Sorocaba, Sorocaba, SP**1. Introduction**

Metallic glasses are materials that present absent of periodic atomic order of long scale and seems to be promised to application in the science and engineering field [1]. They were obtained first in 1960 through the technique of rapid cooling with thinner thickness, but the development of new production techniques and combination of elements allowed the amorphous condition in millimeter-thick alloys, which received the denomination of bulk metallic glass [2-4]. Its properties are usually superior when compared to polycrystalline materials of same composition. The elasticity is greater in metallic glasses because this kind of materials do not have slip plans or linear defects.

2. Experimental

In this work were studied two alloys of metallic glasses with the compositions Cu47,5Zr45,5Al5Er2 and Cu47,75Zr47,75Al4,5. They were produced using arc furnace and characterized through X-ray diffraction, with Cu K_α radiation ($\lambda = 0.154$ nm), and Atomic Force Microscopy (AFM), from Nanoscope IIIA. Before the AFM, the samples were subjected to surface polishing treatment.

3. Results and Discussions

The analysis of the atomic structure of the Cu47,5Zr45,5Al5Er2 alloy showed great structural disorder, and the Cu47,75Zr47,75Al4,5 sample presented peaks from crystalline phases, like Zr₄Cu₂O (big cubic phase) formed due to the affinity between zirconium and oxygen [5], into the amorphous matrix. Using the AFM technique was possible to get the roughness average (Ra) and the Root Mean Square (RMS) from the surfaces. The sample Cu47,5Zr45,5Al5Er2 presented the values of 2.15 nm from Ra and 3.14 nm from RMS. Another sample shown better results of roughness, where Ra was 1.88 nm and the RMS was 2.53 nm. As is known, roughness is an import tribological parameter in materials and lower values allow less surface area exposed to harmful atmospheric effects such as corrosion. While the erbium sample is the best amorphous alloy, the other sample has advantage due to present higher surface regularity and lower roughness.

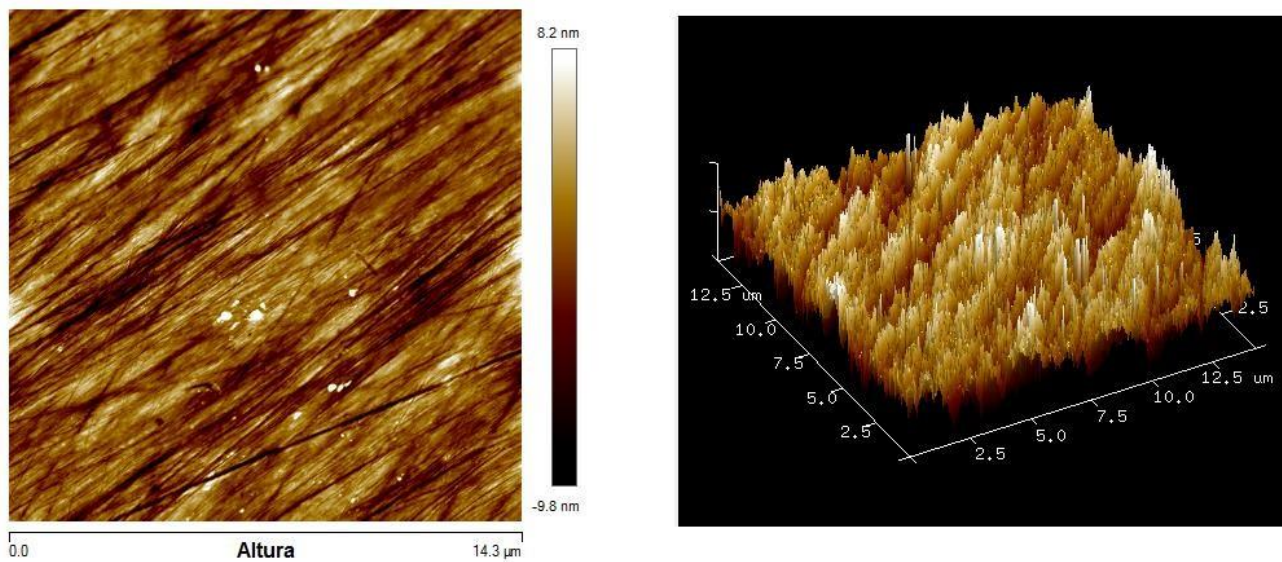


Fig. 1. AFM on sample composed by Cu_{47,75}Zr_{47,75}Al_{4,5}. This micrography presented better roughness than the sample with erbium in alloy.

4. References

- [1] N. T. Ngoc Nu and T. V. Luong, Jour. of Scien. Envin. And Tech, 5(4), 2209-2216, (2016).
- [2] W. Klement, R. H. Willens and P. Duwez, Nature, 187(4740), 869-870, (1960).
- [3] H. S. Chen and D. Turnbull, Acta Metallurgica, 17(5), 1021-1031, (1969).
- [4] J. Löffler, Intermetallics, 11(6), 529-540, (2003).
- [5] M. F. de Oliveira, Journal of Non-Crystalline Solids, 304, 51-55, (2002).

Acknowledgments

The authors thank to FAPESP (grant#2017/08913-6), CAPES and IFUSP for help on development of this project.

ANALYSIS OF THE YIELD STRENGTH USING O SOLIDWORKS SIMULATION CONSULTANT

Felipe Camargo Brito Matias^{1*}, Marco Antônio Pereira do Rosário², Belmira Benedita de Lima Kuhn¹ and Antonio Renato Bigansolli¹

¹Universidade Federal Rural do Rio de Janeiro – UFRRJ, Seropédica - RJ

²Neo Kinetika - Pesquisa e Desenvolvimento - ME / CNPJ: 15.339.431/0001-54 – Seropédica - RJ

1. Introduction

The Computer-Aided Engineering – CAE is a engineering and simulation software projects lets exploit the benefits of simulation when developing new products: shorten the time, increase flexibility, and improve performance. CAE allows a physics-based simulation to verify materials properties. This verification helps you detect and correct errors in the digital model. The aim of this work is to demonstrate this technology by simulation of the flexion effort applied in a metal sheet with and without constraints in the specific case.

2. Experimental

Solidworks® 2020 software, in student version, was used to simulate the flexion effort applied in a metal sheet in static condition. Firstly, the metal sheet was built using the Computer Aided Design (CAD) system with dimensions of 10 mm x 300 mm x 1000 mm. Then, the CAE mode was activated to define the parameters referring to physical characteristics, such as material, applied load and fixation. The metal sheet was simulated under a load of 10 kN and 70 kN.

3. Results and Discussions

The behavior resulting from the application of a load of 10 kN distributed along the sheet was simulated in order to analyses the flexion effort, greater load carrying capacity and greater deflection at break, and was observed that the stress values were below the yield strength of material, as expected. However, the behavior simulated from the application of a load of 70 kN show the deformation of the metal sheet (Fig.1). From the deformation of the metal sheet, solutions for improving the model were indicated by the software, such as new material, new load, new dimensions. Finally, a new simulation was carried out, replacing the initial dimensions by the indicated, that is, increasing the thickness of the metal sheet from 10 mm to 15 mm. Then, the simulation shows the metal sheet, with a greater thickness, without deformation (Fig. 2). This imply that the model gained resistance to the flexion effort, was possible to notice that the acting stresses were below the yield strength of material. It is possible to observe that the excessive loading causes the model to work above the yield stress, a condition that must be avoided in a project. Figure 2 shows that after the increase in thickness, there was a reduction in stresses acting along the body, where it is noted that the maximum stress is less than 551.48 MPa. Project aid technologies are very effective and have an integration capability between multidisciplinary teams, which for organizations in general helps in all stages of a project, reducing operational costs and avoiding wasted resources.

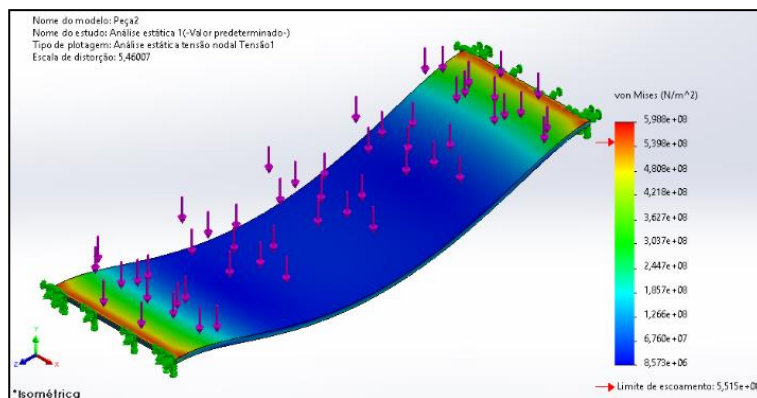


Fig. 1. Plot of von Mises stresses with maximum values acting above the material yield strength (551.48 MPa).

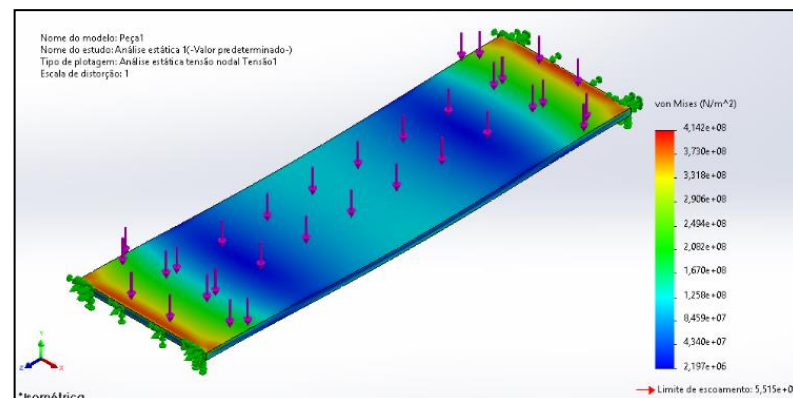


Fig. 2. Plot of von Mises stresses with maximum values acting below the material yield strength (551.48 MPa).

4. References

- [1] I.H. Shames, Introdução à Mecânica dos Sólidos, Prentice-Hall do Brasil (1983).
- [2] F.P. Beer and E.R. Johnston, Resistência dos Materiais, McGraw-Hill (1982).

THE APPLICATION OF CAE TECHNOLOGY IN THE TEACHING OF MATERIALS ENGINEERING

Felipe Camargo Brito Matias¹, Marco Antônio Pereira do Rosário², Belmira Benedita de Lima Kuhn¹ and Antonio Renato Bigansolli^{1,*}

¹Universidade Federal Rural do Rio de Janeiro – UFRRJ, Rodovia BR 465, Km 7, Seropédica - RJ

²Neo Kinetika - Pesquisa e Desenvolvimento - ME / CNPJ: 15.339.431/0001-54 – Seropédica – RJ

1. Introduction

Computer-Aided Engineering - CAE - is able to perform tests by simulating the structures and components, allowing a predictive analysis of the problems or failures that may occur in future phases of the project. The analyses that go into these tests include stress, dynamic, fluid, thermal, and static, among others, to verify the behavior of the object based on the input parameters. Most of these simulation parameters are based on the conditions of the environment and the interaction of the model with it. Thus, it is possible to input experimental variables such as temperature, pressure, forces, number of cycles and obtain answers that indicate whether all project constraints are controlled and whether the model meets the technical specifications. Virtual modelling methods bring a tremendous advantage in the formulation and execution of projects and research in materials engineering. The main objective of this study was to investigate the impact of simulated models on teaching in materials engineering.

2. Experimental

The software chosen for the simulations in this work was Solidworks Premium 2020 and Fusion 360, both in the student version. With them it was possible to create three-dimensional models of specimens using CAD technology and then perform simulations using CAE technology. First, a three-dimensional model of a prismatic shape (25.4mm x 25.4mm x 300mm) was created using the CAD system. When the CAE simulation mode was activated, an alloy steel was selected as the material and the tensile force was applied. The applied force was 100 kN and acted on a surface with a straight cross section of 645.16 mm². The other end was used to create the attachment points. The analysis was carried out under static conditions and a fine mesh was created for higher precision of the results.

3. Results and Discussions

Figure 1 is the CAD drawing of the specimen used in the simulation. Figure 2 is the demonstration of the body after the applied traction. It is possible to see the level of von Mises stress, with the predominant green color indicating a stress value well below the yield strength of the material.

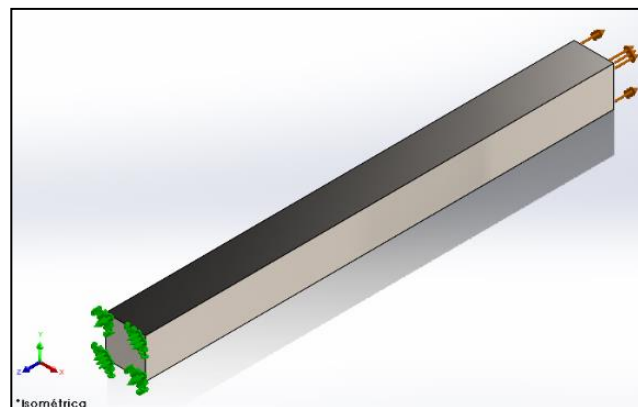


Fig. 1. Test body in Alloy Steel.

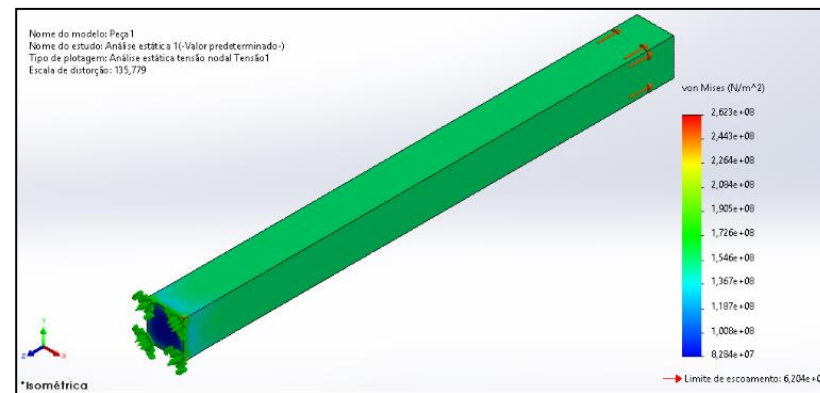


Fig. 2. Plot of voltage levels of de von Mises.

From a technological point of view, knowledge of the support systems for projects, CAD and CAE, can increase the opportunities for professionals in the job market and allow them to work in research and development in engineering fields. Although the systems obtained by CAE technology are not definitive, they allow to study the static stability taking into account the dynamics of the object behavior, which helps in decision making and reducing costs and time.

4. References

[1] Fábio A. O. Fernandes, Nilo Fuchter Júnior, Anderson Daleffe, Daniel Fritzen, Ricardo J. Alves de Sousa, Educ. Sci., 10 (5), 125, (2020).

STUDIES ON ADDITION OF NANOSTRUCTURED ZIRCONIA ONJC(H) OF (Y,ND)-123 SAMPLES

Leonardo Picanço Peixoto Abreu^{1*}, Ana Carolina de Léo Silva², and Marcelo Azevedo Neves³¹Undergraduate student in Materials Engineering – Escola Politécnica - UFRRJ²LMDS/DEFIS (Associated Researcher) – Instituto de Ciências Exatas – UFRRJ³Departamento de Física – Instituto de Ciências Exatas - UFRRJ**1. Introduction**

The (Y/RE)Ba₂Cu₃O_{7-X} (RE = Rare-Earth) oxide is a high critical temperature (T_c) superconductor and is also a Type-II superconductor. This means that in this material Abrikosov vortices can be formed. Nanoparticles can be used as pinning centers for those vortices and can artificially increase the value of the critical current density as a function of the applied magnetic field $J_c(H)$ [1]. In this work we study a processing route in order to a nanostructured zirconia powder can be used as artificial pinning centers in (Y/Nd)Ba₂Cu₃O_{7-X} High T_c superconductor.

2. Experimental

The obtained samples were prepared by usual solid state grinding, mixing and pelletizing of the reactant oxides and carbonates, and submitted to thermal treatment to produce YBa₂Cu₃O_{7-X} and NdBa₂Cu₃O_{7-X} phases [2]. After furnace cooling, the HTS pellets were grinded and nanostructured zirconia powder was added (6% wt.) to some of them in order to improve pinning forces. All samples were characterized by means of X-ray diffraction, scanning electron microscopy and magnetic moment measurements (including isothermal AC loops). The following synthesis program was studied: solid state reaction of powders of BaCO₃ and CuO with Nd₂O₃ or Y₂O₃, with addition of nanostructured ZrO₂ powder in NdBa₂Cu₃O_{7-X} samples after synthesis in a tubular furnace with oxygen flow, and a thermal program with one plateau of 950°C for 12 h (for the synthesis of the semiconductor phase, X = 1) followed by a plateau of 390°C for 6 h (for oxidation, to convert from the semiconductor phase to the superconductor phase X < 1).

3. Results and Discussions

Samples of NdBa₂Cu₃O_{7-X} showed higher $J_c(0)$ than samples of YBa₂Cu₃O_{7-X} and the introduction of nanostructured ZrO₂ powder in the NdBa₂Cu₃O_{7-X}, in the percentage by mass used (6%) and with the thermal programming used, does not affect the critical temperature $T_c = 87$ K nor the critical field $H_c = 250$ Oe, but increases by 1 order of magnitude the critical current density, to a value $J_c(0) = 3.06 \times 10^{16}$ A/cm², with a wide transition to the superconducting state, making the sample operable in subcooled liquid nitrogen. It is proposed to continue the research on that synthesis route, increasing the reaction and oxidation times, as well as the sintering times with ZrO₂.

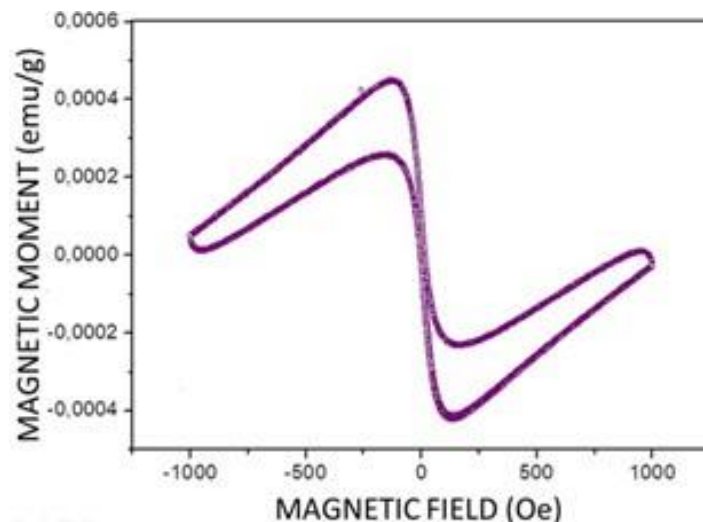


Fig. 1. Magnetization loop for NdBa₂Cu₃O_{7-X} without ZrO₂ addition with calculated $J_c(0) = 8.75 \times 10^{15}$ A/cm².

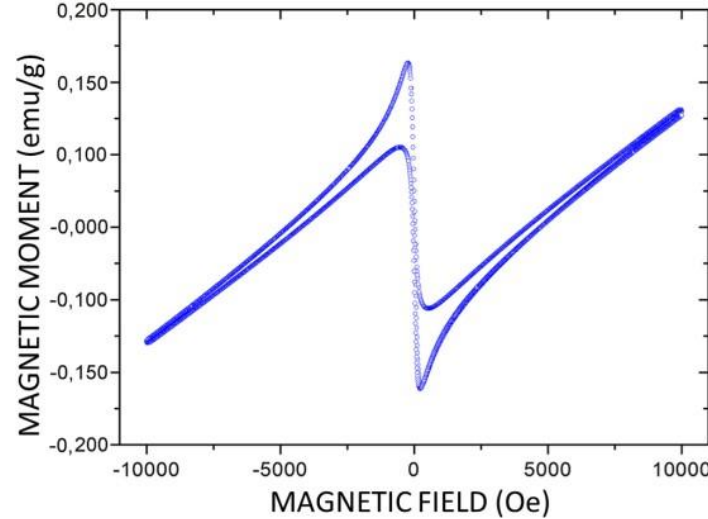


Fig. 2. Magnetization loop for NdBa₂Cu₃O_{7-X} with ZrO₂ addition with calculated $J_c(0) = 3.06 \times 10^{16}$ A/cm².

4. References

[1] WANG, Y., “Fundamental Elements of Applied Superconductivity in Electrical Engineering”. Singapore: John Wiley & Sons, 2013.
 [2] De LÉO, A.C. *et al.*, *IEEE Trans. App. Supercond.*, 28 (4), 2018, 7200305.

Acknowledgments

To the technical staff at LMDS–UFRRJ, LIETA–UERJ and LIMMT–CBPF, ANEEL R&D Program and PIBIC–CNPq.

PROCESSES FOR OBTAINING TYPE I COLLAGEN FROM RESIDUAL BOVINE BONE

Vanessa Ricas Biancardi^{1*}, Antonio Renato Bigansolli² and José Lucena Barbosa Junior¹

¹*Federal Rural University of Rio de Janeiro. Institute of Technology. Department of Food Science and Technology.*

²*Federal Rural University of Rio de Janeiro. Institute of Technology. Department of Chemical Engineering.*

1. Introduction

Establishing methodologies for obtaining collagen from bovine bone requires innovation and emerging technology, reinventing possible uses of the protein as an industrial input. Processes for obtaining type I collagen are mainly via hydrolysis to isolate fibers, peptides or amino acids with a preserved functionality [2,5]. Therefore, the present work aimed to validate such processes to obtain type I collagen and reuse residual bovine bones.

2. Experimental

Type I collagen was obtained from residual bovine tibia. It was started by manually removing the meat and fat with boiling at 100 °C. Followed by drying at 40 °C for 24 hours. Followed by grinding with hammermill (Tecnal TE-330) and analytical mill (Ika A11) with particle standardization at 0.5 cm. Followed by boiling at 100 °C for 1 h. Followed by solubilization in 0.5M acetic acid at 4 °C for 48h. Followed by enzymatic hydrolysis with Neutrase (Pango Enzymes) at 5% and 52 °C for 4h, with constant pH 7.5 adjustment with 2NNaOH. Finally, solubilization in 2M NaCl. Proteins in the supernatants were quantified by the Lowry method[1,3,4].

3. Results and Discussions

A difficulty and relevance in handling the grinding of the residual bones was observed. The sequential combination of mills was extremely important for the standardization of the particles. With this, solubilization and hydrolysis were possible to reproduce in sequence.



Fig. 1. Residual bovine tibia after boiling.



Fig. 2. Residual bovine tibia after grinding.

Acid and enzyme treatments have effects on the residues. Bones are rich in Ca+ and the acid solubilization helps the removal, besides interfering with the exogenous protein structures, preparing the collagen and bone for enzymatic hydrolysis. Non-covalent bonds are broken so as to disorganize the protein structure, producing swelling and dissolution, facilitating further enzyme action. The concentration, temperature and pH adopted in the enzymatic hydrolysis also had an effect on the residues. Since the enzyme needs favorable conditions to act and release type I collagen into the supernatant. Each step applied to the residue was crucial for obtaining type I collagen. At the end of the treatments the sample obtained 16.5 g/mL of protein concentration, according to Lowry's method. Therefore, the proposed treatments are valid processes to obtain type I collagen and reuse the residual bovine bones.

4. References

- [1] Ferraro, v. Et al. International journal of biological macromolecules, 97, 2017).
- [2] Gomez-guillen, m. C. Et al. Food hydrocolloids, 25, (2011).
- [3] Lowry, o.h., et al. J. Biol. Chem. 193, (1951).
- [4] Paola, c. M. Et al. Heliyon, 5, (2019).
- [5] Strøm-andersen, n. Journal of cleaner production, 253, (2020).

Acknowledgments

To CNPQ for the research support. To Beltec Group for the support of the materials.

ENERGY FLUX AND DISCHARGE WAVEFORMS IN ARGON PLASMA GENERATED BY BIPOLAR PULSED POWER SUPPLY

Thaís Macedo Vieira^{1*} and Julio César Sagás¹¹Laboratório de Plasmas, Filmes e Superfícies - Universidade do Estado de Santa Catarina (UDESC)**1. Introduction**

Plasmas are often used for surfaces treatment, however, each process receives influence from the electric discharge's characteristics. Therefore, the knowledge about these properties gives the ability to have control over them. A way of studying them is by electrostatic and thermal probes [1]. In particular, it is possible to measure the incoming energy flux to a given surface by using a calorimetric probe [2]. Our main goal is to study and compare the energy flux and the discharge waveforms for different bipolar pulsed power supplies.

2. Experimental

Argon plasmas were created by two asymmetric bipolar-pulsed plasma supplies, one commercial (Pinnacle Plus – Advanced Energy) and one developed at our laboratory (ABiPPS) [3]. Pinnacle Plus allows the control over power, frequency, and current, while ABiPPS allows finer control over the discharge waveform. In the first case, the frequency was varied in the range 10- 200 kHz with the power kept at 300 W. Using ABiPPS, the length of short positive and negative pulses (0.5 - 2.5 μ s), the length of the long negative pulse (5 - 50 μ s) and the number of short pulses (1 - 4) were changed. The floating potential, current, and voltage waveforms were measured with a digital oscilloscope. The frequency spectra were determined using Fast Fourier Transform (FFT) and the energy flux was obtained from the slope of temperature-time curves measured with the calorimetric probe [2]. The calorimetric probe is a Cu disc (20 mm of diameter and 2.0 mm of thickness) inserted in a ceramic (Macor) support. All experiments were carried out at 0.85 Torr.

3. Results and Discussions

The energy flux for each frequency using Pinnacle Plus (Fig. 1) is of the same order as the energy flux measured in the experiments using ABiPPS. For Pinnacle Plus, the energy flux is linear with discharge power and the frequency has only a minor effect, decreasing the energy flux above 150 kHz. For ABiPPS, there is no relevant relation between energy flux with the number of pulses and the length of the long negative pulse. However, the energy flux decreases with the length of short pulses (positive and negative), stabilizing for lengths above 1.5 μ s (Fig. 2). The floating potential is quite similar for both supplies.

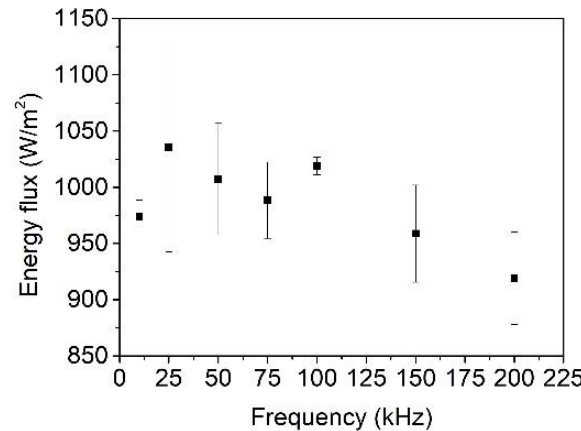


Fig. 1. Energy flux for different frequencies using Pinnacle Plus. The positive pulse length is 4.0 μ s except for 150 and 200 kHz, which are 2.6 and 2.0 μ s, respectively.

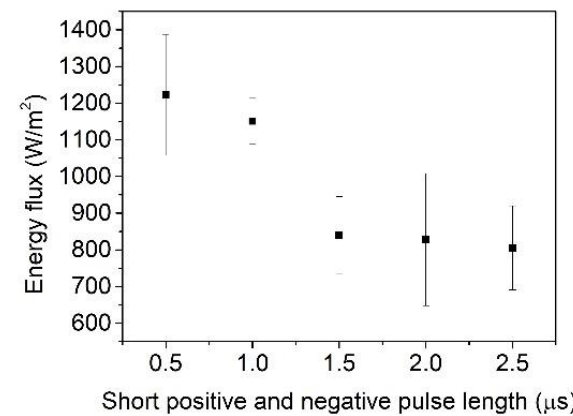


Fig. 2. Energy flux for different short pulse lengths using ABiPPS. The number of pulses is 1 and the long negative pulse length is 10 μ s.

4. References

- [1] Mott-Smith, H. M. and Langmuir, I., *Physical Review*, **28**, 727-763, (1926).
- [2] H. Kersten *et al*, *Vacuum*, **63**, 385-431, (2001).
- [3] Scholtz, J. S., Fontana, L. C. and Mezaroba, M., *IEEE Transactions on Plasma Science*, **46**, 2999-3007, (2018).

Acknowledgments

The authors are grateful for the financial support from Fundação de Amparo a Pesquisa de Santa Catarina (FAPESC) through the grants 2020TR730 (PRONEM-FAPESC) and 2021TR000563 (Universal-FAPESC).

Author Index

Abrahão, A. B. R. M.	34
Abreu, L. P. P.	91
Almeida, A. C. P. L.	18, 37
Almeida, G. S.	75, 83
Almeida, L. S.	62, 84
Alves Jr., C.	19
Amaral-Labat, G. A.	50
Anjos, M. L. S.	66
Aoki, F.	83
Aoki, I. V.	39
Apolinario, R.	86
Ávila, P. T.	86
Baldan, M. R	16, 50
Barbosa Junior, J. L.	92
Barbosa, A. A.	18, 37
Barbosa, E. A.	58
Barros, H. C. S.	16
Becker, D.	64
Bento, R. T.	24
Biancardi, V. R.	92
Bigansolli, A. R.	60, 62, 66, 74, 76, 78, 79, 89, 90, 92
Borges, S. P. T.	38
Bortoleto, J. R. R.	48
Botelho, E. C.	34
Brito A. A. R.	81
Brunatto, S. F.	31
Bueno, C. F.	42
Bufon, C. C. B.	41
Camargo, D. H. S.	41
Campedelli, R. R.	72
Cardoso, G. C.	69, 75
Cardoso, P.	79
Cardoso, R. P.	31
Carvalho, B.	16
Carvalho, D. F.	60
Castanho, M. A. P.	63
Cesare, M. P.	67
Chaves, J. P. M.	79
Chiappim Júnior, W.	82
Coan, K. S.	73
Corrêa, D. O. G.	75, 83
Correa, D. R. N.	23, 27, 30, 46, 49
Correa, O. V.	24
Costa, F. J.	81
Costa-Neto, J. L. S.	76, 78
Couto, A. A.	68, 70
Cruz Lopes, T. G.	61, 62
Cruz, N. C.	41, 44, 46, 48, 49, 85

Cunha, T. H. R.	35
Dalmolin, C.	72
Damasceno, B.	16
Danelon, M. R.	40, 73
de Almeida, L. S.	40, 73, 84
Degasperi, F. T.	58, 77
Emidio, G.	72
Esmonde H.	19
Fabrício Jr., C. A.	63
Fachini, E. R.	53
Ferreira, A. H. R.	80
Ferreira, D. C.	35
Ferreira, M. J.	17
Fin, P.	72
Florêncio, O.	88
Flores, I. C. C.	58
Fonseca, L. P.	46
Fontana, L. C.	28, 29, 55, 64, 72
Freitas, L. R.	36
Fricke, K.	43
Galindo, E. L.	69
Garcia, A. C. M.	63
Garcia, Y. A.	32, 33, 54
Gelamo, R. V.	35, 36, 39
Godoy-Jr, A.	16
Gomes, M. C.	16
Gonzaga, A. B.	70
Grandini, C. R.	22, 23, 27, 30, 75, 83, 87
Issaka, R. K.	85
Kalinke, C.	35
Karnopp, J.	59
Klok, L. A.	64
Kodaira, F. V. P.	18, 25, 43
Koga-Ito, C. Y.	18, 51, 52, 79, 82
Kostov, K. G.	18, 25, 37, 43, 45, 51, 52, 65, 79
Kühn, B. B. L.	60, 61, 66, 74, 76, 78, 89, 90
Lago, N. M.	61
Laur, A.	28, 29
Leal, B. H. S.	18, 25
Legendre, D.	79
Leite, D. M. G.	16
Leite, L. D. P	51
Lenz e Silva, G. F. B.	50
Letichevsky, S.	33
Lima G. M. G.	18
Lima, M. S. F.	81
Lopes, R. E. L.	69, 83
Lucas, R.R.	34
Lustosa, C. J. R.	88
Magaldi, B. V.	67

Makhneva, E.	43
Manfrinato, M. D.	40, 57, 71, 73, 84
Marcuzzo, J. S.	50
Marciano F. R.	21
Marino, C. E. B.	36
Marques, P. W.	88
Martinez-Orozco, K.	86
Martins, C. A.	67
Massi, M.	28, 29
Matias, F. C. B.	89, 90
Matsushima, J. T.	50
Meireles, A.	54
Mendonça, R. H.	32, 33, 54
Mendonça, T. S.	33
McGuinness G.	20
Milhan, N. V. M.	52
Monteiro, M. J.	33
Morais, A. M.	55
Moreto, J. A.	35, 36, 39
Moretti, M. L.	26
Moro, J. R.	63
Mota, R. P.	34
Moura, F. O.	63
Moura, G. M.	35
Mui, T. S. M.	52, 79
Munhoz, M. G. C.	50
<i>Nanuh, A. C.</i>	46
Nascente, P. A. P.	86
Nascimento, A. M.	74
Nascimento, F.	18, 37, 45, 65
Nascimento, J. P. L.	36, 39
Nascimento, M. S.	68, 70, 74
Naves, E. A. A.	35
Neves, M. A.	91
Nishime, T. M. C.	18, 51
Oliveira, F. S.	38
Oliveira, L. P. G.	48
Oliveira, L. S.	42
Oliveira, M. A. C.	51
Oliveira, P. R.	35
Oliveira, R. N.	62
Orea, A. C.	14
Palmeira, E.	68
Pasa, A. A.	13
Passaro, A.	81
Passeti, T.	85
Patrício, B. F. C.	54
Pavani, R. R.	57, 84
Pereira, A. L. J.	16
Pereira, D. B.	54

Perez, J. L. J.	15
Perosa, B. S.	23
Pessoa, R. S.	59, 67, 80, 82
Petroski, K. A.	18, 65
Pillis, M. F.	24
Pintão, C. A. F.	69
Pinto, B. O.	27
Pinto, H. C.	86
Proença, J. P.	49
Quadros, F. F.	87
Rangel, E. C.	41, 44, 46, 48, 49, 85
Recco, A. A. C.	26, 55, 72
Ribeiro, A. A.	67
Ribeiro, R. P.	44, 48, 85
Rocha, H. V. A.	54
Rodrigues, A. C.	50
Rodrigues, I. R.	69, 83
Rosário, M. A. P.	89, 90
Rossino, L. S.	40, 57, 71, 73, 84
Sagás, J. C.	28, 29, 55, 59, 72, 93
Sampaio, A. G.	52, 82
Santos Filho, S. G.	53
Santos Fo., S. G.	56
Santos, A. M.	84
Santos, G. A.	68, 70
Santos, L. C.	56
Santos, M. L.	85
Santos, O. A. M. R.	57, 84
Santos, V. T.	68, 70
Scalvi, L. V. A.	42, 47
Scarminio, J.	35, 39
Secco, K. M. S.	77
Siervo, A.	35
Silva Sobrinho, A. S.	16
Silva, A. C. L.	91
Silva, A. G.	12
Silva, A. N. R.	53
Silva, B. P.	39
Silva, C. C.	35
Silva, C. E. R.	32, 33
Silva, D. M.	79
Silva, F. L. F.	57, 84
Silva, M. L. P.	53, 56
Silva, M. R.	68, 70
Silva, T. G.	32, 33
Silvestre-Filho, F. A.	78
Sousa, G. G. J.	77
Sousa, J. O.	60
Sousa, R. R. M.	40

Sousa, T. S. P.	30
Spigarollo, D. C. F. S.	41
Steffen, T. T.	64
Stryhalski, J.	28, 29, 55
Tanaka, M. H.	18
Teram, R.	68, 70
Torrento, J. E.	23, 27, 30
Vatavuk, J.	68, 70
Vegan M. R. C	52, 79
Vieira, T. M.	93
Weltmann, K. D.	43
Zambuzzi, W. F.	75, 83
Zanella, I. G	31

ICONISMUS XI



ISBN: 978-65-00-79418-2

9



9 786500 794182